



International Committee for Future Accelerators

Sponsored by the Particles and Fields Commission of IUPAP

Beam Dynamics Newsletter

No. 63

**Issue Editors:
I. S. Ko, J.-H. Han**

**Editor in Chief:
W. Chou**

April 2014

Contents

1	FOREWORD	7
1.1	FROM THE CHAIR	7
1.2	FROM THE EDITORS	8
2	LETTER TO THE EDITOR.....	9
2.1	PARTICLE ACCELERATORS AND THE INTERNATIONAL YEAR OF LIGHT	9
2.1.1	Introduction.....	9
2.1.2	Accelerators and the Light Sciences	10
2.1.3	International Year of Particle Accelerators and Accelerator-based Technologies	12
2.1.4	References.....	13
3	THEME SECTION: MICROBUNCHING INSTABILITY	16
3.1	OVERVIEW AND ISSUES OF EXPERIMENTAL OBSERVATION OF MICROBUNCHING INSTABILITIES.....	16
3.1.1	Introduction.....	16
3.1.2	Instability Effects	16
3.1.2.1	<i>Context</i>	16
3.1.2.2	<i>Diagnostics Options</i>	17
3.1.3	Thermionic Cathode Gun Beams.....	18
3.1.3.1	<i>SCSS Results</i>	18
3.1.3.2	<i>SACLA Results</i>	20
3.1.3.3	<i>APS/ANL Results</i>	21
3.1.4	NLCTA X-band Results	22
3.1.5	Discussion	22
3.1.6	Some Issues.....	23
3.1.7	Summary	23
3.1.8	Acknowledgments.....	24
3.1.9	References.....	24
3.2	MICROBUNCHING INSTABILITY SUPPRESSION VIA ELECTRON MAGNETIC PHASE MIXING.....	25
3.2.1	Introduction.....	25
3.2.2	Suppression of Microbunching via Energy Landau Damping.....	25
3.2.3	Experiment Setup	26
3.2.4	Experimental Results vs. Analytical Predictions	28
3.2.5	Application to FELs.....	29
3.2.6	Acknowledgments.....	30
3.2.7	References.....	30
3.3	COHERENT SYNCHROTRON RADIATION IN WHISPERING GALLERY MODES: THEORY AND EVIDENCE	32

3.3.1	Introduction.....	32
3.3.2	The Electromagnetic Problem in the Vacuum Chamber of an Accelerator	34
3.3.3	Comparison with Spectrum Measured at NSLS VUV Light Source.....	39
3.3.4	High Resolution CSR Spectra at the Canadian Light Source (CLS).....	41
3.3.5	Implications for the Wake Field	42
3.3.6	Experimental Evidence for Interbunch Communication	43
3.3.7	Direct Observation of a Long Range Wake Field.....	44
3.3.8	Simulation of Interbunch Communication	45
3.3.9	Outlook	46
3.3.10	Acknowledgment.....	47
3.3.11	References	47
3.4	COHERENT SYNCHROTRON RADIATION STUDIES AT THE EMITTANCE EXCHANGE BEAMLINE.....	48
3.4.1	Introduction.....	48
3.4.2	CSR Studies at the A0 Emittance Exchange Beamline	49
3.4.2.1	<i>Experimental Setup</i>	49
3.4.2.2	<i>CSR Power Measurements</i>	50
3.4.2.3	<i>Polarization of CSR</i>	51
3.4.2.4	<i>Bunch-Length Measurements</i>	51
3.4.2.5	<i>Skew-Quadrupole Measurements</i>	52
3.4.2.6	<i>Emittance Exchanger with an Energy-Chirped Beam</i>	53
3.4.3	Other Exact-Emittance Exchange Configurations.....	55
3.4.4	Conclusion	57
3.4.5	References.....	57
3.5	MITIGATION PLANS FOR THE MICROBUNCHING-INSTABILITY-RELATED COTR AT ASTA/FNAL.....	59
3.5.1	Introduction.....	59
3.5.2	ASTA Facility and Diagnostics Aspects	60
3.5.2.1	<i>Facility</i>	60
3.5.2.2	<i>Diagnostics Options</i>	61
3.5.3	Temporal Mitigation Option in Diagnostics.....	64
3.5.4	Summary.....	64
3.5.5	Acknowledgments	65
3.5.6	References.....	65
3.6	CANCELLATION OF COHERENT SYNCHROTRON RADIATION KICKS WITH OPTICS BALANCE	65
3.6.1	Introduction.....	65
3.6.2	Suppression of CSR-driven Emittance Growth with Optics Symmetry.....	66
3.6.3	Cancellation of CSR Kicks Extended to Asymmetric Optics	67
3.6.3.1	<i>Theoretical Model</i>	67
3.6.3.2	<i>Experimental Results</i>	69
3.6.4	Conclusions.....	72
3.6.5	References.....	73
4	WORKSHOP AND CONFERENCE REPORTS	74

4.1	ICFA MINI WORKSHOP ON SUPERKEKB BEAM COMMISSIONING	74
4.1.1	Review of Extant Facilities and Lessons Learned (Convenor: J.T. Seeman, SLAC).....	76
4.1.2	More Lessons-learned for SuperKEKB (Convenor: Y. Funakoshi, KEK)..	76
4.1.3	Linac and DR Commissioning (Convenor: K. Oide, KEK)	77
4.1.4	Ring Optics and Intensity Effects (Convenor: F. Zimmermann, CERN)....	77
4.1.5	IP Commissioning/Background and Lifetime (Convenor: M. E. Biagini, INFN-LNF)	78
4.1.6	Feedback, Injection and Commissioning Strategies, (Convenor: J. Flanagan, KEK).....	79
5	RECENT DOCTORIAL THESES	80
5.1	STUDY ON ELECTRON BEAM OPTIMIZATION AT PAL-XFEL INJECTOR TEST FACILITY	80
6	FORTHCOMING BEAM DYNAMICS EVENTS.....	80
6.1	55 TH ICFA ADVANCED BEAM DYNAMICS WORKSHOP ON HIGH LUMINOSITY CIRCULAR E^+E^- COLLIDERS FOR HIGGS FACTORY (HF2014)	80
6.2	INTERNATIONAL BEAM INSTRUMENTATION CONFERENCE (IBIC 2014).....	82
6.3	XXIV RUSSIAN PARTICLE ACCELERATORS CONFERENCE	82
7	ANNOUNCEMENTS OF THE BEAM DYNAMICS PANEL	84
7.1	ICFA BEAM DYNAMICS NEWSLETTER	84
7.1.1	Aim of the Newsletter	84
7.1.2	Categories of Articles.....	84
7.1.3	How to Prepare a Manuscript.....	84
7.1.4	Distribution	85
7.1.5	Regular Correspondents	85
7.2	ICFA BEAM DYNAMICS PANEL MEMBERS.....	86

1 Foreword

1.1 From the Chair

Weiren Chou, Fermilab
Mail to: chou@fnal.gov

The International Committee for Future Accelerators (ICFA) met on February 20-21, 2014 at DESY, Hamburg, Germany. Nigel Lockyer, Fermilab Director and ICFA Chair chaired the meeting. This meeting was preceded by a Linear Collider Board (LCB) meeting earlier on February 20 in the same place.

The Funding Agencies for Large Colliders (FALC) gave a report on the status and plans for particle physics in the 3 regions (America, Asia and Europe) over the next 2-3 years. The Japanese funding agency MEXT will conduct a comprehensive study to examine the viability of building the ILC in Japan. A Common Fund for the Linear Collider Collaboration (LCC) was established with equal contributions from the 3 regions. The Japan Science Council issued a review report, which expressed two concerns about hosting the ILC in Japan: possible resulting funding cuts to other research fields; and the difficulty of finding enough scientists and technicians for this big project. Meanwhile, the Japanese government took a significant and positive action by allocating a special line item fund to the ILC in the 2014 budget. An ILC Planning Office has been set up at KEK.

Since the discovery of the Higgs particle in 2012 at CERN, there has been a renewed interest in building a new large circular collider. Presently there are two large (50-100 km) future circular colliders – FCC and CEPC-SppC – under emerging consideration by the world HEP community. In Europe, a tunnel of 80-100 km has been considered for the FCC, A study group has been formed and is looking at the pp , $e+e-$ and ep options. In China, there is a window of opportunity after ~2020 to build a 50-70 km tunnel to host a 240 GeV $e+e-$ collider for a Higgs factory (CEPC), with later conversion to a pp collider (SppC). IHEP (Beijing) is planning to write a Preliminary Conceptual Design Report (Pre-CDR) by the end of this year. ICFA encouraged the two studies to work as close together as possible and issued a statement: “*ICFA supports studies of energy frontier circular colliders and encourages global coordination.*” As part of the global coordination, ICFA approved the 55th ICFA Advanced Beam Dynamics Workshop on High Luminosity Circular $e+e-$ Colliders for a Higgs factory (HF2014), which will take place from October 9 to 12, 2014 in Beijing, China. The announcement can be found in Section 6.1. (<http://hf2014.ihep.ac.cn>)

The ICFA Seminar, which takes place once every three years, will be hold from October 27 to 30, 2014 at IHEP, Beijing. It is a valuable meeting because it brings together the funding agency representatives, lab directors and scientists all over the world. There will also be a significant media attendance.

As Lockyer’s term as the ICFA Chair will end this year, ICFA approved Joachim Mnich, Research Director of DESY, to be the new ICFA Chair for the period January 1, 2015 to December 31, 2017.

ICFA discussed the status of the Linear Collider School, which started in 2006 and has been very successful in educating and training the next generations of accelerator scientists for future colliders. However, the DOE support for this school was cut last year because of the zeroing out of the ILC fund in the US. ICFA suggested forming a

working group that will produce a plan for the future of the School and report to the July 2014 ICFA meeting. The next school will be in Vancouver, Canada and hosted by TRIUMF.

2015 has been proclaimed by the United Nations as the *International Year of Light and Light-based Technologies* (IYL2015). Sameed Ahmed Khan, a Regular Correspondent of this newsletter, wrote a Letter to the Editor discussing the significance of IYL2015 and its relationship with particle accelerators.

The editor of this issue is Dr. In Soo Ko, a panel member and a senior scientist at PAL, Korea, and Dr. Jang-Hui Han, also from PAL. They collected 6 articles in the theme section “*Microbunching Instability*,” which were selected from a recent workshop at Pohang, Korea. These articles give a comprehensive review of this important beam dynamics topic in the study of high brightness electron beams. In this issue there is also a workshop report (SuperKEKB Commissioning), one recent PhD thesis abstract (Moonsik Chae, PAL) and three workshop announcements (*HF2014*, *IBIC2014*, *RuPAC2014*). I thank In Soo and Jang-Hui for editing and producing a newsletter of good quality and great value to the accelerator community.

1.2 From the Editors

In Soo Ko and Jang-Hui Han, Pohang Accelerator Laboratory
Mail to: isko@postech.ac.kr, janghui_han@postech.ac.kr

High brightness beams become crucial for modern storage rings, linear colliders and free electron lasers. However, high brightness electron beams may generate unwanted microbunching instabilities. The 4th Microbunching Instability Workshop, organized by Pohang Accelerator Laboratory, was held at the POSCO International Center in Pohang, Korea, May 8-10 2013. This workshop was reported shortly in the 61st issue of Beam Dynamics News Letter. For the theme section of the 63rd issue of this Letter, we have chosen selected contributions of the workshop. The first article by **A. H. Lumpkin** overviews experimental observations of microbunching instabilities. After discussing experimental results from LCLS, SCSS, SACLAL, APS, and NLCTA, he claims that the instability detected through the generation of coherent optical transition radiation (COTR) occurs in various types of accelerators and electron guns. Some issues on the experimental side are summarized. **S. Di Mitri** reports the first experimental demonstration of control and suppression of microbunching instability by means of particles’ longitudinal phase mixing in a magnetic chicane. The article is extended to a discussion of applications of magnetic phase mixing to the generation of quasi-cold high-brightness ultra-relativistic electron beams. **R. Warnock** discusses the theory and evidence of coherent synchrotron radiation (CSR) in whispering gallery modes. Starting from Lord Rayleigh’s study on a whispering gallery phenomena at St. Paul’s Cathedral in London, he explains the theory and experimental observations in modern particle accelerators. **J. Thangaraj** reports coherent synchrotron radiation studies at the A0 emittance exchange (EEX) beamline of Fermi Lab. The measurements of CSR power as a function of bunch charge and length and the measurement of polarization of the CSR are shown. He then discusses a peak current increase with an energy-chirped beam. Finally, the latest developments in EEX configuration are described and two new configurations are proposed. The second article of **A. H. Lumpkin** shows mitigation plans for the microbunching instability related CORT at ASTA/FNAL. They plan to use

the spectral differences between OTR and COTR, the scintillators in combination with bandpass filters, and temporal gating techniques to mitigate the diagnostics effects by a total factor of 100-1000. In the second contribution from **S. Di Mitri**, he shows how to cancel CSR kicks with optics balance. Cancellation of CSR kicks is extended to asymmetric optics. The theoretical model is first described in detail and then experimental results at FERMI@Elettra are compared with ELEGANT simulation.

We thank the contributors for providing these excellent articles and also the participants of the workshop for exciting discussions. We hope this Theme Section is useful to accelerator physicists.

2 Letter to the Editor

2.1 Particle Accelerators and the International Year of Light

Sameen Ahmed Khan

Engineering Department, Salalah College of Technology (SCOT), Sultanate of Oman

Mail to: rohelakhan@yahoo.com

2.1.1 Introduction

The year 2013 ended with the much awaited and anticipated announcement from the United Nations, when it proclaimed 2015 as the *International Year of Light and Light-based Technologies* (IYL 2015). It is a cross-disciplinary educational and outreach project with over one hundred partners from more than 85 countries and will involve participation in many more. The partner base includes scientific societies, research infrastructure networks, industry consortia, museums, educational institutions, national and international academies, and other associations. The IYL commemorates the achievements of light science; its applications; and its contributions to humankind. The resolution A/RES/68/221 proclaiming the IYL 2015 was adopted without vote on 20 December 2013 during a plenary meeting of the 68th Session of the UN General Assembly, with the General Assembly acting on the recommendation of its Second Committee (Economic and Financial) during consideration of an Agenda item on Science and Technology for Development. This marked a culmination of three years' work to bring the international year into being. The text of the resolution, which was adopted as part of a more general agenda item on science and technology for development, stated: "*Applications of light science and technology are vital for existing and future advances in medicine, energy, information and communications, fiber-optics, astronomy, architecture, archaeology, entertainment and culture.*" [1-3]



Light is at the origin of all life and it plays a central role in human activities. At the very basic level it provides us vision. At the most fundamental level through photosynthesis (mostly in the green leaves of the plants), light is at the origin of all life. In human skin, the sunlight induces the synthesis of the essential vitamin-D. Light and the technologies based on it have revolutionized society through medicine and communications, entertainment and culture. Without recent advances in photonics (as this science is now known), there would be no DVDs, barcode scanners, no smart phones or flat screen televisions, and no worldwide web. It is to be recalled that the worldwide web or www as it is known was born at CERN the European Organization for Nuclear Research [4]. Advances in lighting and solar energy are considered crucial for future sustainable development.

The year 2015 commemorates a remarkable series of important milestones in the history of the physics of light. A number of major scientific anniversaries will be celebrated in 2015, starting with the early work on optics by the medieval Arab scholar Ibn Al-Haytham in 1015. The notion of light as a wave proposed by Fresnel in 1815; the electromagnetic theory of light propagation proposed by Maxwell in 1865; Einstein's theory of the photoelectric effect in 1905; Einstein's embedding of light in cosmology through general relativity in 1915; the discovery of the cosmic microwave background by Penzias and Wilson in 1965; and Charles Kao's achievements in 1965 concerning the transmission of light in fibers for optical communication [2].

The International Year of Light is endorsed by *International Council of Science* and a number of other international scientific unions. IYL 2015 will be administered by an International Steering Committee in collaboration with the UNESCO International Basic Sciences Program at UNESCO headquarters in Paris and a Global Secretariat at ICTP: the Abdus Salam International Centre for Theoretical Physics in Trieste, Italy, which is a UNESCO Category 1 Institute. The international committee will run a number of cornerstone projects while encouraging national committees to inspire celebrations at a more local level [5].

2.1.2 Accelerators and the Light Sciences

Accelerator optics and light optics have an intimate relationship. At the level of the formalism and language, we have the Hamilton's analogy. Historically, variational principles played a fundamental role in the evolution of mathematical models in classical physics, and many equations were derived using them. Here the relevant examples are Fermat's principle in optics and Maupertuis' principle in mechanics. The

corresponding beam-optical Hamiltonians are $H = -\{n^2(\mathbf{r}) - \mathbf{p}_\perp^2\}^{1/2}$ and $H = -\{p_0^2 - \boldsymbol{\pi}_\perp^2\}^{1/2} - qA_z$ respectively. The analogy between the trajectory of material particles in potential fields and the path of light rays in media with continuously variable refractive index was formalized by Hamilton in 1833. This Hamiltonian analogy led to the development of electron optics in 1920s, when Busch derived the focusing action and a lens-like action of the axially symmetric magnetic field using the methodology of geometrical optics. Around the same time, Louis de Broglie associated his now-famous wavelength to moving particles. Schrödinger extended the analogy by passing from geometrical optics to wave optics through his wave equation incorporating the de Broglie wavelength. This analogy played a fundamental role in the early development of quantum mechanics [6]. On the other hand, the analogy, led to the development of practical electron optics, and one of the early inventions was the electron microscope by Ernst Ruska [7-9]. Recent works have extended the Hamilton's analogy to the wavelength-dependent regime [10-15]. It is seen in these works that the traditional Hamiltonians due of Fermat and Maupertuis are modified by wavelength-dependent parts [16-19]. The beginning of the analogy between geometrical optics and mechanics is usually attributed to Descartes (1637), but it can actually be traced back to Abu Ali Al-Hasan Ibn Al-Haytham (0965–1037) who is more commonly known by his Latinized name Alhazen; see [20-21] for a detailed historical account.

The aforementioned relationship between accelerator optics and light optics is at the level of the formalism. For the end users the relationship is seen through synchrotron-light. Synchrotrons produce electromagnetic radiation beyond the visible range that too with special properties. The advent of the free-electron lasers (FEL) has further strengthened the links between the two optics. The free-electron laser has the widest frequency range of any laser type, and can be widely tunable, currently ranging in wavelength from microwaves, through terahertz radiation and infrared, to the visible spectrum, ultraviolet, and X-Rays. There are proposals exploring laser-based particle accelerators. In principle, laser-based schemes could offer a complementary technological approach to future high-energy particle accelerators.

The IYL 2015 is aimed at stimulating worldwide interest, especially among young people in light and related sciences & technologies. It will highlight to the citizens of the world the importance of light and optical technologies in their lives, for their futures, and for the development of society. A variety of events and activities will be organized throughout 2015 world-wide. In view of the strong relationship between the world of accelerators and light sciences, IYL will be an excellent platform to conduct accelerator related outreach programmes. Cornerstone projects such as a *Synchrotron Day* or *Synchrotron Week* (or an Accelerator Day or Accelerator Week) can be organized, when synchrotron radiation facilities (and other accelerator facilities) around the world will open their doors to public visitors. This will enable to highlight the role of accelerators in human endeavours, ranging from basic particle physics research to diverse applications in medicine and industry.

The ongoing year is the International Year of Crystallography (IYCr 2014). It is a century since, it was discovered that crystals could diffract X-Rays, a finding that helped revolutionize our ability to visualize matter at the atomic scale. It was found that X-Rays can be used to determine accurately the positions of atoms within a crystal and thus unravel its three-dimensional structure. This discovery has contributed hugely to the modern development of all the natural sciences, because atomic structure governs

chemical and biological properties of matter, and the crystal structure determines most of its physical properties. The insights gained from the structure of matter have impacted chemistry, solid state physics, biology and medicine. This has resulted in the synthesis of novel materials, new drugs and our understanding of the structure of proteins and DNA. The United Nations adopted that 2014 be the International Year of Crystallography (IYCr 2014) at its Sixty-Sixth Assembly on 3rd July 2012. This is to commemorate the centennial of X-Ray diffraction and related discoveries [22]. IYCr provides yet another venue for the accelerator community to highlight the role of X-Rays, Synchrotrons and other accelerator-based techniques used extensively in crystallography.

2.1.3 International Year of Particle Accelerators and Accelerator-based Technologies

Accelerators are finding an increasing use in numerous fields such as medicine; industries; accelerator-based nuclear energy programmes and others. A global survey reveals that very few (about twenty or so) accelerators are high-energy devices used in academic particle research and there are thousands of accelerators routinely used in hospitals [23]. Today there are over ten thousand electron linacs world-wide dedicated to cancer therapy [24]. Besides, there are other types of medical accelerators covering therapies such as hadron therapy and ion therapy. There are over seventy-five synchrotron radiation sources in various stages of operation, construction or planning in twenty-six countries. Iran is the latest country to join this elite group. The Iranian Light Source Facility (ILSF) is a 3GeV facility, presently in the design phase and to be located at Qazvin 150km northwest of the capital Tehran [25]. From this list it is evident that the world of synchrotron sources has its own share of haves and have-nots! The continent of Africa is yet to have a synchrotron [26-28]. There are more than 20,000 synchrotron users per year and a strong growth is predicted [29]. There is an increasing demand for medical accelerators and synchrotrons. There are some synchrotrons operated jointly such as the ESRF: European Synchrotron Radiation Facility [30]; and SESAME: the Synchrotron-Light for Experimental Science and Applications in the Middle East [31]. The proposal for regional synchrotron radiation facilities (RSRF) is not new [32-34]. It has been aptly pointed out by Sessler and Wilson in their book, *Engines of Discovery*, “*The appetite of the particle physicists for particles of higher and higher energy seems never to be satisfied*” [23]. This appetite has necessitated international collaborations. The future machines in this direction will require hefty funding in tens of billions of US dollars. Many nations will find it difficult to meet the financial requirement individually. Moreover, the technology to individually build and run such large facilities will be beyond the reach of many nations. For such projects to become a reality, we need awareness and outreach programmes. Same is true for the (relatively modest) synchrotron programmes. To keep pace with the demand of the accelerators, there needs to be awareness. It is time to have an *International Year of Particle Accelerators and Accelerator-based Technologies* (IYPA). An IYPA will promote the central role of particle accelerators in basic sciences and its numerous applications such as ion implantation and lithography in industry, medicine, radiotherapy, food sterilization, management of nuclear waste. The proposed IYPA shall provide the ideal platform to educate the public and the policy makers about the role of accelerators and the spin-off technologies; and thereby reach the potential

sources of funding. It will provide a forum to support and strengthen the underlying beam physics programmes [35]. It will address the themes such as: accelerator-based international cooperation; creation of global accelerator facilities and regional accelerator facilities where applicable; and other themes related to the world of accelerators.

It is a useful coincidence that several institutional jubilees related to accelerators fall during the year of IYCr 2014. These include the sixty years of CERN: European Organization for Nuclear Research [4]; ESRF: European Synchrotron Radiation Facility completes twenty years of User Operation [30]; and fifty years of ICTP: Abdus Salam International Centre for Theoretical Physics [5]. A detailed account of the accelerator-related activities at ICTP can be found in [36]. The younger jubilees of the three institutions were covered in this newsletter a decade back [36]. These institutional jubilees in 2014 will be marked with several programmes bringing together scientists, engineers, policy makers and government officials together; thus providing an excellent occasion to interact and chalk out strategies towards the proposed International Year of Particle Accelerators and Accelerator-based Technologies.

Since, 1959 the UN has been observing international years under its auspices. For instance, World Refugee Year (1959), International Health and Medical Research Year (1960), International Year of Physics (2005), International Year of Astronomy (2009), International Year of Chemistry (2011), International Year of Sustainable Energy for All (2012), and International Year of Crystallography (2014). Years can also be established by the UN bodies and other international entities. So why not have an International Year of Particle Accelerators? A year in the 2020s coinciding with the anniversaries of the milestones from the 1920s would be too far in the future. An earlier year would be ideal. Many accelerator projects do not go beyond the drawing stage. Accelerator projects take a long time to mature. The outreach programmes are an urgent necessity to realize the accelerator projects. The proposed International Year of Particle Accelerators would be an ideal vehicle to reach the goals of the accelerator community. ICFA is in the best position to initiate the proposed International Year of Particle Accelerators and Accelerator-based Technologies.

2.1.4 References

1. “Proclamation of 2015 as the United Nations International Year of Light”, <http://unesdoc.unesco.org/images/0022/002225/222574e.pdf> (13 August 2013); “Resolution adopted by the General Assembly on 20 December 2013”, http://www.un.org/en/ga/search/view_doc.asp?symbol=A/RES/68/221 (20 December 2013).
2. See the Prospectus at the European Physical Society Website, <http://www.eps.org/light2015> and http://www.eps.org/resource/resmgr/events/EPS_IYL2015prospectus.pdf (September 2013).
3. Sameen Ahmed Khan, “2015 declared the International Year of Light and Light-based Technologies”, *Current Science*, **106** (4), 501 (25 February 2014). (Fortnightly Publication of the Indian Academy of Sciences). <http://www.currentscience.ac.in/Volumes/106/04/0501.pdf>
4. “CERN where the web was born”, <http://home.web.cern.ch/about/topics/birth-web/where-web-was-born>; “The birth of the web”, <http://home.web.cern.ch/topics/birth-web>

5. “A Celebration of Light: ICTP to coordinate UN International Year of Light”, *ICTP News Highlights* (27 February 2014); Abdus Salam International Centre for Theoretical Physics (ICTP), Trieste, Italy, <https://www.ictp.it/about-ictp/media-centre/news/2014/2/year-of-light.aspx>
6. Barry R. Masters, “Erwin Schrödinger’s Path to Wave Mechanics”, *Optics & Photonics News*, **25** (2), 32-39 (February 2014).
7. P. W. Hawkes and E. Kasper, “Principles of Electron Optics”, Vols. I and II (Academic Press, London, 1989); P. W. Hawkes and E. Kasper, “Principles of Electron Optics Vol.3: Wave Optics” (Academic Press, London and San Diego, 1994).
8. M. Born and E. Wolf, “Principles of Optics”, Cambridge University Press, United Kingdom, 7th edition (1999).
9. G. W. Forbes, “Hamilton’s Optics: Characterizing Ray Mapping and Opening a Link to Waves”, *Optics & Photonics News*, **12** (11), 34-38 (November 2001).
10. R. Jagannathan, R. Simon, E. C. G. Sudarshan and N. Mukunda, “Quantum theory of magnetic electron lenses based on the Dirac equation”, *Phys. Lett. A* **134**, 457-464 (1989).
11. R. Jagannathan, “Quantum theory of electron lenses based on the Dirac equation”, *Physical Review*, **A42**, 6674-6689 (1990).
12. M. Conte, R. Jagannathan, S. A. Khan and M. Pusterla, “Beam optics of the Dirac particle with anomalous magnetic moment”, *Particle Accelerators*, **56** 99-126 (1996).
13. R. Jagannathan and S. A. Khan, “Quantum theory of the optics of charged particles”, Chapter-4 in *Advances in Imaging and Electron Physics*, Editors: P. W. Hawkes, B. Kazan and T. Mulvey, (Academic Press, San Diego, 1996) **Vol. 97**, 257-358 (1996). [http://dx.doi.org/10.1016/S1076-5670\(08\)70096-X](http://dx.doi.org/10.1016/S1076-5670(08)70096-X)
14. S. A. Khan, “Quantum theory of charged-particle beam optics”, University of Madras, Chennai, India, 1997 (PhD thesis). Complete thesis available from Dspace of IMSc Library, The Institute of Mathematical Sciences (IMSc), Chennai, India, where the doctoral research was done, <http://www.imsc.res.in/xmlui/handle/123456789/75?show=full> and <http://www.imsc.res.in/xmlui/>
15. R. Jagannathan and S. A. Khan, “Quantum mechanics of accelerator optics”, *ICFA Beam Dynamics Newsletter*, **13**, 21-27 (April 1997). (ICFA: International Committee for Future Accelerators).
16. Sameen Ahmed Khan, “Analogies between light optics and charged-particle optics”, arXiv:physics/0210028 [physics.optics]; *ICFA Beam Dynamics Newsletter*, **27**, 42-48 (June 2002). (ICFA: International Committee for Future Accelerators).
17. Sameen Ahmed Khan, “Wavelength-dependent modifications in Helmholtz Optics”, arXiv:physics/0210001 [physics.optics]; *International Journal of Theoretical Physics*, **44** (1), 95-125 (January 2005), (Kluwer Academic Publishers). <http://dx.doi.org/10.1007/s10773-005-1488-0>
18. Sameen Ahmed Khan, “The Foldy-Wouthuysen Transformation Technique in Optics”, *Optik - International Journal for Light and Electron Optics*, **117** (10), 481-488 (October 2006) (Elsevier, 2006), <http://dx.doi.org/10.1016/j.ijleo.2005.11.010>; Chapter-2 in *Advances in Imaging and Electron Physics*, Editor: Peter W. Hawkes, (Elsevier, 2008) **Vol. 152**, 49-78 (August 2008). [http://dx.doi.org/10.1016/S1076-5670\(08\)00602-2](http://dx.doi.org/10.1016/S1076-5670(08)00602-2)
19. Sameen Ahmed Khan, “Maxwell Optics of Quasiparaxial Beams”, *Optik - International Journal for Light and Electron Optics*, **121** (5), 408-416 (March 2010) (Elsevier, 2010), <http://dx.doi.org/10.1016/j.ijleo.2008.07.027>; “Aberrations in Maxwell Optics”, *Optik - International Journal for Light and Electron Optics*, **125** (3), 968-978 (February 2014) (Elsevier, 2014). <http://dx.doi.org/10.1016/j.ijleo.2013.07.097>.
20. D. Ambrosini, A. Ponticello, G. Schirripa Spagnolo, R. Borghi and F. Gori, “Bouncing light beams and the Hamiltonian analogy”, *European Journal of Physics*, **18**, 284-289 (1997).

21. Alistair Kwan, John Dudley and Eric Lantz, "Who really discovered Snell's Law?", *Physics World*, **15** (4), 64 (April 2002). <http://physicsworldarchive.iop.org/full/pwv15i4a44.pdf>.
22. International Year of Crystallography (IYCr 2014), <http://www.iycr2014.org/>
23. Andrew Sessler and Edmund Wilson, "Engines of Discovery: A Century of Particle Accelerators", World Scientific (2006).
24. Ugo Amaldi, "Particle Accelerators take up the fight against Cancer", *AAPPS Bulletin*, **18** (1), 19-23 (February 2008). (AAPPS: Association of Asia Pacific Physical Societies).
25. The Iranian Light Source Facility (ILSF), <http://ilsf.ipm.ac.ir/>
26. Keith Jackson, Sameen Ahmed Khan, Abebe Kebede and Azher Majid Siddiqui, "SESAME the Nearest Synchrotron Radiation Facility to Africa", at the website of the *African Synchrotron User Forum*. <http://sirius-c.ncat.edu/asn/Africasynchrotron/index.html> (20 March 2003). <http://synchrotron.org.za/>
27. Sameen Ahmed Khan, "The Middle East Synchrotron is Launched; Armenian Synchrotron; To Launch the African Synchrotron Programme", *AAPPS Bulletin*, **13** (2), 35-36 (April 2003). (AAPPS: Association of Asia Pacific Physical Societies).
28. Sameen Ahmed Khan, "Ground Breaking for the Middle East Synchrotron; Armenian Synchrotron; Time to Launch the African Synchrotron Research Programme", *ICFA Beam Dynamics Newsletter*, **30**, 88-89, (April 2003). (ICFA: International Committee for Future Accelerators).
29. Light Sources Website, <http://www.LightSources.org/>
30. Website of the ESRF: the European Synchrotron Radiation Facility, <http://www.esrf.eu/>
31. Website of SESAME: the Synchrotron-Light for Experimental Science and Applications in the Middle East, <http://www.sesame.org/jo/>
32. Sameen Ahmed Khan, "Need to Create Regional Synchrotron Radiation Facilities", *IRPS Bulletin*, **17** (2), 7-13 (July 2003). (IRPS: International Radiation Physics Society).
33. Sameen Ahmed Khan, "When will there be an Asian Accelerator Laboratory?", *ICFA Beam Dynamics Newsletter*, **28**, 49-54 (September 2002). (ICFA: International Committee for Future Accelerators).
34. Sameen Ahmed Khan, "Prospects for an Asian Accelerator Laboratory", *AAPPS Bulletin*, **12** (2), 21-27 (June 2002). (AAPPS: Association of Asia Pacific Physical Societies).
35. Sameen Ahmed Khan, "Call for Creation of Accelerator & Beam Physics Forums", *ICFA Beam Dynamics Newsletter*, **17**, 5-6 (August 1998). (ICFA: International Committee for Future Accelerators); *Europhysics News*, **30** (2), 49-50 (March/April 1999). <http://dx.doi.org/10.1007/s00770-999-0049-0>. (Publication of the *European Physical Society*).
36. Sameen Ahmed Khan, "2004 - the Year of Jubilees; Fifty Years of CERN; Forty Years of ICTP, Ten Years of ESRF User Operation", *IRPS Bulletin*, **19** (1), 4-8 (June 2005). (IRPS: International Radiation Physics Society); *ICFA Beam Dynamics Newsletter*, **37**, 12-18 (August 2005). (ICFA: International Committee for Future Accelerators).

3 Theme Section: Microbunching Instability

3.1 Overview and Issues of Experimental Observation of Microbunching Instabilities

Alex H. Lumpkin, Fermilab, Batavia, IL 60510, USA
Mail to: lumpkin@fnal.gov

3.1.1 Introduction

The generation of the ultra-bright beams required by modern accelerators and drivers of free-electron lasers (FELs) has generally relied on chicane-based bunch compressions that often result in the microbunching instability [1,2]. Following compression, spectral enhancements extend even into the visible wavelengths through the longitudinal space charge (LSC) impedances. Optical transition radiation (OTR) screens have been extensively used for transverse electron beam size measurements for the bright beams, but the presence of such longitudinal microstructures (microbunching) in the electron beam or the leading edge spikes can result in strong, localized coherent enhancements (COTR) that mask the actual beam profile. Generally, we have observed effects in rf photocathode (PC) injected linacs with chicane compressions since an R_{56} term is needed. In the past COTR had been only reported in S-band and L-band photoinjected based linacs with single or double bunch compression. Drive laser modulations and charge shot noise have been suspected of contributing to the cause. We now have evidence for the effects in both rf PC-gun injected linacs and thermionic-cathode (TC)-gun injected linacs (the latter do not involve a drive laser). Since the first observations, significant efforts have been made to characterize, model, and mitigate COTR effects on beam diagnostics [3-6]. An update on the state-of-the-art for diagnosing these effects will be given as illustrated by examples at the Linac Coherent Light Source (LCLS), Spring-8 Compact SASE Source (SCSS), Spring-8 Angstrom Compact Free Electron LAser (SACLA), Advanced Photon Source (APS), and the Next Linear Collider Test Accelerator (NLCTA). These observations continue to be of interest to the accelerator community.

3.1.2 Instability Effects

3.1.2.1 Context

It should be kept in mind that the energy modulation amplitude is even stronger in the several-micron-period regime where it impacts the effective energy spread and can reduce FEL gain. As reference the original description by Saldin, Schneidmiller, and Yurkov [1] provides an analysis of the charge density noise being amplified via LSC impedances with the gain as a function of wavelength as shown in Fig. 1. In this case curve 1 includes energy spread as compared to curve 2 which is for a cold beam. Experimentally, one images the 0.4- to 0.7- μm regime of COTR with our standard CCD cameras in the various linac facilities. Another gain calculation has been given by Huang et al. [2] with maximum gain calculated at about 10 μm under an initial 150- μm period modulation with 8% amplitude as also shown in Fig. 1.

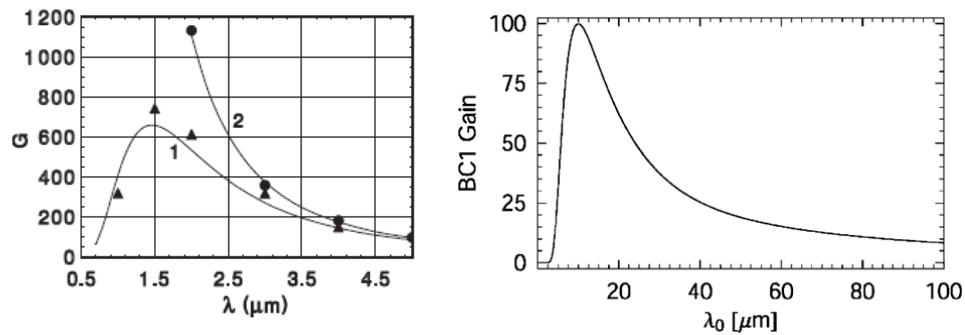


Figure 1: Calculated gain (G) for the microbunching instability versus wavelength from reference [1] (left) and reference [2] (right).

3.1.2.2 Diagnostics Options

Some of the diagnostics for assessing the μBI via COTR and other techniques include:

- 1) Bunch length monitors for tuning and verifying the compression. These might be based on coherent radiation sources based on transition radiation (CTR), synchrotron radiation (CSR), edge radiation (CER), diffraction radiation (CDR), etc. in the frequency domain or on incoherent sources in the temporal domain with an ultrafast streak camera or deflecting mode cavity plus an imaging screen.
- 2) OTR beam profile monitor screens are used for detecting the presence of COTR and its spatial distribution, intensity fluctuations, and intensity enhancements. The latter can be factors of 100 to 10,000 which make the profiles no longer representative of the true charge distribution and obviate the technique for profiling.
- 3) Optical spectrometers have been used for characterizing the NIR COTR vs the bluish OTR. This information provides a concept for mitigation of the COTR effects in the diagnostics with spectral filtering.
- 4) NIR and FIR spectrometers for evaluation of the spectral content in the 1-30 μm regime. These experiments have predominately been done at FLASH [7,8].
- 5) Deflecting mode cavities are needed with very high resolution (fs) to see directly the longitudinal structure even for FIR modulations. This is one diagnostics issue [6].
- 6) Electron energy spectrometers need high resolution to resolve the modulation [6].
- 7) X-ray spectrometer with high resolution. There are direct spectral effects in the FEL spectra driven by such beams with modulations which can be detected as discussed below [9].

These techniques have been applied on PC rf gun beams initially, but we have been able to apply them now to the TC gun beams as also will be described in a later section.

The instability effects were graphically demonstrated in the high energy spectra at LCLS as presented at FEL 10 by J. Welch [9]. The modulation in energy attributed to such microbunching is seen with the laser heater off in Fig. 2a, while it is suppressed with the laser heater on in Fig. 2b. Concomitantly, the observed x-ray spectra for the two cases showed the dramatic simplification of the spectrum with laser heater “on” in Fig. 3.

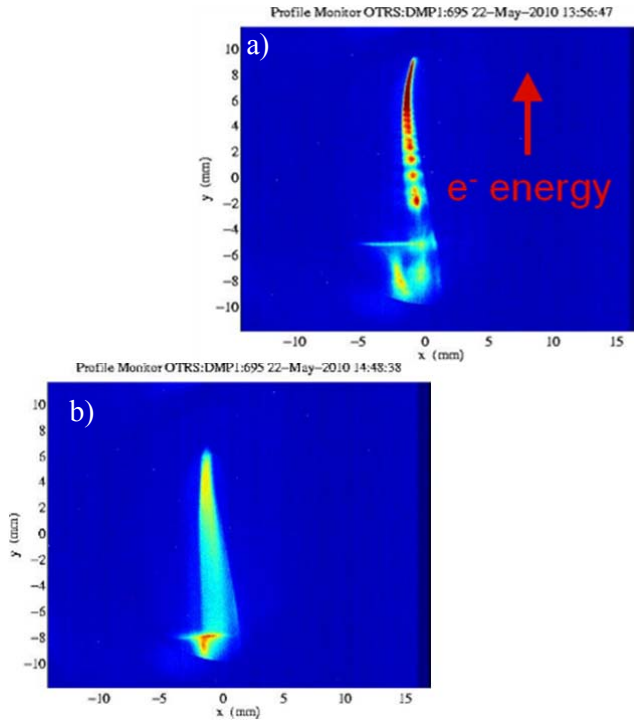


Figure 2: Examples of the LCLS electron beam high energy spectrum a) without and b) with the laser heater active [9].

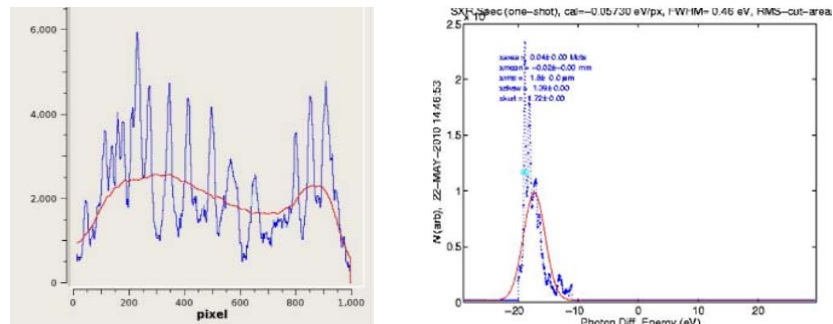


Figure 3: Corresponding x-ray spectra at LCLS for Fig.2 without (left) and with (right) the laser heater active [9].

3.1.3 Thermionic Cathode Gun Beams

One of the major developments in the past year in this μ BI subfield involves the observations of the COTR effects attributed to the microbunching instability in TC gun beams, in both DC and rf guns. Example results are provided in this section.

3.1.3.1 SCSS Results

The SCSS linac is based on a DC TC gun with deflector, subharmonic bunchers, a S-band accelerator section, a chicane bunch compressor, a C-band accelerator and another chicane for filtering the dark current beam as shown in Fig. 4 [10]. Using the

second chicane as a bunch compressor was suggested in discussions at the μ BI-4 workshop and following the FEL12 conference as well as looking for OTR enhancements at the station after this chicane. The experiments were initiated in October 2012 and were immediately successful.

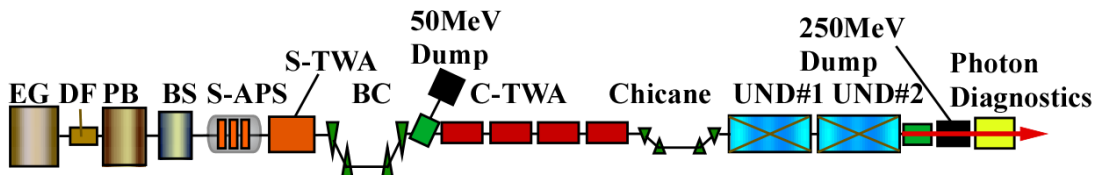


Figure 4: Schematic of the injector for the SCSS facility showing TC DC gun, accelerators, FEL, and beamlines. (courtesy of K. Togawa.)

An example image is shown in Fig. 5 with about 250 pC micropulse charge, and the plot of OTR intensity in such images versus C-band phase setting is shown in Fig. 6. The intensity doubles at the -10 degrees off-crest phase point, and the fluctuations of the intensity dramatically increase compared to those at -5 and -15 degrees. This increase is attributed to a coherent process starting from noise in the beam due to the LSC microbunching instability, and the second compression shifted the effects into the visible light regime where they were sensed by the CCD camera. In the previous tests they had observed the OTR *before* this second chicane and with the C-band accelerator run on crest so no COCTR effects were observed.

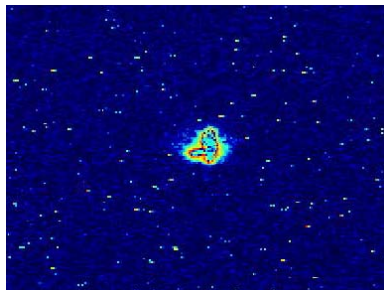


Figure 5: Image of the OTR and COCTR generated at the beam profile station after the second bunch compressor at SCSS [11]. The x and y axes cover 4 x 3 mm.

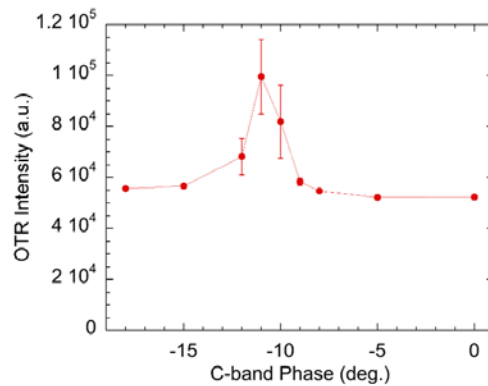


Figure 6: Plot of the C-band phase dependence of the OTR from the station after the second chicane at SCSS [11].

3.1.3.2 *SACLA Results*

The SACLA accelerator injector shown in Fig. 7 is based on the SCSS design with a few modifications such as the C-band correcting cavity. It also uses a DC TC gun with a deflector to select a part of the beam that is then subharmonically bunched. There are then three chicane-based compression stages with further acceleration to 1.4 GeV. After the third chicane bunch compression, they encountered significant COTR enhancements that saturated their CCD cameras [12]. To mitigate this effect they used spatial filtering with a scintillator crystal to obtain beam images. However, in the last year the staff revisited the stations to quantify the effects per suggestions from the Microbunching Instability Workshop 2012 attendees.

SACLA staff now report that the enhancement, or gain, is about 6000 over OTR [11], and they also showed the characteristic gradient-operator-related doughnut shape in the near field beam image in Fig. 8 as described by Loos et al. previously in the LCLS COTR images [4]. Additionally, they reported the enhanced red wavelength regime with intensity modulated spectrum in Fig. 9 as identified in the earlier APS/ANL PC rf gun based linac studies [13].

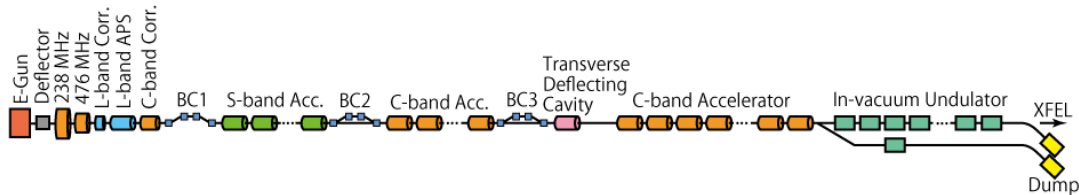


Figure 7: Schematic of the SACLA beamline with DC gun, bunchers, and accelerators with three chicanes for bunch compression. (courtesy of K. Togawa).

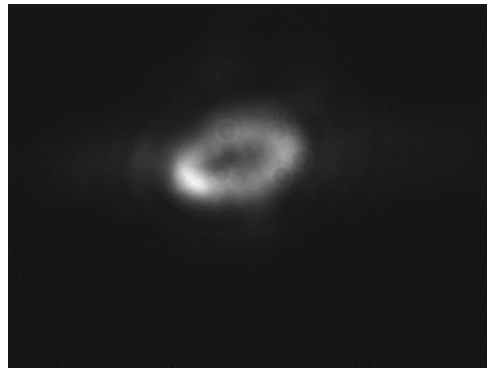


Figure 8: Beam image at 1.4 GeV after the third chicane at SACLA showing the COTR halo in the near field [11].

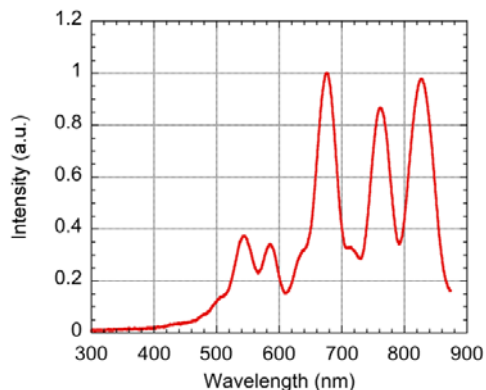


Figure 9: COTR spectrum obtained at 1.4 GeV after the third chicane at SACLA [11].

3.1.3.3 *APS/ANL Results*

The initial experiments at ANL were on the PC rf gun beam, and the first look at the TC rf gun beam was also done. At that time the signature of COTR spiking in the beam profiles was only seen in the PC rf gun OTR images [5]. However, because the TC rf gun beam involves a set of 25 micropulses at the S-band frequency, the statistical fluctuations of COTR might be averaged out in the CCD camera integration. More recent tests show the increase in the integrated profiles when the compression in the chicane occurs following implementation of energy chirp in the beam entering the chicane. In these cases we operated with higher current in the gun than previously. Adjusting the compression was done by evaluating the autocorrelations of FIR CTR at stations located in the linac before and after the chicane as shown in Fig. 10. The alpha magnet did provide an initial compression of about ten prior to the chicane's factor of two compression measured. As shown in Fig. 11, two different horizontal profiles from 10 OTR-image sums were taken without (black and green circles) and with chicane compression (blue and red circles). The intensity of the profile peaks increased by 4-8 when operating at the rf phase that peaked the FIR CTR signal in the Golay cell after the chicane [7]. The profile data shown at the workshop have been replotted in this figure to facilitate the direct comparison of the intensities. The charge transport at the end of the linac was tracked at $2 \text{ nC} \pm 10\%$ during the acquisition of these sets of images so charge-transport variation cannot explain the effects.

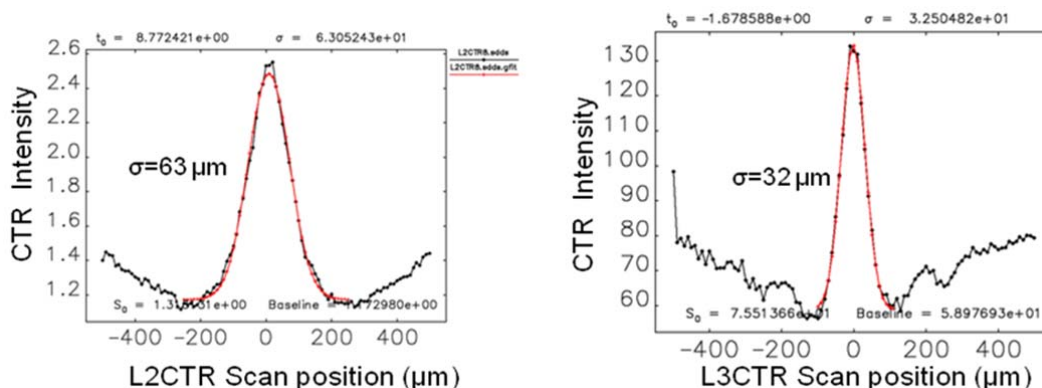


Figure 10: Autocorrelation results of CTR taken at the L2CTR and L3CTR locations which are before and after the chicane, respectively. A compression factor of two was observed.

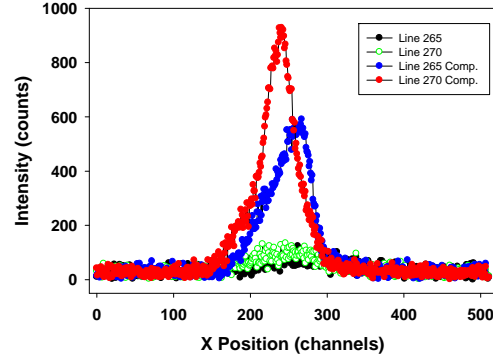


Figure 11: Profiles at lines 265 and 270 through the OTR sum images from TC rf gun beam uncompressed and compressed (blue and red symbols) with a final beam energy of 325 MeV at APS.

3.1.4 NLCTA X-band Results

Another interesting piece of the puzzle involves the observation of COTR with only 20-pC of charge in the micropulse following two chicane compressions at NLCTA as shown in Fig. 12. This facility has an S-band PC rf gun with two X-band accelerator sections that produce the 120-MeV beams [14]. Additionally, coherent optical undulator radiation has been reported [15].

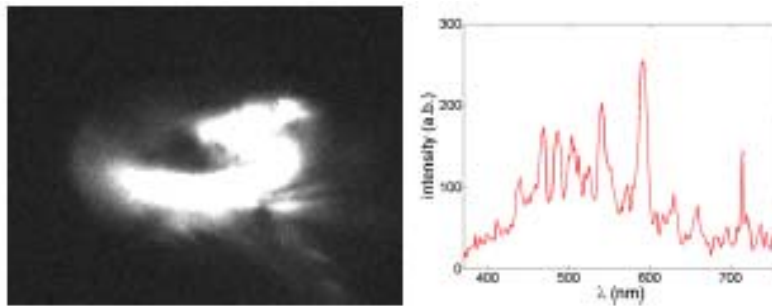


Figure 12: Typical COTR image (left) and wavelength spectrum following double compression at NLCTA [14].

3.1.5 Discussion

Table 1 is a summary of the scope of the observations in the various linacs including LCLS, DESY, and NLCTA and with the new TC gun beam results at SCSS, SACLA, and APS. The role of compression factors is indicated where second compressions in SCSS and APS were needed to display the COTR effect in TC gun beams. It is noted that the final enhancement of 6000 in SACLA after three chicanes in the TC DC gun beam approaches the very large enhancements in LCLS after two chicane compressions of the PC rf gun beam. Also, it is noted the transverse normalized emittances vary from 6-10 mm mrad in APS and NLCTA beams while LCLS, DESY, SCSS, and SACLA beams have emittances at about 1 mm mrad or below. All cases below exhibit some COTR effects.

Table 1: Summary of the COTR Effects Observed in Various Accelerator Facilities Including the Gun Type, Linac Energy, and Number of Chicanes or Compressions.

Facility	Gun	Linac, Energy	Chicanes	COTR Effects
LCLS	PC, S-band	S-band, 250, 14 GeV	two	very strong, $\times 10^4$
APS	PC, S-band rf TC, S-band	S-band, 150, 325 MeV	one alpha magnet, one	$\times 10$ -100 localized $\times 4$ integral
DESY	PC, L-band	SCRIF, L-band, 1.2 GeV, linearizer	two	$\times 10$ -100 localized
SACLA	TC, DC gated	S-band, C-band, 1.4 GeV	three	$> 6 \times 10^3$ after 3 compressions
SCSS	TC, DC gated	S-band, C-band, 250 MeV	two	$\times 2$, Observable after two compressions
NLCTA	PC, S-band	X-band, 120 MeV	two of four	$\times 20$ after two

3.1.6 Some Issues

There are some issues on the experimental side to consider in the future. These include:

- extending measurements in the NIR and FIR where the instability gain is stronger in more of the accelerator configurations;
- obtaining detailed longitudinal measurements with adequate resolution in time and energy;
- defining of beam parameters needed for simulations;
- evaluating longitudinal impedances involved in C-band and X-band accelerating structures compared to those of L-band and S-band structures;
- collecting more statistical data on intensity fluctuations and the Gamma function for the process;
- benchmarking of the relevant codes with the more extensive data sets we now have.

The question of whether the PC gun beams have more charge fluctuations than TC gun beams, and hence they are more prone to the larger μ BI effects needs consideration.

3.1.7 Summary

In summary, the microbunching instability as detected through the generation of COTR has become worldwide in interest. The observations of the microbunching instability attributed to longitudinal space charge impedances and CSR effects has become recognized as a more general phenomenon with cases reported in L-band, S-band, C-band, and X-band accelerators and with beams generated by both PC rf guns and TC rf and DC guns. There is an opportunity for using this broader empirical data base to elucidate the effect via further modeling efforts based on LSC impedances and shot noise. Modeling of the TC gun beams still seems to be needed since the slice

energy spread may not be as well understood at this time. Mitigations in the diagnostics have been reported in several labs [5,6,12], and suppression of the instability itself has been ongoing with laser heaters and dispersive elements. Further investigations are encouraged as it has now been demonstrated that the instability is not only observed in PC rf gun beams initiated with drive lasers as was implied a few workshops ago.

3.1.8 Acknowledgments

The author acknowledges: discussions with D. Dowell, Z. Huang, and H. Loos of SLAC; W. Fawley (LBNL); D. Rule (NSWC); and R. Fiorito (UMD); support from K.-J. Kim, R. Gerig, and H. Weerts of the Argonne Accelerator Institute; the collaborations on ANL linac tests of N. Sereno, J. Dooling, S. Pasky, Y. Li, and Y. Sun of ANL; the support of M. Wendt and N. Eddy of Fermilab; and the figures provided by K. Togawa (Riken, SPring-8) and S. Weathersby (NLCTA/SLAC).

3.1.9 References

1. E.L. Saldin, E.A. Schneidmiller, and M.V. Yurkov, Nucl. Instr. and Methods, A490, 1 (2002).
2. Z. Huang, M. Borland, P. Emma, J. Wu, C. Limborg, G. Stupakov, and J. Welch, Phys. Rev. ST-AB 7, 077701 (2004).
3. D. Dowell et al., Proc. of FEL07, WEAAU01, JACoW.org.
4. H. Loos et al., Proc. of FEL08, THBAU01, JACoW.org.
5. A.H. Lumpkin et al., Phys. Rev. ST-AB 12, 080702 (2009).
6. C. Behrens et al., Phys. Rev. ST-AB 15, 062801 (2012).
7. B. Schmidt et al., Proc. of FEL'08, Gyeongju, Korea, TUPPH06, (2008), JACoW.org.
8. S. Wesch, C. Behrens, B. Schmidt, and P. Schmuser, Proc. of FEL09, Liverpool UK. WEPC50, (2009), JACoW.org.
9. J. J. Welch, "X-ray Diagnostics Commissioning at LCLS", Talk presented at FEL10, FROA11 (2010), JACoW.org.
10. K. Togawa et al., Proc. of the Fourth Microbunching Instability Workshop, Univ. of Maryland, April 11-13 2012.
11. K. Togawa et al., Proc. of the Fifth Microbunching Instability Workshop, Pohang, Korea, May 8-10, 2013.
12. H. Tanaka, Proc. of IPAC11, MOYCA01, 21, JACoW.org.
13. A. H. Lumpkin et al., Proc. of FEL09, TUPC47, 352, JACoW.org.
14. M. Dunning et al., Proc. of PAC11, MOP014, 130, JACoW. Org.
15. S. Weathersby et al., Proc. of PAC11, THP170, 2426, JACoW.org.

3.2 Microbunching Instability Suppression via Electron Magnetic Phase Mixing

S. Di Mitri¹, S. Spampinati^{2,3}

¹Elettra Sincrotrone Trieste, S.S. 14 km 163,5 in AREA Science Park, 34149
Basovizza, Trieste, Italy

²University of Liverpool, Department of Physics, Liverpool, UK

³Cockcroft Institute, Sci-Tech Daresbury, Warrington, UK

Mail to: simone.dimitri@elettra.eu

3.2.1 Introduction

Control of the microbunching instability is a fundamental requirement in modern high brightness electron linacs, in order to prevent misleading responses of beam optical diagnostics and contamination in the generation of coherent radiation, such as free electron lasers. We report the first experimental demonstration of control and suppression of microbunching instability by means of particles' longitudinal phase mixing in a magnetic chicane. In the presence of phase mixing, the intensity of the beam-emitted optical transition radiation, which is used as an indicator of the instability gain at optical wavelengths, is reduced by one order of magnitude and brought to the same level provided, alternatively, by beam heating. The experimental results are in agreement with particle tracking and analytical evaluations of the instability gain. This article is extended to a discussion of applications of magnetic phase mixing to the generation of quasi-cold high-brightness ultra-relativistic electron beams. This work has been submitted for publication to Physical Review Letters (2014).

3.2.2 Suppression of Microbunching via Energy Landau Damping

The understanding and control of the electron beam energy and density modulations is vital for high brightness linac-driven light sources such as free electron lasers (FELs). In the framework of the so-called microbunching instability [1–6], some undesired bunching – that is the Fourier transform of the longitudinal charge distribution, which is a measure of the density modulation amplitude – starts from electron beam shot noise and/or macroscopic density non-uniformities, and is further amplified along the accelerator by the interplay of the longitudinal space charge (LSC) force, non-isochronous energy dispersive insertions and the emission of coherent synchrotron radiation (CSR). The strength of the microbunching instability is usually quantified by its spectral gain, which is the ratio of the final to the initial bunching [1, 2]. When only LSC is considered, the gain can be evaluated by [1]:

$$G(k) = Ck |R_{56}| \frac{I}{\gamma I_A} \frac{|Z(k)|}{Z_0} \exp\left(-\frac{1}{2} C^2 k^2 R_{56}^2 \sigma_{\delta,0}^2\right), \quad (1)$$

where C is the electron bunch length compression factor provided by one magnetic insertion with momentum compaction R_{56} , k is the wave number of the energy modulation induced upstream of the compressor by the LSC impedance $Z(k)$, γ is the beam's relativistic Lorentz factor at the compressor, $\sigma_{\delta,0}$ is the beam fractional

incoherent energy spread just before compression, $Z_0 = 377 \Omega$ and $IA = 17045 \text{ A}$. A gain as large as 10^2 to 10^4 is common in linac-driven FELs and peaks at final wavelengths $\leq 1 \mu\text{m}$ [7, 8]. Large bunching is accompanied by large energy modulation with analogous spectral content. The final energy modulation may act on the FEL process as large local (slice) energy spread that, depending also on the spatial scale of the cooperative FEL process, may reduce the FEL output power and/or enlarge the FEL spectral bandwidth [9–11]. A “laser heater” (LH) system was first proposed in [12] to counteract those disrupting effects. In a LH, the electrons interact with an external infrared laser pulse in a short undulator, at beam energies typically around 100 MeV. As a consequence of the interaction, the electron beam incoherent energy spread is increased and the microbunching gain suppressed, as suggested by Eq.1. A LH is routinely adopted at LCLS [13] and FERMI [14] FEL facilities where, in standard operating conditions, $\sim 20 \text{ keV}$ and $\sim 7 \text{ keV}$, respectively, are added to the 1–3 keV beam incoherent energy spread (all rms values). When the LH is turned off, a high instability gain leads to large coherent optical transition radiation (COTR) signal at screen targets intercepting the time-compressed beam for diagnostic purposes. COTR emission limits the utility of beam profile imaging systems [15, 16]. This can be recovered by the LH action which is able to reduce the OTR intensity to the incoherent emission level [10]. The OTR intensity is thus an indicator of the strength of the instability at optical wavelengths. In our experiment, we made use of this relationship, finding agreement of the OTR intensity behavior with numerical and analytical predictions for the instability gain.

3.2.3 Experiment Setup

Initially proposed in [17, 18] as an alternative to the beam heating process described above and to other recently proposed schemes in [19, 20], phase mixing has the advantage of relying on a relatively simple and robust system, *i.e.*, a four dipoles, non-isochronous magnetic chicane (hereafter named “mixing chicane”) installed at intermediate linac energies. Although not strictly necessary the mixing chicane is preferred to be achromatic, like in the case of a symmetric magnetic bunch length compressor. The idea consists in smoothing the electron bunch current and energy distribution by forcing the electrons to “rotate” in the longitudinal phase space (z, δ) , where z is the particle’s longitudinal coordinate along the bunch and δ is the particle’s fractional energy deviation. The rotation is actually a phase slip, primarily induced by the first order momentum compaction (R_{56}) of the mixing chicane that couples to the (z, δ) correlation established by the upstream instability at its characteristic (short) wavelength scale. This dynamics is illustrated in Figure 1 [18].

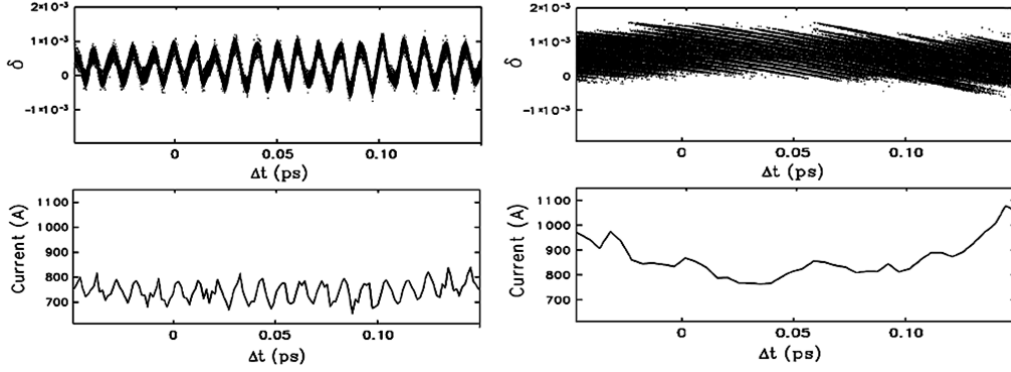


Figure 1. A 30 μm wavelength, 1% amplitude density modulation is superimposed to an electron beam at 100 MeV. The bunch is then compressed by a factor 10, transported to the entrance of a mixing chicane (left plots) and subjected to phase mixing with $|R_{56}|=30$ mm. Top row: electron beam longitudinal phase space. Bottom row: current profile. Elegant code [21] particle tracking results [18].

The experiment was carried out at the FERMI S-band linac, which is sketched in Figure 2. A 500 pC, 2.8 ps rms long electron bunch was photo-injected [22] into the linac and time-compressed by a factor 12 in a magnetic chicane (BC1) at 0.27 GeV. The second magnetic compressor (BC2) was used as the mixing chicane. The beam was then accelerated to the energy of 1.23 GeV. In general, phase mixing should not affect the bunch length σ_z . This implies that the correlated fractional energy spread σ_δ evaluated on the bunch length scale (linear energy chirp) has to be small enough to ensure $R_{56}\sigma_\delta \ll \sigma_z$. Bunch length compression in the mixing chicane has also to be avoided because, defeating its scope, it would enhance the total instability gain at short wavelengths, as it happens in a two-stage compression scheme with respect to the one-stage [8, 18, 23]. If the electron bunch were time-compressed in the early stage(s) of the accelerator, a residual energy chirp, including nonlinear terms, would be present at the mixing chicane, thus potentially inducing bunch length variation. The total chirp would be a resultant of: the linear energy chirp required for previous magnetic compression; the energy spread induced by the RF curvature of the accelerating electric field; the action of linac longitudinal wakefield; adiabatic damping due to acceleration. The latter two contributions tend to reduce the former. The linac wakefield and the RF curvature add quadratic and cubic energy chirp to the beam longitudinal phase space [24]. In order to remove the linear chirp at the BC2 location, the RF phase of two upstream S-band accelerating structures, L3 in Figure 2, was scanned and set to 140 deg S-band, which is 50 deg off the phase of maximum energy gain. That value gave the minimum horizontal beam size in the middle of BC2, measured with a beam profile imaging system. Beam optics matching upstream of BC2 ensured that the horizontal beam size in the middle of BC2 was dominated by the chromatic particle motion, with estimated contributions to the total beam size $\sqrt{\beta_x \varepsilon_x} = 89 \mu\text{m}$ and $\eta_x \sigma_\delta = 319 \mu\text{m}$, $\beta_x = 5$ m being the design betatron function, $\varepsilon_x = 1.6$ nm rad the beam geometric emittance and $\eta_x = 255$ mm the energy dispersion function, all quantities intended in the bending plane and in the middle of BC2. Accordingly, the residual correlated energy spread, now dominated by a quadratic energy chirp, was lowered to 0.1% rms level. Figure 3 shows the agreement between the experimental behavior of the energy-dominated horizontal beam size in

BC2 and the particle tracking result, which included geometric wakefields in the accelerating structures. The beam energy at BC2 turned out to be 0.62 GeV. With this linac set up and 90 mrad bending angle in BC2, the Elegant code [21] predicts $\sim 10\%$ bunch length variation at the exit of the mixing chicane relative to ~ 1 ps full width bunch duration at its entrance.

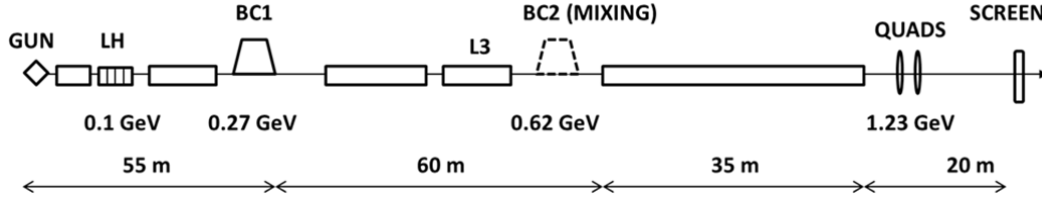


Figure 2. Sketch of the FERMI linac (not to scale).

3.2.4 Experimental Results vs. Analytical Predictions

At the linac's end, an OTR-based beam profile imaging system was used to measure the beam transverse sizes and the beam spot's OTR intensity as the BC2 bending angle was varied in the range 0–90 mrad; $|R_{56}|$ was varying in the range 0–46 mm. During the scan, the beam sizes were kept almost constant at the observation point by tuning upstream quadrupole magnets. The geometric mean of the horizontal and vertical rms beam size had average value of 250 μm over the BC2 angle range, with standard deviation of 15 μm and peak-to-peak variation of 30 μm . Beam optics mismatch induced by edge focusing of the mixing chicane's dipole magnets was recovered with a dedicated matching insertion at the linac's end. The effect of CSR emission in BC2 on the beam transverse emittance was counteracted with a manipulation of the beam optics across the chicane [25]. The projected emittance was not varying by more than 10% at the linac's end over the entire BC2 angles' range. The OTR intensity, integrated over the region occupied by the beam spot and averaged over many shots, was recorded vs. the $|R_{56}|$ in BC2, with and without the LH action. When turned on, the LH provided approximately 50 keV rms incoherent energy spread to the uncompressed beam. Such a strong beam heating was used on purpose since, as discussed below, the analytical model ensures total suppression of microbunching at optical wavelengths and shorter. When the LH was off the OTR intensity increases sharply even for small values of $|R_{56}|$; it then drops for values equal or larger than 9.1 mm. At $|R_{56}| = 27.8$ mm, the OTR intensity was the same as in the presence of beam heating. A similar behavior was also observed, in a different preliminary experimental session, with a beam time-compressed in BC1 by a factor 8, whose emitted OTR intensity explored ~ 3 orders of magnitude over the same $|R_{56}|$ range. The OTR data are consistent with those collected at a 5 m downstream OTR screen. As a revival of microbunching may be expected downstream the linac, the same tuning of the mixing chicane should be repeated but looking to the OTR intensity at the location of interest. In other words, the optimum strength of phase mixing shall be chosen on the basis of the instability gain for the entire beam line under consideration.

For the case of LH off, we computed the microbunching instability gain at the end of the FERMI linac, at the optical wavelength of 550 nm vs. $|R_{56}|$ in BC2, starting from shot noise and on the basis of the one-dimensional linear theory developed in [1] (see

Eq.1) and [2], for a beam with 1 μm transverse normalized emittance and initial 2 keV rms incoherent energy spread. The behavior of the instability gain is in agreement with that of the OTR intensity previously depicted. We remark that the same gain's behavior holds in the entire optical range, *e.g.*, at the wavelength of 220 nm and 800 nm, shown in the same plot. As far as the *peak* gain is concerned, namely its maximum value evaluated over the entire spectrum, the analytical model predicts an increase of up to two orders of magnitude as $|R_{56}|$ in BC2 moves from 0 to 46 mm. However, as the momentum compaction is increased and phase mixing becomes more effective, the wavelength of maximum gain red-shifts from 1.1 μm to 7.1 μm . Consequently, the amount of phase mixing can be tuned through the mixing chicane's bending angle to bring the instability gain far enough from the spectral range of interest. With LH on the optical gain is strongly suppressed for any $|R_{56}|$ in BC2 in the range 0–46 mm and the peak gain is shifted to final wavelengths longer than tens of micron. The experimental behavior of the OTR intensity confirms the analytical prediction of the gain. This confirmation together with our finding that the instability gain can be controlled with BC2, are the principle results of our study.

3.2.5 Application to FELs

In order to investigate the expected performance of magnetic phase mixing in terms of slice energy spread, we consider three possible locations for the mixing chicane: low, intermediate and high linac energy. Since the process takes advantage of the instability itself to minimize its impact on the beam *final* longitudinal phase space, the adoption of a mixing chicane at the beginning of the linac, where the bunching has not grown enough yet, inhibits the electrons' phase slip and is therefore ineffective. Phase mixing at late linac stage smoothes the longitudinal phase space, but the final slice energy spread remains of the same order as the (possibly large) energy modulation amplitude accumulated up to that point (see Figure 1). These considerations point to the conclusion that phase mixing should take place at an intermediate linac longitudinal coordinate – let us call it \bar{s} – to be most effective. Roughly speaking, for an FEL to be efficient we impose that the energy modulation amplitude accumulated up to \bar{s} and normalized to the *final* linac energy, be smaller than the so-called FEL parameter, ρ [26]. We then require that the energy modulation amplitude from \bar{s} to the undulator be smaller than that accumulated upstream of the mixing chicane: $\Delta\gamma(\bar{s} \rightarrow s_f) < \Delta\gamma(s_i \rightarrow \bar{s}) < \gamma(s_f)\rho$, with γ the relativistic Lorentz factor. If such an \bar{s} exists, depending on several electron beam and machine parameters, an increase of the slice energy spread will be allowed along the beam line, but not to the extent that it overwhelms the FEL normalized energy bandwidth. Based on this plausible model, the presence of multiple mixing chicanes appears a viable solution in long linacs. We remark that the criterion we are proposing for the production of quasi-cold electron beams can be verified through the same analytical model [1, 2, 18] used to produce Figure 5. The model is able to estimate, *e.g.*, energy and density modulation amplitude at any point of the accelerator, thus can be used for finalizing the machine design. For the FERMI moderate one-stage compression, we found that there is no further growth of the instability after phase mixing. The final slice energy spread is then expected to be approximately 100 keV rms (the maximum energy modulation amplitude accumulated up to BC2), which is close to that measured at FERMI during standard operation of the LH [27].

It might be worth to mention that an *enhancement* of bunching through a series of magnetic chicanes has been pursued for the generation of x-ray coherent radiation [28–35]. We recognize a common denominator to all these schemes in that, similarly to phase mixing, they take advantage of the correlation established in the beam’s longitudinal phase space by either an external laser interacting with the electron beam in the linac [28] and in the undulator [29, 30], or by FEL emission [31, 32], or LSC [33–35]. As a by-product of our experimental work we have shown that simultaneous control of the electron bunch length, energy chirp and bunching factor can be achieved in a reproducible way just as required, *e.g.*, by the two-chicane “compressed harmonic” scheme proposed in [32] to generate coherent x-ray radiation. Preserving coherent microbunching through a two-stage compression system as proposed in [32], however, requires additional optics optimization which is outside the scope of our work. In conclusion, we have demonstrated that magnetic phase mixing is a viable alternative to the LH in controlling microbunching instability, with the advantage of a more robust system and of a less intrusive impact on the accelerator layout. Tunability of the wavelength at which the microbunching instability gain is suppressed is provided by the chicane’s bending angle, thus ensuring a simple and flexible operation for different machine set-ups. The presence of the mixing chicane imposes a control of the linac RF phases in order to remove the linear energy chirp at its entrance. This control aims at minimizing the correlated energy spread on the scale of the bunch length, and is therefore beneficial, *e.g.*, to FELs. At the same time, it may imply additional RF power, both to cancel the chirp at the mixing chicane and to counterbalance the longitudinal wake potential in the downstream RF structures, while leaving the final beam energy unchanged. In general, the RF budget should also allow one to adjust the energy chirp while the bunch current is changed upstream of the mixing chicane, as this implies a different strength of the linac wakefields. Depending on the linac setting, the additional RF power required for phase mixing may make it a less attractive alternative to a LH. We finally remark that a careful control of higher order energy chirp, as *e.g.* reviewed in [24], would help to avoid the production of current spikes at the bunch edges as the beam passes through the mixing chicane and, at the same time, minimize the bunch length variation.

3.2.6 Acknowledgments

The authors are indebted to L. Badano who provided the calibration curves of the beam profile imaging system; these were used to compute the OTR integrated intensity over all ranges of attenuation. The authors also thank: H.-S. Kang for his revision of the script used to compute the instability gain; M. Veronese, for instructive discussions about COTR; E. Allaria, who inspired the software tool used for data collection; M. Venturini for instructive discussions on topics covered by this article, and M. Cornacchia, J. Wu, G. Penco and R. Bosch, for careful reading and suggestions. We thank the FERMI commissioning team for the time available to carry out the reported measurements.

3.2.7 References

1. E.L. Saldin, E.A. Schneidmiller and M.V. Yurkov, Nucl. Instrum. Methods Phys. Research, Sect. A 490, **1** (2002).

2. Z. Huang and K.-J. Kim, Phys. Rev. Special Topics – Accel. Beams **5**, 074401 (2002).
3. M. Borland et al., Nucl. Instrum. Methods Phys. Res., Sect. A **483**, 268 (2002).
4. T. Shaftan and Z. Huang, Phys. Rev. Special Topics Accel. Beams **7**, 080702 (2004).
5. R. Akre et al., Phys. Rev. Special Topics Accel. Beams **11**, 030703 (2008).
6. A. H. Lumpkin, T. J. Dejus and N. S. Sereno, Phys. Rev. Special Topics Accel. Beams **12**, 040704 (2009).
7. Z. Huang, M. Borland, P. Emma, J. Wu, C. Limborg, G. Stupakov and J. Welch, Phys. Rev. Special Topics – Accel. Beams **7**, 074401 (2004).
8. M. Venturini, Phys. Rev. Special Topics – Accel. Beams **10**, 104401 (2007).
9. Z. Huang *et al.*, Phys. Rev. Special Topics – Accel. Beams **13**, 020703 (2010).
10. S. Spampinati *et al.*, in Proc. of the 34th Intern. Free Electron Laser Conf., MOPD58, Nara, Japan (2012).
11. E. Allaria *et al.*, in Proc. of the 34th Intern. Free Electr. Laser Conf., TUOB02, Nara, Japan (2012).
12. E. L. Saldin, E. A. Schneidmiller and M. V. Yurkov, Nucl. Instrum. Methods Phys. Res., Sect. A **528**, 355 (2004).
13. P. Emma *et al.*, Nature Photon. **4**, 641 (2010).
14. E. Allaria *et al.*, Nature Photon. **6**, 699 (2012).
15. H. Loos et al., in Proc. of the 30th Free Electron laser Conf., THBCU01, Gyeongju, Korea (2008).
16. C. Behrens et al., Phys. Rev. Special Topics – Accel. Beams **15**, 062801 (2012).
17. M. Cornacchia, S. Di Mitri, S. Spampinati, S. V. Milton, in Proc. of the 11th European Part. Accel. Conf., TUPP033, Genoa, Italy (2008).
18. S. Di Mitri, M. Cornacchia, S. Spampinati and S. Milton, Phys. Rev. Special Topics – Accel. Beams **13**, 010702 (2010).
19. C. Behrens, Z. Huang, and D. Xiang, Phys. Rev. Special Topics – Accel. Beams **15**, 022802 (2012).
20. J. Qiang, C. E. Mitchell and M. Venturini, Phys. Rev. Letters **111**, 054801 (2013).
21. M. Borland, APS Tech Note LS-207 (2000).
22. G. Penco *et al.*, JINST **8**, P05015 (2013).
23. S. Di Mitri, M. Cornacchia, P. Craievich, G. Penco, S. Spampinati, M. Venturini, and A.A. Zholents, in Proc. of the 32th Free Electron Laser Conf., THPB03, Malmö, Sweden (2010).
24. S. Di Mitri and M. Cornacchia, “Electron Beam Brightness in Linac Drivers for Free-Electron-Lasers” in press in Physics Reports (2014).
25. S. Di Mitri, E.M. Allaria, P. Craievich, W. Fawley, L. Giannessi, A. Lutman, G. Penco, S. Spampinati, and M. Trovo’, Phys. Rev. Special Topics – Accel. Beams **15**, 020701 (2012).
26. R. Bonifacio, C. Pellegrini and L. Narducci, Opt. Commun. **50**, 373-378 (1984).
27. G. Penco, E. Allaria, D. Castronovo, M. B. Danailov, A. Demidovich, G. De Ninno, S. Di Mitri, W.M. Fawley, E. Ferrari, L. Giannessi, C. Spezzani and M. Trovo’, in Proc. of the 35th Intern. Free Electron Laser Conf., TUOCNO01, New York, NY 10036, USA (2013), submitted to Phys Rev. Letters (2013).
28. D. Ratner, A. Chao and Z. Huang, Phys. Rev. Special Topics – Accel. Beams, **14**, 020701 (2011).
29. G. Stupakov, Phys. Rev. Lett. **102**, 074801 (2009).
30. D. Xiang et al., Phys. Rev. Lett. **105**, 114801 (2010).
31. E.L. Saldin, E.A. Schneidmiller and M.V. Yurkov, Phys. Rev. Special Topics – Accel. Beams, **13**, 030701 (2010).
32. D. Ratner et al., Phys. Rev. Special Topics – Accel. Beams, **14**, 060701 (2011).
33. E.A. Schneidmiller and M.V. Yurkov, Phys. Rev. Special Topics – Accel. Beams, **13**, 110701 (2010).

34. M. Dohlus, E.A. Schneidmiller and M.V. Yurkov, Phys. Rev. Special Topics – Accel. Beams, **14**, 090702 (2011).
 35. A. Marinelli et al., Phys. Rev. Letters, **110**, 264802 (2013).

3.3 Coherent Synchrotron Radiation in Whispering Gallery Modes: Theory and Evidence

Robert Warnock
 SLAC National Accelerator Laboratory
 in collaboration with
 Jack Bergstrom, Canadian Light Source
 Marit Klein, Synchrotron SOLEIL
 Mail to: warnock@slac.stanford.edu

3.3.1 Introduction

Whispering galleries in certain public buildings have been a curiosity for centuries. In a building with a cylindrical wall, one person whispering in a tangential direction near the wall can be heard clearly by another person at a remote location near the wall. Lord Rayleigh [1] was inspired to study this phenomenon at St. Paul's Cathedral in London (Fig.1), where there is a famous whispering gallery running near the base of the huge dome (Fig.2). George Biddell Airy, Astronomer Royal at the time of Rayleigh's study, thought the effect had to do with a concentration of an echo in which the symmetry of the dome played a role. Rayleigh raised doubts about this view since it would require speaker and auditor to be at opposite sides of the gallery, contrary to observations. As it turned out later, Airy functions play a role in a correct description of the effect, since they provide approximations to high order Bessel functions.

One need not be Christopher Wren to design a whispering gallery. I observed the effect in a distinctly incomparable setting, namely a Starbucks Coffee House with a cylindrical front wall, on Central Avenue in Albuquerque, New Mexico. In spite of perturbations to the cylindrical geometry in the form of persons eating bagels, etc., I could hear every word of a conversation at the other side of the room, against a noisy background.

The high frequency components of a speaking voice, prominent in a whisper, are emitted within a narrow cone, say of opening angle θ . Then the minimum distance from an emitted ray to the center of the gallery of radius b is $b \cos \theta$, as shown in Fig.3. Thus Rayleigh expected the acoustical disturbance to be localized near the wall, and performed a charming experiment to verify this ray picture, as in Fig.4. He set up a sheet of zinc in cylindrical form (2 feet wide by 12 feet long), making an arc of 180 degrees, and employed a tangentially directed bird call as source and a sensitive flame as detector. The flame flared when the bird call sounded, but the flare could be stopped by imposing a narrow barrier, only 2 inches wide, near the wall. Barriers along the straight line between whistle and flame had no such effect. In Rayleigh's nicely turned expression, "Especially remarkable is the narrowness of the obstacle, held close to the concave surface, which is competent to intercept most of the effect."



Figure 1: St. Paul's Cathedral;
Christopher Wren, architect.



Figure 2: Whispering Gallery.

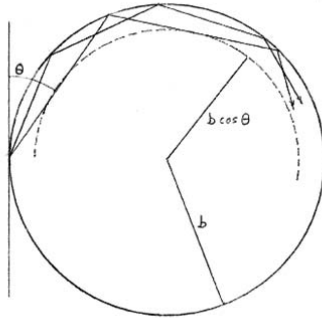


Figure 3: Rayleigh's ray picture.

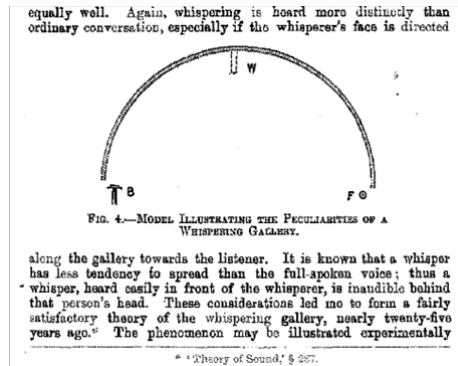


Figure 4: Rayleigh's lab experiment.

Rayleigh went on to develop a wave theory of the phenomenon, in two interesting papers from which we can still learn today [3]. Let ψ be the velocity potential of a sound field in a two-dimensional region specified in polar coordinates (r, θ) with $r \leq b$. It satisfies the wave equation

$$\Delta\psi - \frac{1}{v^2} \frac{\partial^2\psi}{\partial t^2} = 0. \quad (1)$$

An elementary solution is in terms of the Bessel function J_n ,

$$\Psi = J_n(kr) \cos(n\theta - kvt) \quad (2)$$

This is a wave traveling in the azimuthal direction with frequency $k\nu$ and wave number $n/R = 2\pi/\lambda$. The boundary condition is that the radial velocity $v_r = \partial\psi/\partial r$ be zero on the boundary $r = b$:

$$J'_n(kb) = 0 \rightarrow kb = j'_{ns}, s = 1, 2, \dots \quad (3)$$

where the j'_{ns} are the zeros of $J'_n(x)$ enumerated by the integer s . The j'_{ns} and the corresponding zeros j_{ns} of $J_n(x)$ are all greater than n , and are given by asymptotic series at large n ; see [4].

This is a resonance condition, satisfied only at discrete frequencies $\omega_* = k_* \nu$. The solution of the inhomogeneous wave equation with source blows up at those frequencies. One can also think of the resonance condition as a dispersion relation, which relates frequency to wave number at discrete frequencies.

Rayleigh showed that this set-up describes whispering gallery behavior, because the wave function with factor $J_n(k_* r)$ is concentrated at values of r near the boundary, the concentration being more pronounced at large n . The mathematics of this concentration, very relevant to the present work, was explored more thoroughly in his second paper.

3.3.2 The Electromagnetic Problem in the Vacuum Chamber of an Accelerator

Consider a perfectly conducting vacuum chamber of circular toroidal form with rectangular cross section, as illustrated in Fig. 5. After appropriate integral transforms, one can solve Maxwell's equations in the interior of the torus, with correct boundary conditions on the walls, using separation of variables in cylindrical coordinates [5]. We take the Laplace transform with respect to time, the variable conjugate to time being $-i\omega$. The complex frequency ω initially has positive imaginary part ν , so that convergence of the transform is guaranteed if the field is bounded. Since the field excited by a circulating beam does not decay at large time, the Fourier transform does not exist. Nevertheless, many papers incorrectly use the Fourier transform, Ref.[5] among them. We employ Fourier series in θ and z , the latter chosen so as to meet the boundary conditions on the upper and lower planar surfaces of the chamber. For E_z the Laplace-Fourier transform is

$$\begin{aligned} \hat{E}_z(r, n, p, \omega) &= \frac{1}{2\pi} \int_0^{2\pi} d\theta e^{-in\theta} \frac{1}{g} \int_{-g}^g dz \cos \alpha_p(z + g) \\ &\cdot \frac{1}{2\pi} \int_0^\infty dt e^{i\omega t} E_z(r, \theta, z, t), \end{aligned} \quad (4)$$

where $\alpha_p = \pi p/h$ with $h = 2g$ being the height of the chamber. All components of the fields can be expressed in terms of $\hat{E}_z(r, n, p, \omega)$, $\hat{H}_z(r, n, p, \omega)$ and their r -derivatives [5]. The wave equations for E_z and H_z imply that \hat{E}_z and \hat{H}_z satisfy Bessel equations with source terms, which can be solved in terms of Bessel functions by variation of parameters [5].

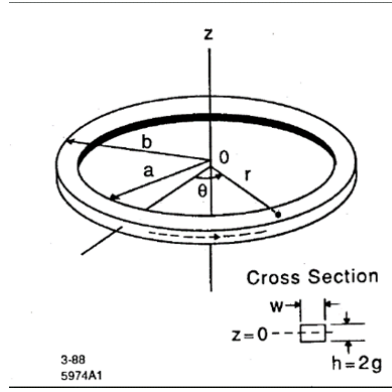


Figure 5: Toroidal chamber with rectangular cross section.

The charge-current source can be arbitrary, but to get the simplest possible expression we take a ribbon beam with rigid longitudinal form. Its charge density is

$$\rho(r, \theta, z, t) = q\lambda(\theta - \omega_0 t)H(z) \frac{\delta(r - R)}{R}, \quad (5)$$

$$\int \lambda(\theta) d\theta = \int H(z) dz = 1, \quad (6)$$

with $H(z)$ an arbitrary vertical profile. The Laplace-Fourier transform of this function is

$$\hat{\rho}_{np}(r, \omega) = \frac{iq\lambda_n H_p \delta(r - R)}{2\pi R(\omega - n\omega_0)}, \quad (7)$$

$$\lambda_n = \frac{1}{2\pi} \int_0^{2\pi} e^{-in\theta} \lambda(\theta) d\theta, \quad H_p = \frac{1}{g} \int_{-g}^g \sin \alpha_p(z + g) H(z) dz. \quad (8)$$

The corresponding current density is $(J_r, J_\theta, J_z) = (0, \beta cr\rho/R, 0)$. A general charge density,

$$\rho(r, \theta, z, t) = q\phi(\theta - \omega_0 t, r, z, t), \quad (9)$$

has Laplace-Fourier transform

$$\hat{\rho}_{np}(r, \omega) = \frac{q}{2\pi} \int_0^\infty e^{i(\omega - n\omega_0)t} \hat{\phi}_{np}(r, t) dt,$$

$$\hat{\phi}_{np}(r, t) = \frac{1}{2\pi} \int_0^{2\pi} e^{-in\theta} d\theta \frac{1}{g} \int_{-g}^g \sin \alpha_p(z + g) \phi(\theta, r, z, t) dz. \quad (10)$$

Notice that the t -independent part of $\hat{\phi}_{np}$ again gives a pole at $\omega = n\omega_0$. In allowing a general form of charge-current one must account for the continuity equation, which can be done by constructing charge and current densities from a distribution function in

phase space, evolving by correct dynamics.

If the beam is centered in the chamber, the fields at the position of the beam are hardly affected if the radius a of the inner wall is pushed to zero, thus obtaining a “pill box” chamber rather than a torus. This is not obvious, but comes out of a detailed analysis. Solving for the longitudinal electric field $E_\theta(r, \theta, z, t)$ in the pill box by the method sketched above we find its Laplace- Fourier transform as follows (SI units):

$$\hat{E}_\theta(r, n, p, \omega) = -\frac{q\beta c Z_0 \lambda_n H_p}{4(\omega - n\omega_0)} \cdot \left[\frac{\omega}{c} \left(\frac{J'_n(\gamma_p r)}{J'_n(\gamma_p b)} s_n(\gamma_p b, \gamma_p R) + \Theta(r - R) s_n(\gamma_p r, \gamma_p R) \right) + \frac{n}{\beta R} \left(\frac{\alpha_p}{\gamma_p} \right)^2 \left(\frac{J_n(\gamma_p r)}{J_n(\gamma_p b)} p_n(\gamma_p b, \gamma_p R) + \Theta(r - R) p_n(\gamma_p r, \gamma_p R) \right) \right] \quad (11)$$

$$\gamma_p^2 = (\omega/c)^2 - \alpha_p^2, \quad \alpha_p = \pi p/h,$$

$$p_n(x, y) = J_n(x)Y_n(y) - Y_n(x)J_n(y),$$

$$s_n(x, y) = J'_n(x)Y'_n(y) - Y'_n(x)J'_n(y) \quad (12)$$

Here $Z_0 = 120\pi \Omega$ is the impedance of free space and $\Theta(x)$ is the unit step function, equal to 1 for $x \geq 0$ and zero otherwise. This formula displays the same concentration near the outer wall as in Rayleigh’s case and similar resonances. Resonances result from boundary conditions, as in the Rayleigh theory, and give poles in the ω -plane:

$$J'_n(\gamma_p b) = 0 \text{ (TE)}, \quad J_n(\gamma_p b) = 0 \text{ (TM)} \quad (13)$$

In our nomenclature the TE and TM modes have electric and magnetic fields transverse to the symmetry axis of the problem (z -axis). Thus the TE mode has electric field polarized in the plane of motion of the beam, while the TM mode has electric field perpendicular to that plane.

As remarked above the toroidal and pill box models give nearly the same field at the position of the beam, and indeed at any point not too close to the inner torus wall. The corresponding wave functions for a typical choice of parameters are shown in Fig.6.

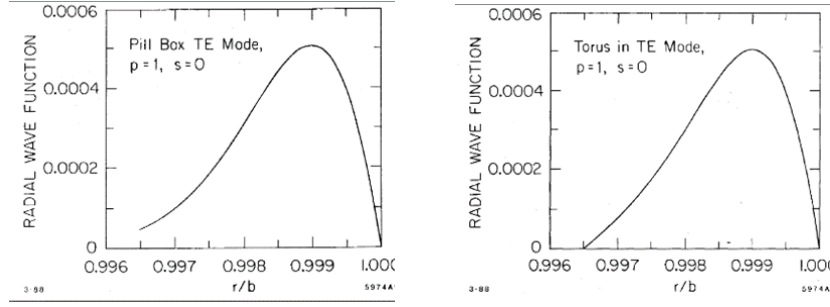


Figure 6: Wave functions vs. r/b for pill box and torus. Here $s = 0$ corresponds to $s = 1$ in the main text.

The longitudinal field (averaged over transverse distributions) can be expressed in terms of the impedance $Z(n, \omega)$:

$$-2\pi R \mathcal{E}_\vartheta(n, \omega) = Z(n, \omega) I(n, \omega), \quad I(n, \omega) = \frac{iq\omega_0 \lambda_n}{2\pi(\omega - n\omega_0)} \quad (14)$$

The wake voltage is given by the inverse Laplace-Fourier transform,

$$V(\theta, t) = \sum_n e^{in\theta} \int_{\text{Im } \omega = v} e^{-i\omega t} Z(n, \omega) I(n, \omega) d\omega, \quad v > 0, \quad (15)$$

and the power is $\mathcal{P}(t) = -dW/dt$, where W is the work done per unit time by the wake field,

$$\mathcal{P}(t) = q\omega_0 \sum_n e^{in\omega_0 t} \lambda_n^* \int_{\text{Im } \omega = v} e^{-i\omega t} Z(n, \omega) I(n, \omega) d\omega \quad (16)$$

The impedance deduced from (11) is

$$Z(n, \omega) = i\pi^2 Z_0 g R \sum_{p=0}^{\infty} H_p^2 \left[\frac{\omega R J'_{|n|}(\gamma_p R)}{c J'_{|n|}(\gamma_p b)} S_{|n|}(\gamma_p b, \gamma_p R) + \frac{n}{\beta} \left(\frac{\alpha_p}{\gamma_p} \right)^2 \frac{J_{|n|}(\gamma_p R)}{J_{|n|}(\gamma_p b)} p_{|n|}(\gamma_p b, \gamma_p R) \right]. \quad (17)$$

This is correct at positive and negative n alike.

Now the wake voltage (16) may be evaluated by pushing the ω -contour to infinity in the lower half-plane, and in so doing one encounters poles at $\omega = n\omega_0$ from the factor in the current, at resonant frequencies $\omega = \pm\omega_r$, defined by Eqs.(13), and at wave guide poles $\omega = \pm\alpha_p c$ which appear in the impedance. The contour at infinity in the lower half plane gives no contribution. Thus we have [6]

$$\begin{aligned}
V(\theta, t) &= \sum_n e^{in\theta} \int_{Im \omega = v} e^{-i\omega t} Z(n, \omega) \hat{I}(n, \omega) d\omega \\
&= q\omega_0 \sum_n \lambda_n Z(n, n\omega_0) e^{in(\theta - \omega_0 t)} \\
&\quad + q\omega_0 \sum_n e^{in\theta} \lambda_n \sum_j \left[\frac{e^{-i\omega_j t} R(n, \omega_j)}{\omega_j - n\omega_0} - \frac{e^{i\omega_j t} R(n, -\omega_j)}{\omega_j + n\omega_0} \right] \\
&= V_1(\theta - \omega_0 t) + V_2(\theta, t). \tag{18}
\end{aligned}$$

Here the (positive) resonance and wave guide pole positions are denoted generally by ω_j , and $R(n, \omega_j)$ is the residue of the pole in $Z(n, \omega)$ at $\omega = \omega_j$.

The first term V_1 in (19) depends only on the angular distance $\theta - \omega_0 t$ from the reference particle and is the usual expression of the induced voltage that one finds in the literature, with $Z(n, n\omega_0)$ being a more precise designation of what is usually called $Z(n)$. The second term $V_2(\theta, t)$ is conceptually important, but as far as I know does not appear in the literature before Ref.[6]. It exactly cancels the first term V_1 if $n\omega_0$ should approach one of the resonance frequencies ω_r , where $Z(n, n\omega_0)$ is infinite. Without the cancelation we have a potentially infinite induced voltage, which hardly seems physical.

When wall resistance is included in the boundary condition, as was done in Ref.[5], the resonance poles are displaced to nearby points in the lower half plane: $\pm\omega_r \rightarrow \pm\omega_r - i\epsilon$. Then the corresponding terms in V_2 vanish at large t with a damping factors $\exp(-\epsilon t)$. There is also a third term $V_3(\theta, t)$ arising from a branch point of the impedance at $\omega = 0$ due to the square root singularity in the skin depth. This too vanishes at large t , being an integral along the negative imaginary axis with factor $\exp(-i\omega t)$ in the integrand. It appears that the contribution of the wave guide poles to V_2 averages to zero with increasing t , but a careful analysis of this point remains to be done.

We invoke wall resistance and carry out a similar treatment of the power (17). Furthermore, we suppose that when the bunch form evolves in time, the constant λ_n can simply be replaced by $\lambda_n(t)$. As was shown in Refs. [7] and [8] for the case of the parallel plate model of the vacuum chamber, this is only an approximation, and not always an accurate one. A careful study of the approximation for both parallel plates and the toroidal model would be desirable. For now we just declare the time-dependent induced voltage and power to be

$$V(\theta, t) = q\omega_0 \sum_{n=-\infty}^{\infty} e^{in(\theta - \omega_0 t)} Z(n, n\omega_0) \lambda_n(t), \tag{19}$$

$$\begin{aligned}
&P(t) \\
&= 2(q\omega_0)^2 \sum_{n=1}^{\infty} \text{Re} Z(n, n\omega_0) |\lambda_n(t)|^2. \tag{20}
\end{aligned}$$

3.3.3 Comparison with Spectrum Measured at NSLS VUV Light Source

The vacuum chamber in the NSLS-VUV synchrotron light source at Brookhaven has relatively little deviation from the toroidal form with rectangular cross section, in the bending magnets where CSR is observed. Ignoring the effect of straight sections and chamber corrugations elsewhere in the ring we make a comparison of the observed CSR power spectrum to the real part of the impedance computed from the toroidal model with resistive wall, shown in Fig.7. The parameters are $R = 1.91\text{m}$, $w = 8\text{cm}$, $h = 4\text{cm}$, where R is the bending radius and w and h are the horizontal width and vertical height of the chamber. Vertical modes up to $p = 25$ are included. The wall conductivity is that of the stainless steel chamber, but that is not a critical parameter. The outer wall of the torus is at $r = b = 1.948\text{m}$, and the beam is at $r = R$, putting it 2mm off center; this improves somewhat the fit to the data in comparison to a centered beam. Measurements [10] were done with a Michelson interferometer (Fig.8) and, at the lowest frequencies near the cut-off of the radiation impedance, with RF methods (horn antenna, wave guides, and frequency analyzer) (Fig.9). For details of our fit see [9]. Here we show only the comparison of experimental and theoretical lines in Table 1. The entries marked with an asterisk correspond to somewhat doubtful small shoulders in the data, rather than clear peaks.

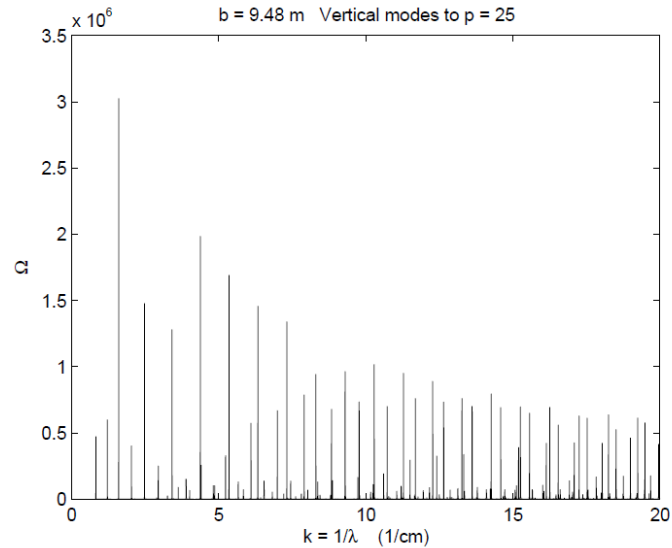


Figure 7: $\text{Re } Z(n, n\omega_0)$ for parameters of VUV light source, vs. wave number $1/\lambda$ in units of cm^{-1} .

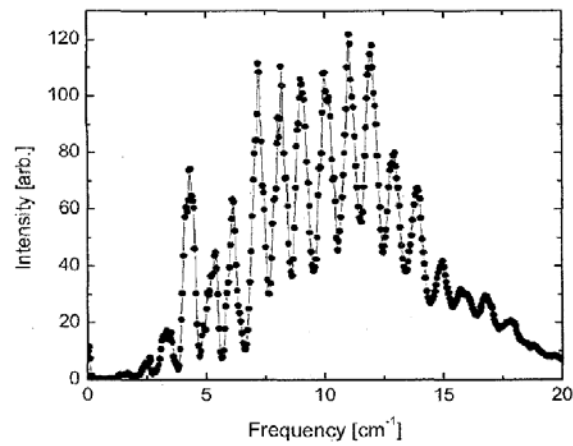


Figure 8: Far IR spectrum measured at NSLS.

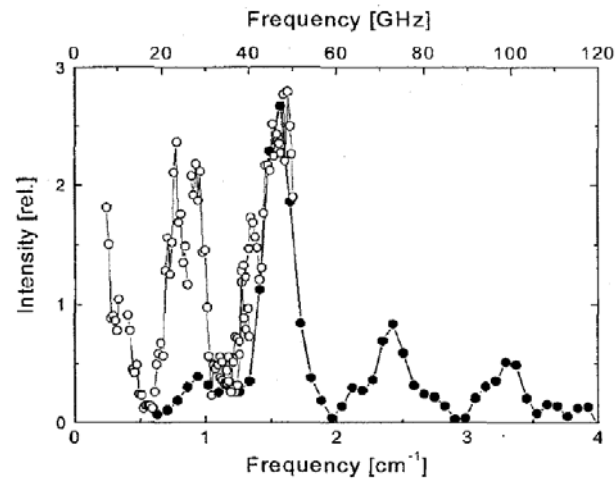


Figure 9: Low frequency spectrum measured at NSLS. The black dots are IR data from an interferometer, the open dots from RF measurements.

Table 1: Theoretical frequencies compared to data of Figs.8,9.

Exp.	Thy.	Exp.	Thy.
0.80	0.827	6.10	6.31
0.93	-	7.25	7.32
1.32	1.21	9.00	8.32
1.57	1.60	10.0	9.29
2.10*	2.04	11.1	10.28
2.40	2.48	12.0	11.29
2.76*	2.94	12.8	12.33
3.10*	3.26	13.8	13.31
3.66*	3.62	15.0	14.3
3.88*	3.90	15.7-15.9	15.3
4.20	4.38	16.7	16.3
5.25	5.34	18.0	17.3
		18.8*	18.3

In a follow up to this fit, D. Zhou [11] has done a calculation including straight sections, but without imposing periodicity of fields around the ring. Periodicity is hard to impose in the paraxial approximation that Zhou employed. Peaks in the impedance in this calculation have non-zero widths, which Zhou tries to identify with experimental widths. I am skeptical of this identification for two reasons. First, I suspect that periodicity will imply sharp resonances, even in the presence of bends; second, there are eminent sources of experimental widths, such as dispersion in the IR beam lines. Nevertheless, Zhou raises an interesting issue which certainly should be explored.

3.3.4 High Resolution CSR Spectra at the Canadian Light Source (CLS)

In view of the impressive agreement between theory and the data from VUV, taken a long time ago, one is encouraged to look at more recent data and other machines. On the one hand, there are now superb instruments such as the Bruker IFS 125 HR interferometer at CLS and Soleil, with a resolution down to 0.0009 cm^{-1} . On the other hand, comparison with theory is more difficult at machines more modern than the VUV, since their vacuum chambers at the location where IR is extracted do not have the simple form of the toroidal model with constant rectangular cross section. Rather, there is usually a fluted chamber with an outer wall receding from the beam by a large distance, perhaps tens of centimeters. Fig.10 shows the plan of one of two similar IR chambers at the CLS. Within the chamber are two significant metallic structures that can reflect radiation, a copper photon absorber, and a mirror near the beam to send radiation into the IR beam line leading to the interferometer. We can hardly expect the simple toroidal model to describe fields in this structure, and indeed experiment indicates that it does not.

Nevertheless, observations at the CLS leave little doubt that there are sharp peaks in the power spectrum, which are determined by the vacuum chamber and the bending field alone. Spectra taken with the Bruker show a remarkable stability with respect to changes in the machine setup and the structure of the IR beam line. Figure 11 compares a power spectrum (red) taken in the bursting mode of CSR with one bunch at 2.9 GeV, on 18/5/2010, with another (blue) taken in the continuous mode with 210 bunches at 1.5 GeV, on 30/1/2012. The latter was multiplied by a factor of 8 to aid comparison. Because of the large change in the beam one expects the positions of peaks to agree better than the relative heights, as is found, but even the relative heights show a lot of similarity between the two runs. We take this stability as a strong indication that the spectrum is determined primarily by the vacuum chamber and bends.

The peaks in the fine structure of Fig.11 have a spacing $\Delta k = \Delta(1/\lambda) \approx 0.073 \text{ cm}^{-1}$. If we try to get that spacing from the toroidal model, the distance from the beam to the outer wall must be $d = b - R = 33 \text{ cm}$, which happens to be near the actual distance at the maximum excursion of the wall. Here the spacing referred to is that of the strongly dominant TE modes.

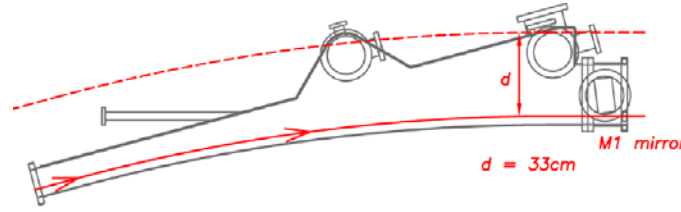


Figure 10: Vacuum chamber of CLS at dipole where IR is extracted.

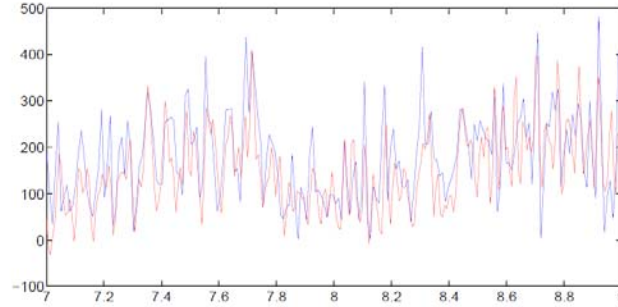


Figure 11: CLS spectra from two very different runs, power (a.u.) vs. k in cm^{-1} .

3.3.5 Implications for the Wake Field

Suppose there is only one bunch in the ring. The wake field within the confines of the bunch turns out to be almost the same for the toroidal and parallel plate impedance models, at least for a Gaussian bunch that is short compared to the bending radius. This in spite of the utterly different appearance of the two impedances. This behavior was noticed long ago [12] and unfortunately led to my opinion that the whispering gallery modes would have no great influence on bunch dynamics.

When there are two or more bunches in the ring and the bunch currents are large the situation is quite different. The toroidal model predicts a very long wake field, which can affect the dynamics of a following bunch. In Fig.12 we show the real part of the toroidal impedance for parameters of the ANKA light source in Karlsruhe. The corresponding wake potential, computed from (20) with $\lambda_n = 1/2\pi$ and maximum n corresponding to $k = 65\text{cm}^{-1}$, is shown in Fig.13; the head of the bunch is on the right. A feature of the model, if not of the real system, is that the wake wraps all the way around the ring, so that there is a precursor field in front of the bunch.

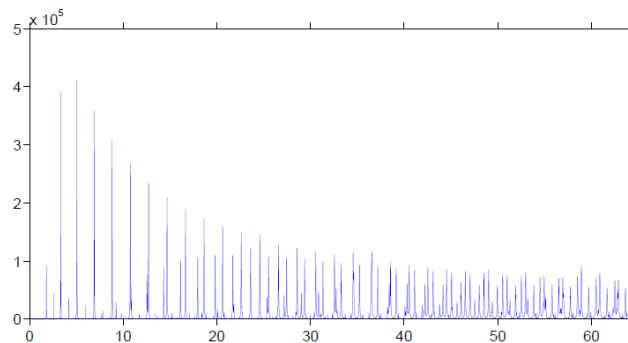


Figure 12: $\text{Re } Z(k)$ in ohms for ANKA parameters, vs. $k = 1/\lambda$ in cm^{-1} .

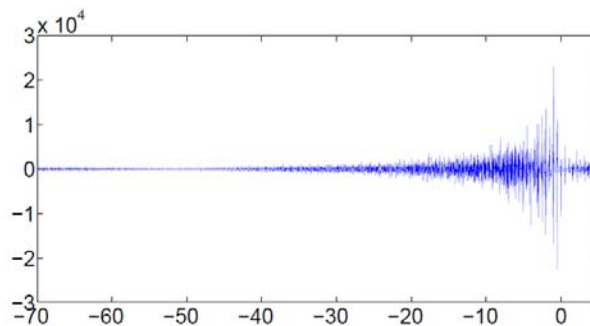


Figure 13: Wake potential $W(z)$ in V/pC from Z of Fig.12, vs. z in cm.

3.3.6 Experimental Evidence for Interbunch Communication

Evidence of a long range wake field comes from an experiment at ANKA by V. Judin and collaborators [13], [14]. They observed THz radiation with a fast bolometer having sufficient time resolution to distinguish radiation from individual bunches. A large number of buckets were filled with known but varying amounts of charge. Bolometer signals from the various bunches were sorted into two groups: the blue group in which the preceding bunch in the fill has at least 10% less charge, and the red group in which the preceding bunch has at least 10% greater charge. The power signals were preponderantly greater for the red group, as is seen in the histogram of Fig. 14. The histogram gives the distribution of red and blue signals relative to a curve which is a global fit to all the signals.

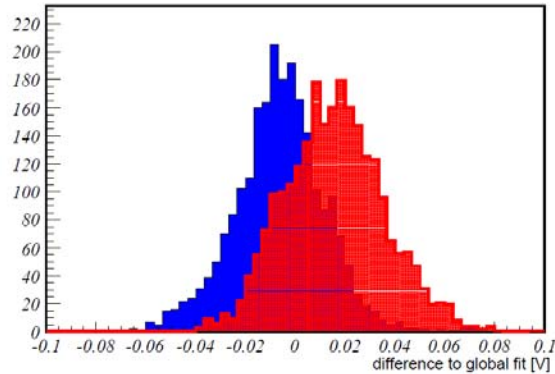


Figure 14: Radiation enhancement by higher charge in preceding bunch.

3.3.7 Direct Observation of a Long Range Wake Field

Experiments which aspire to observe the wake field directly were carried out at the CLS, following an idea of S. Kramer to put a microwave horn and diode detector at a backward port (in the horizontal pipe seen in Fig. 10) in one of the two IR dipole chambers. The diode has a bandwidth of roughly 50-75 GHz, and receives signals traveling opposite to the direction of the beam, which might come from backward reflections off structures present in the chamber. Fig. 15 shows a typical oscilloscope trace of the diode signal. Labeling the prominent *downward* peaks from left to right as 1 to 4, we have a plausible explanation as follows: 1 and 2 are reflections from the first downstream obstacle in the flared chamber, a copper photon absorber (in second circle from right in Fig. 10), whereas 3 and 4 are from the next obstacle, a structure supporting the M1 pick-off mirror. The 1-3 separation corresponds closely to the separation of these obstacles. Peak 1 is seen as the prompt wake field from the bunch, while peak 2 is a delayed pulse in the wake field, about 13.5 cm behind the bunch; similarly for 3 and 4, coming from the later reflection. The point to emphasize is that the distance from bunch to delayed wake pulse is very close to the reciprocal of the average spacing of peaks in the power spectrum shown in Fig. 11, namely $\Delta k \approx 0.073 \text{cm}^{-1}$. Correspondingly, the distance between the center burst and the first side peak in the interferogram is 13.5cm.

The interpretation of the peaks in terms of reflections is given added weight by a second experiment in which the diode was moved to a “normal” dipole chamber. That resembles the special IR chamber, but lacks the pick-off mirror and has a slotted wall (centered slot of width 1 cm) between the beam and the large flared box. The analog of peaks 1-2 is seen, but that of 3-4 goes away, in accord with the absence of the mirror support structure.

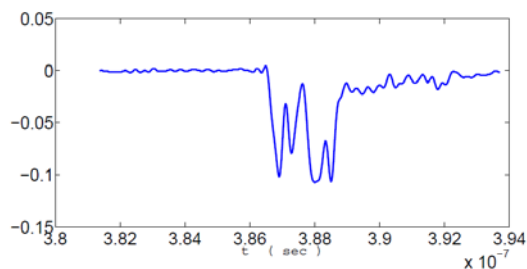


Figure 15: Signal (a.u.) from backward viewing diode at CLS vs. time in seconds.

3.3.8 Simulation of Interbunch Communication

In collaboration with Marit Klein, I have demonstrated the effect of the long range wake field from whispering gallery modes by solving a nonlinear Vlasov- Fokker-Planck (VFP) system for two bunches in two adjacent buckets. We take ANKA parameters for which the interbunch spacing is 60cm. The impedance is that of Fig. 12. We have two coupled VFP equations, each referring to the longitudinal phase space distribution for a bunch in its beam frame, but with a term in the wake field defined by the distribution of the other bunch. The equations are solved by the method of Ref.[15], but with bi-cubic rather than bi-quadratic interpolation to update the distribution. The initial distributions are Haïssinski equilibria, which are highly unstable at the currents considered.

We plot the total coherent power (a.u.) radiated by each of the two bunches vs. time in synchrotron periods. There are $N_a = 1.14 \cdot 10^9$ particles (0.49mA) in bunch (a), and an unperturbed bunch length for both bunches of $\sigma_z = 1.92\text{mm}$, typical for a low- α setup of ANKA used in CSR runs. The longitudinal damping time is given its realistic value. For Fig. 16 we have $N_a = N_b$, but the power from the trailing bunch (blue) is consistently greater than that from the leading bunch (red).

Fig. 17 shows the power from trailing bunch (a), without a leading bunch (red) and with a leading bunch having 50% more charge (blue). The strong enhancement due to the leading bunch is perhaps surprising in view of the seemingly small wake potential at 60cm shown in Fig. 13, but is believed to be an authentic consequence of the model, evidently a feature of the unstable bunch dynamics at the large (but realistic) currents considered. Of course, the corresponding calculation with the parallel plate impedance shows no inter-bunch communication.

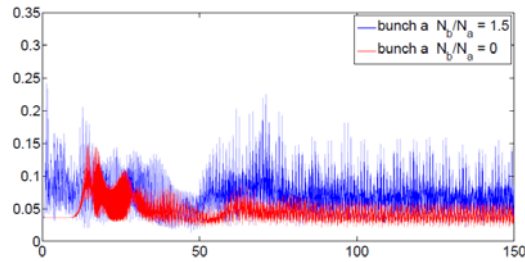


Figure 16: Power from two bunches with equal charges.

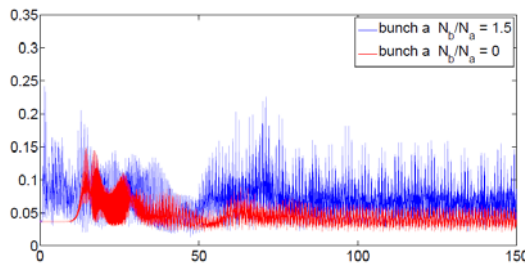


Figure 17: Power from trailing bunch (a), with and without leading bunch (b), which has 50% more charge.

3.3.9 Outlook

I have reviewed the prediction of sharp peaks in the power spectrum of CSR on the basis of an idealized model of the vacuum chamber, and have compared the prediction to experiment. For more precise comparisons, one will need a theory accounting for the specific geometric shape of the vacuum chamber in the bend region where radiation is produced and sent to the spectrometer. It will be important to understand the question of locality of the phenomenon: does it depend in part on fields produced in upstream bends, or not? I hope that these issues will be clarified by a new frequency domain theory which takes a global view of a closed vacuum chamber with arbitrary bends and straights and arbitrary outer wall excursions.

On the experimental side there are ongoing experiments at the CLS, using backward and forward viewing diodes, sensitive to polarization, together with the Michelson interferometer. With more precision and a greater range of tests, a consistent picture seems to be emerging. It is hoped that a better understanding might lead to a way of smoothing out peaks in the spectrum, which are an annoyance to users of the IR facility.

I have not touched on the implications for bunch dynamics, beyond showing that radiation from a trailing bunch is enhanced compared to that of a leading bunch. Dynamical questions clearly need more theoretical and experimental study. Simulations with a large number of bunches are feasible with parallel computation, as has been shown at SOLEIL. Among other efforts one tries to reproduce “waterfall plots” obtained

experimentally, that is to say the Fourier transform of the radiated power with respect to time, versus the current, the latter naturally declining during a fill.

For simulation of bunch dynamics it may be less important to understand the fields in the fluted IR chambers, since the average wake field over a turn is all that we need, one turn being much less than a synchrotron period. The chamber is simpler in most of the bends, and much easier to model.

3.3.10 Acknowledgment

We sincerely thank Steven Kramer, Brant Billingham, Vitali Judin, and all the others who contributed to the experiments cited. Partial support of work at SLAC was from U.S. Dept. of Energy contract DE-AC03-76SF00515; support at CLS was from CFI, NSERC, NRC, The Canadian Institutes of Health Research, and the Government of Saskatchewan.

3.3.11 References

1. Lord Rayleigh (John William Strutt, 3rd Baron Rayleigh [1842-1919]), "The Theory of Sound, Vol. 2" (1896), §287, p.126 (Dover Publications reprint, 1945)
2. Lord Rayleigh, Royal Institution of Great Britain, Weekly Evening Meeting, January 15, 1904.
3. Lord Rayleigh, Phil. Mag., Ser. 6, **20**,1001-1004 (1910); **27**, 100-109 (1914).
4. M. Abramowitz and I. A. Stegun, "Handbook of Mathematical Functions", (National Bureau of Standards, 1964), §9.5.22, 9.5.24.
5. R. L. Warnock and P. Morton, SLAC-PUB-4562 (1988), Part. Accel. **25**, 113 (1990).
6. R. L. Warnock, pp. 113-135 in "Doing Physics: a Festschrift for Thomas Erber", (IIT Press, Chicago, 2010). Errata: In Eq.(11.31) the factor $-2\pi R$ belongs on the left hand side. In Eq.(11.38) the first term on the right hand side should be summed over n .
7. R. Warnock, R. Ruth, M. Venturini, J. A. Ellison, Phys.Rev. ST Accel. Beams **8**, 014402 (2005).
8. R. Warnock and M. Venturini, Proc. PAC 2003, Portland, paper RPP806, p.3144.
9. R. Warnock and J. Bergstrom, Proc. PAC 2011, New York, paper WEP119.
10. G. L. Carr et al., Proc. PAC 2001, Chicago; S. Kramer, Phys. Rev. ST - Accel. Beams **5**, 112001 (2002).
11. D. Zhou, Proc. IPAC 2012, Beijing, paper MOOBBO3.
12. R. Warnock and K. Bane, SLAC-PUB-95-6837 (1995), unpublished.
13. Beam Dynamics Newsletter **57**, §3.13.5.2.
14. V. Judin, "Investigation of Bunch-Bunch Interaction and the Influence of the Geometric Impedance in Production of Coherent THz Radiation" (in German), Ph.D. Dissertation, Karlsruhe Institute of Technology, 2013.
15. R. Warnock and J. Ellison, Proc. 2nd ICFA Workshop on High Brightness Beams, 1999 (World Scientific, 2001), SLAC-PUB-8404.

3.4 Coherent Synchrotron Radiation Studies at the Emittance Exchange Beamline

Jayakar Thangaraj

Fermi National Accelerator Laboratory, Batavia, Illinois 60510

Mail to: jtobin@fnal.gov

3.4.1 Introduction

Springing from the minds of great physicists such as Schott, Schiff, Schwinger, and Nodvick, coherent synchrotron radiation (CSR) was predicted to be a threat to building electron accelerators as far back in the early part of the 20th century [1-4]. This was not seen as a serious concern as the length of the electron bunch used in the accelerators (mostly circular) was long. The accelerator technology quickly provided ultra-short bunches with the onset of the era of photoinjectors and linac-driven light sources in early 1990's and theoretical work shifted to look into tighter bending radius and higher charges [5-8]. In this work, we will restrict further discussion to experimental CSR studies in chicanes. CSR in storage rings continues to be investigated either to mitigate it or to build novel FIR/IR sources [9-12]. An excellent history of CSR in storage rings and CSR in linacs spanning a century of work with seven distinct eras of accelerator science is described in [13]

Synchrotron radiation is the electromagnetic radiation emitted by a radially accelerated charged particle. CSR refers to synchrotron radiation with a wavelength that is longer than the bunch length and thus emitted coherently throughout the bunch. The steady-state CSR power loss based on a free-space model can be expressed as [5] : $P = \frac{N^2 x e^2 c}{\epsilon_0 \rho^{2/3} \sigma_z^{4/3}}$ Watts, where N is the number of particles, x is 0.0279, ρ is the bending radius in m , σ_z is rms the bunch length in m , and e is the charge of electron and c is the speed of light. Therefore, the shorter the bunch at the dipole, larger is the power loss due to CSR. The synchrotron radiated power spectrum is given by $\frac{dP}{d\lambda} = \frac{dp}{d\lambda} [N(1-g(\lambda)) + N^2 g(\lambda)]$, where p is the single particle classical synchrotron radiation power, N is the number of particles and $g(\lambda)$ is the form factor proportional to the Fourier transform of the longitudinal profile of the bunch and λ is the wavelength of the radiation [14]. If the condition for coherency is satisfied i.e. $Ng(\lambda) \gg 1$, the single particle radiation intensity is multiplied by the bunch form factor and N^2 to yield CSR. For a Gaussian bunch with rms bunch length σ_z , the form factor is given by $g(\lambda) = \exp[-(\frac{2\pi\sigma_z}{\lambda})^2]$, indicating that bunches will emit CSR at wavelengths longer than $2\pi\sigma_z$.

The adverse aspect of CSR in the context of linear colliders and free-electron lasers is that the amount of energy that is radiated scales as the square of the number of particles (for Q=3.2 nC, $N \sim 10^{10}$) and such an energy loss inside a bend could lead to a non-linearly correlated energy spread along the bunch and a projected emittance growth. After the millennium, some experimental work on characterizing CSR in a chicane was done at CTF-II [15, 16]. Measurements at FLASH, LCLS, and FERMI@Elettra have

also gained grounds on understanding the impact of CSR on beam dynamics [17-19]. Though these studies have been very revealing, the dynamics of CSR in a linac are complex for non-Gaussian beams and the form factor (shape) of the beam plays a crucial role among other parameters [20, 21]. A recent work has shown that by properly choosing the right shape of the bunch before compression in a 4-dipole chicane, the core-emittance of the beam could be preserved [22]. Such longitudinally shaped beams can be generated using a combination of RF-accelerating and harmonic cavities [23] or by shaping the laser beam at the cathode where a flat current distribution was generated [24].

During the last decade, micro-bunching instability driven by a combination of CSR and longitudinal space charge that leads to fragmentation of the phase space has attracted much attention to investigate and control longitudinal and transverse beam dynamics inside a chicane [21, 25-28] leading to few proposed ideas such as: a laser heater [29], a scheme using bend magnets that damp the longitudinal modulations due to transverse spot size and divergence [30], reversible laser heater [31] and an emittance exchanger [32]. The laser heater has been demonstrated experimentally at LCLS [29] and the emittance exchanger beamline has been demonstrated at A0 [33].

The emittance exchange line (EEX) consists of a TM 110 cavity sandwiched by doglegs [34]. The EEX beamline has been shown to have valuable application in beam shaping applications such as generating sub-ps bunch trains, tailored current distribution for advanced accelerator applications and a short wavelength FEL. In this article, we focus on briefly summarizing the work done on experimentally investigating coherent synchrotron radiation effects (CSR) in the emittance exchange line at the Fermilab A0 photoinjector. We begin with the measurement of CSR power as a function of charge and bunch length, followed by a report on the measurement of polarization of the CSR. We then show how CSR was used to measure the bunch length of the electron beam and compare those results with numerical simulations. After describing results from time-resolved studies of CSR using a skew quadrupole, we conclude our summary with measurements from the emittance exchanger, where a peak current increase by a factor of 2 was obtained with an energy-chirped beam. For more details on the machine parameters and details of the CSR setup, we refer the reader to [35]. At the end we describe the latest developments in EEX configurations and propose two new configurations to the list.

3.4.2 CSR Studies at the A0 Emittance Exchange Beamline

3.4.2.1 *Experimental Setup*

The A0 photoinjector facility (A0PI) shown in Fig. 1 consists of an L-band RF gun followed by a superconducting 9-cell booster cavity, which accelerates the electron beam up to 16 MeV.

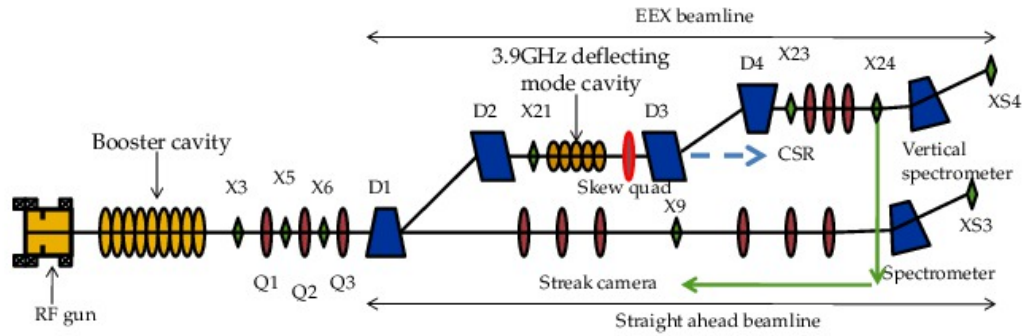


Figure 1: Experimental setup of the A0 photoinjector facility. Electrons generated by the RF gun are accelerated through the booster cavity to 14 MeV. Q1, Q2, Q3 focus the beam before it enters the EEX beamline. D1, D2, D3 and D4 are the dipole magnets. The skew quadrupole located before D3 is used to study time-resolved effects. X# refers to beam imaging stations.

After acceleration, the beam is steered and focused using the dipoles and the quadrupoles (Q1 Q2 Q3). The beam can either continue straight to XS3 or be steered into the dogleg. In our experiments, the beam is sent through the doglegs to the spectrometer (XS4). Located between the doglegs is the liquid-nitrogen-cooled, 5-cell 3.9 GHz TM110 deflecting mode cavity, which was switched on/off during our study. When the bunch passes through the dogleg, CSR is expected to be more pronounced at dipole D3. We installed optics to collect the radiation coming out of the port at dipole D3. The light is collimated using an off axis parabolic mirror onto a plane mirror. The reflected light is then directed either to a single LiTaO₃ crystal pyrodetector (for power measurement) or to a Martin-Puplett interferometer (to measure bunch length).

3.4.2.2 *CSR Power Measurements*

We measured the intensity of the radiation for various bunch charges and at different RF phases. We found that the detector power is maximum at the minimum bunch length for a fixed charge, as expected from the theory. Moreover, the detected power also varies quadratically with charge as expected for coherent radiation, and this is shown in the Figure 2 inset. Comparison between charges with a fixed number of bunches in a bunch train poses a limitation because the pyrodetector is saturated for higher charge at a lower number of bunches. The number of bunches we chose was 10 to prevent the pyrodetector from saturating at 1 nC.

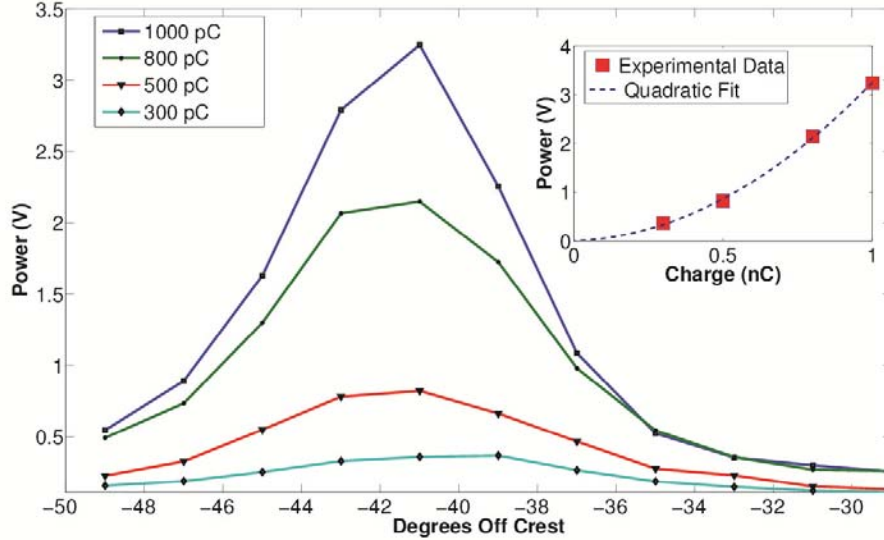


Figure 2: CSR Power measurement at D3 as a function of 9-cell booster cavity phase. Maximum power is observed at 41° off crest. The inset shows the fit of the CSR power as a function of charge.

3.4.2.3 Polarization of CSR

A wire-grid polarizer, which could be remotely rotated, was installed in front of the pyrodetector. The grids consist of 15 micron diameter tungsten wires spaced by 45 micron. The intensity of the CSR was measured as a function of the polarizer angle and is shown in Figure 3 along with a fit function. As expected, the light is mostly horizontally polarized. The measured ratio between the horizontal and the vertical polarization components was 4.6.

3.4.2.4 Bunch-Length Measurements

In order to extract the bunch length, the CSR was directed into a Martin-Puplett interferometer. The results of the measurements and a comparison with the single-particle simulation using both *BeamLattice* - a program based on a linear matrix model - and ELEGANT are shown in Figure 4. The uncertainty in the measurement is primarily due to the choice of the fitting function used to best capture the low-frequency cut-off of the detector. Simulation agrees with the experimental value for shorter bunch length while at longer bunch lengths low-frequency diffraction effects dominate, leading to the discrepancy. Also, the predicted RF phase at which the bunch length is minimum shows good agreement with the experimental value.

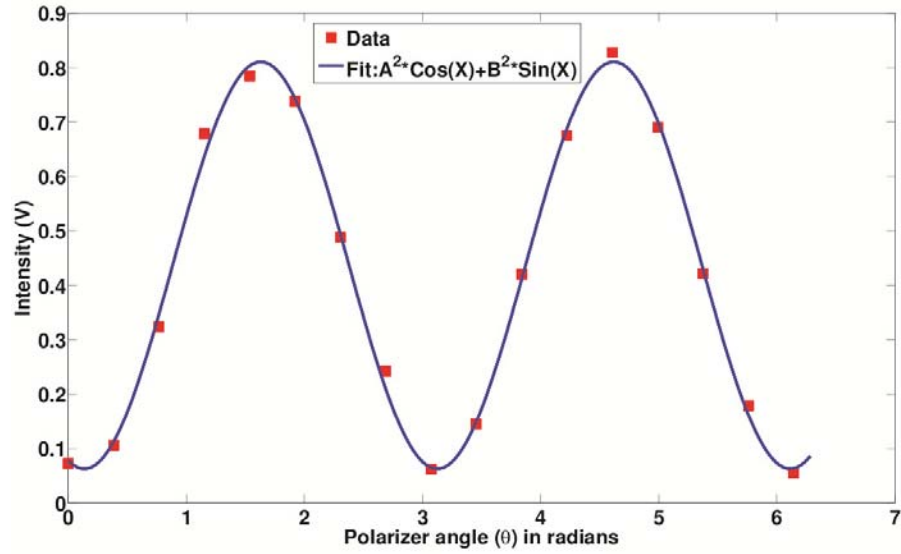


Figure 3: The measured CSR intensity as a function of polarizer angle. While the sinusoidal behavior indicates a horizontally polarized CSR light, the non-zero baseline indicates the vertical polarization component of the CSR. The fit function is given by $A^2 \cos^2(X) + B^2 \sin^2(X)$ where $X = w\theta + \phi$ and w, ϕ, A and B are arbitrary constants and θ is the polarizer angle in radians.

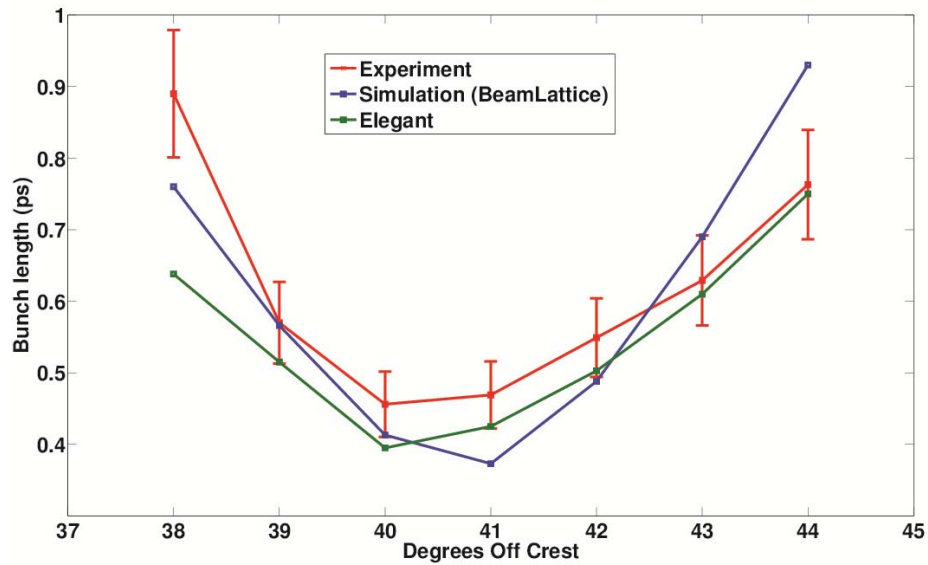


Figure 4: R.M.S. bunch length comparison for an *Elegant* simulation including CSR, a single-particle-matrix simulation without CSR, and the measurements.

3.4.2.5 Skew-Quadrupole Measurements

CSR modulates the energy by accelerating the head of the bunch which results in a change in the transverse positions of the particles as they exit the bend. The measured image profile at X24 for various charges with and without the skew quadrupole on is

shown in Figure 5. As the charge increases, the CSR "bulge" effect is seen on the screen as shown in Figure 5. This is consistent with the CSR power measurement in Figure where increase in charge shows a quadratic increase in CSR power loss indicating that the CSR effect is more pronounced at higher charges. Here we have made a thin-lens approximation for the 5-cell and have ignored other collective effects like space charge and wakefields.

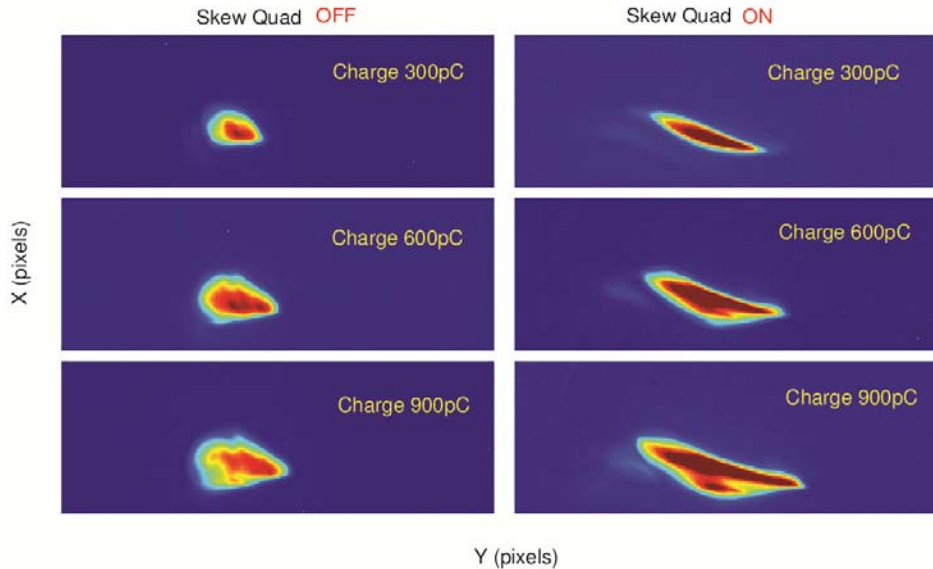


Figure 5: Measured transverse beam profile at X24 as a function of skew quadrupole off (left column) and skew quadrupole on (right column) for various charges. The CSR bulge effect is prominent at higher charges.

3.4.2.6 *Emittance Exchanger with an Energy-Chirped Beam*

In the emittance exchange beamline, if we assume a thick lens for the cavity, the transfer matrix is altered with coupling from incoming z and δ . So, the outgoing particle $z_2 = \kappa \xi x_1 + \left[\frac{-1}{\kappa} + \left(\frac{L_c}{4} + L \right) \xi \right] \kappa x'_1 + \frac{L_c \kappa^2 \xi}{4} (z_1 + \xi \delta_1)$ where ξ is the longitudinal dispersion, x_1, x'_1, z, δ are the incoming x-position, x-angle, longitudinal position, energy spread of the beam and L_c, L, κ are the length of the cavity, the length of the dogleg and the strength of the cavity respectively. If we set the chirp $h = \frac{\delta_1}{z_1} = \frac{-1}{\xi}$, then the last term in the equation will be zero or minimized.

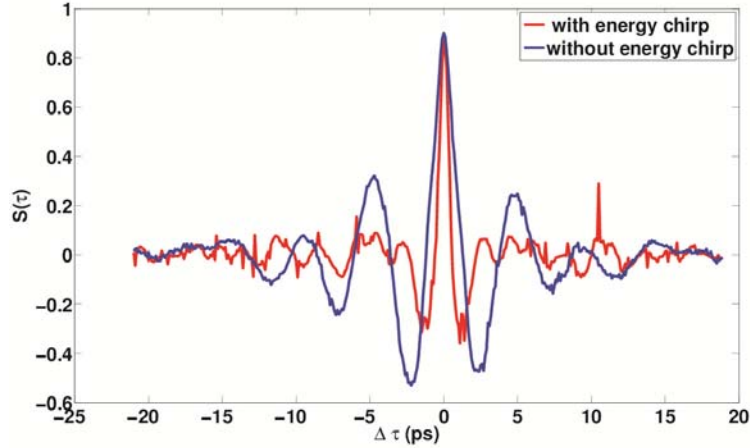


Figure 6: Auto-correlation measurement with Martin-Puplett interferometer with and without energy chirp.

The CTR radiation from X24 was used to measure the auto-correlation of the beam with and without energy chirp. The result is shown in Figure 6. The bunch with chirp (red) shows a shorter auto-correlation width compared with the bunch with no chirp (blue). Assuming a Gaussian bunch and extracting the bunch length from the auto-

correlation using the formula: $\sigma_t = \frac{FWHM_{center}}{2.35\sqrt{(2)}}$ where $FWHM_{center}$ corresponds to the

full-width half maximum of the center peak, yields a bunch length of 0.60 ps (blue) and 0.25 ps (red). Therefore, adding a chirp decreases the bunch length by a factor of ~ 2.4 . In other words, beam with the RF chirp is shorter compared to the one without chirp. This is consistent with the power measurements which also showed a factor of ~ 2 increase in the detector power for a beam with chirp and also agrees with the theoretical predictions and computer simulations. The bunch length formula has been verified through computer simulation which assumes a Gaussian bunch along with a diamond window for the extraction port.

A positive side-effect of using a chirped beam is the decrease in the x' after the cavity. Recall that after the cavity, $\Delta x' = \kappa \Delta z$, where κ is the strength of the deflecting cavity set to $\frac{-1}{\eta}$ for EEX. So if we reduce the bunch length at the cavity by adding

energy chirp, the beam divergence after the cavity is also reduced and thus reducing the emittance growth from second order dispersive aberration. A negative side effect of using a chirped beam is the increase in coherent radiation effects that can spoil the transverse emittance of the beam in the bend plane. Coherent radiation effects increase quadratically with charge and limit our experiment to 400 pC, where the coherent radiation effects are not a significant threat as compared to higher charges.

In the chirped EEX experiment, the beam energy was set to 13.2 MeV. This was done to maintain the same beam energy for different RF-phase settings without driving the gradient too high on the 9-cell cavity. The charge per bunch was 400-450 pC. The incoming rms normalized transverse emittance was $4 \mu\text{m}$. The incoming bunch length was measured at X9 using a streak camera and the minimum energy spread was measured using a RF-phase scan and the spectrometer magnet in the straight ahead

beamline. The rms normalized longitudinal emittance was $20 \mu\text{m}$. The beam was then sent through the emittance exchange line and the transverse and the longitudinal emittances were measured after the exchange. The results of the measurement for different chirp setting are shown in Figure 7. The emittance exchange ratio improves as the RF chirp on the beam increases. Ideally, the ratio should be one, but higher order effects in the dogleg, non-linearity in the field in the deflecting cavity, and space-charge effects could limit the achievable ratio in the laboratory.

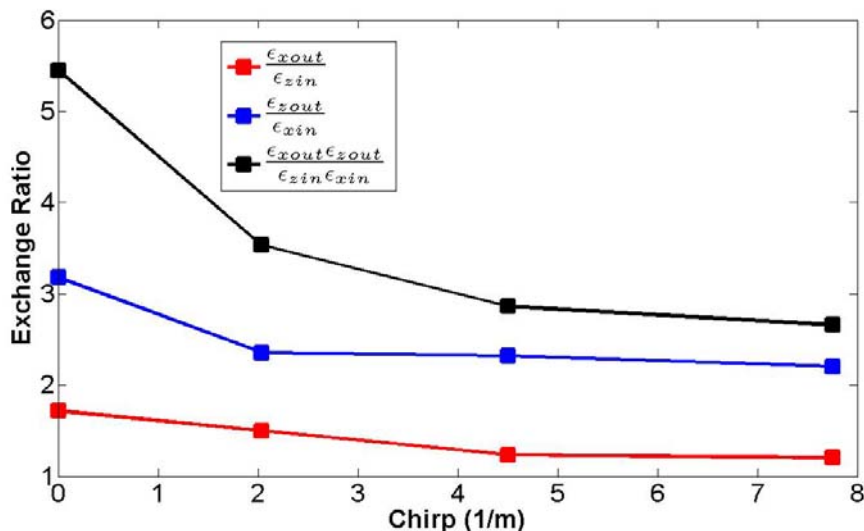


Figure 7: Measured value of the emittance exchange ratio and their products. As the RF-chirp increases, the ratio tends towards one. There is still some emittance dilution possibly due to second order effects and space charge.

3.4.3 Other Exact-Emittance Exchange Configurations

As we have shown in this work, adding the appropriate RF-chirp to the beam increases the performance of the emittance exchange i.e. the coupling due to the thick-lens effect of the TM110 cavity is minimized. Another way to overcome the thick-lens effect of the TM110 cavity is to use an accelerating-mode cavity before or after the deflecting as shown in [36]. By appropriately setting the chirp, the thick-lens effect can be made zero. Alternatively, we can use another TM110 cavity to do the same. In this case, the strength of the deflecting mode cavity must be changed a little bit but the thick-lens effect can be overcome [37]. A negative-drift based EEX was proposed that could be used as a bunch compressor that has significant benefit of compressing without a RF-chirp (energy-phase) correlation, which saves energy by operating on-crest and is less vulnerable to CSR-effects at high beam energy [38]. Most of the EEX listed above has a baseline design that uses dogleg geometry.

A chicane-type EEX which has the benefit of operating both as a chicane and as an EEX was proposed by introducing negative unity transfer matrix using a quadrupole doublet before the TM110 cavity [39]. The chicane being widely available around in many accelerators can take advantage of this scheme. Another option is to use a double emittance exchanger by ganging one EEX followed by another EEX. In the context of microbunching instability, it should be pointed out that in such a configuration adding a few micron thin beryllium foil after the first EEX section increases the energy spread at

the end of the double emittance exchanger beamline (due to multiple scattering). This can be effectively used as a laser heater without a laser, wiggler and a chicane[36].

Chicane style EEX while an improvement still has a major limitation that constrains the deflecting mode cavity to be at the center of the chicane. This sometimes prevents the transverse deflecting mode cavity, an expensive but very useful diagnostic for beamline operations. Under certain conditions, an EEX design that allows the deflecting mode cavity to be in line with the linac would be helpful. Ideally this will allow the beamline to operate as a chicane followed by a deflecting cavity or being used as an EEX. This can be done by the configuration shown in Figure 8 using a flipper EEX based on a double chicane configuration. The flipper EEX converts the chicane into a “dogleg-like” lattice with twice the dispersion thereby the strength needed for the cavity drops by a factor of two. By adding magnification lattice, more reduction is possible but the non-bending y-plane needs to be carefully managed. A triplet to do the negative unity matrix is beneficial but space constraints might allow only a doublet. The advantage of this scheme is that existing beamlines that have two chicanes with transverse deflecting mode cavity between them can be readily converted into a EEX beamline by adding quadrupoles. There are some limitations in this scheme. The chicane needs space that makes this scheme larger. A compact chicane might be helpful. CSR effects still will be a problem at the last few dipoles. In a real beamline, more magnets might be necessary for appropriate transverse control before and after the EEX beamline.

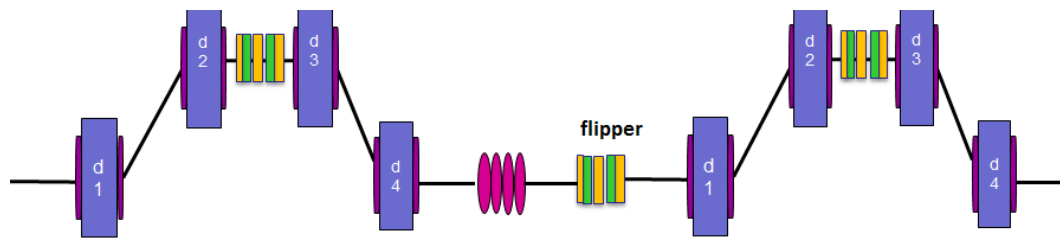


Figure 8: “Flipper” EEX. The deflecting cavity can be used for EEX or for normal linac diagnostic operations.

Finally, most of the emittance exchangers discussed above use the configuration that involves a dispersive section followed by a transverse deflecting mode cavity that is then followed by a dispersive section. This is a cheaper scheme as it involves only one deflecting mode cavity. But typically such a beamline is coupled both to the longitudinal and the transverse dispersion of the lattice unless uncoupled by a properly tuned quadrupole lattice before and after the beamline.

Another possible scheme is to have a deflecting mode cavity followed by dispersive section which is then followed by a deflecting mode cavity as shown in Figure 9. While this is an expensive option, such a beamline has the feature of a “pure” exchange of one phase-space variable (x') to the other (z'). Also, such a beamline could also be used as a reversible laser heater by rotating the deflecting mode cavity to deflect in the y-plane. Further details of such a beamline are discussed in [40]. This “pure” scheme is also made robust against the thick lens effect of the transverse deflecting mode cavity by

chirping the accelerating mode cavity before and after it appropriately for compensation.

The final EEX matrix for this beamline is

$$\begin{pmatrix} 0 & 0 & 0 & 2\eta \\ 0 & 0 & -\frac{1}{2\eta} & 0 \\ 0 & -2\eta & 0 & 0 \\ \frac{1}{2\eta} & 0 & 0 & 0 \end{pmatrix}.$$

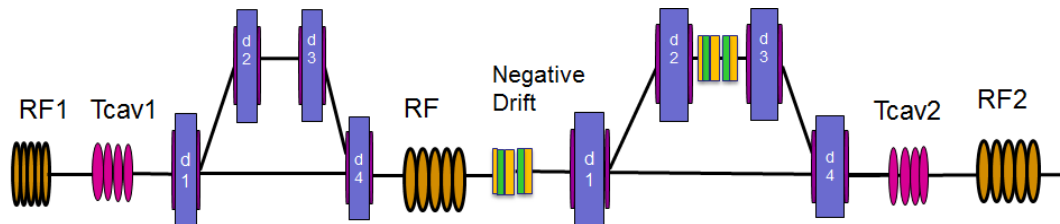


Figure 9: “Pure” EEX. The deflecting cavity can be used for EEX or for normal linac diagnostic operations.

3.4.4 Conclusion

Coherent synchrotron radiation has been studied at the emittance exchanger beamline. The properties of the radiation and its effect on the beam have been discussed. A chirped beam has shown to improve the performance of the emittance exchanger scheme. Possible schemes of next generation emittance exchanger beamline has been listed that could be useful in other context such as microbunching instability, bunch compression and bunch shaping applications.

3.4.5 References

1. Schiff, L., *Production of particle energies beyond 200 MeV*. Review of Scientific Instruments, 1946. **17**(1): p. 6-14.
2. Schwinger, J.S., *On radiation by electrons in a betatron (1945)*. reprinted 1996.
3. Nodvick, J.S. and D.S. Saxon, *Suppression of Coherent Radiation by Electrons in a Synchrotron*. Physical Review, 1954. **96**(1): p. 180.
4. Schott, G.A., *Electromagnetic radiation and the mechanical reactions arising from it*. 1912: University Press.
5. Derbenev, Y.S., et al., *Microbunch Radiative Tail-Head Interaction*. TESLA-FEL 95-05 Note, 1995.
6. Saldin, E.L., E.A. Schneidmiller, and M. Yurkov, *On the coherent radiation of an electron bunch moving in an arc of a circle*. Nuclear Instruments and Methods in Physics Research Section A: Accelerators, Spectrometers, Detectors and Associated Equipment, 1997. **398**(2): p. 373-394.
7. Murphy, J., S. Krinsky, and R. Gluckstern. *Longitudinal wakefield for synchrotron radiation*. in *Particle Accelerator Conference, 1995., Proceedings of the 1995*. 1995. IEEE.
8. Carlsten, B.E. and T.O. Raubenheimer, *Emittance growth of bunched beams in bends*. Physical Review E, 1995. **51**(2): p. 1453.

9. Carr, G., et al., *Observation of coherent synchrotron radiation from the NSLS VUV ring*. Nuclear Instruments and Methods in Physics Research Section A: Accelerators, Spectrometers, Detectors and Associated Equipment, 2001. **463**(1): p. 387-392.
10. Sannibale, F., et al., *A model describing stable coherent synchrotron radiation in storage rings*. Physical review letters, 2004. **93**(9): p. 94801.
11. Nakazato, T., et al., *Observation of coherent synchrotron radiation*. Physical review letters, 1989. **63**(12): p. 1245-1248.
12. Kheifets, S. and B. Zotter, *Shielding effects on coherent synchrotron radiation*. AIP Conference Proceedings 367, 1996. **367**: p. .
13. Murphy, J.B., *'An Introduction to Coherent Synchrotron Radiation in Storage Rings*. ICFA Beam Dynamics Newsletter, 2004(35).
14. Williams, G.P., et al., *Coherence effects in long-wavelength infrared synchrotron radiation emission*. Physical review letters, 1989. **62**(3): p. 261-263.
15. Braun, H., et al., *Emittance growth during bunch compression in the CTF-II*. Physical review letters, 2000. **84**(4): p. 658-661.
16. Braun, H.H., et al., *Emittance growth and energy loss due to coherent synchrotron radiation in a bunch compressor*. Physical Review Special Topics-Accelerators and Beams, 2000. **3**(12): p. 124402.
17. Bane, K., et al., *Measurements and modeling of coherent synchrotron radiation and its impact on the Linac Coherent Light Source electron beam*. Physical Review Special Topics-Accelerators and Beams, 2009. **12**(3): p. 030704.
18. Beutner, B., *Measurement and analysis of coherent synchrotron radiation effects at FLASH*. 2007.
19. Di Mitri, S., et al., *Transverse emittance preservation during bunch compression in the Fermi free electron laser*. Physical Review Special Topics - Accelerators and Beams, 2012. **15**(2): p. 020701.
20. Li, R., *Sensitivity of the CSR self-interaction to the local longitudinal charge concentration of an electron bunch*. Nuclear Instruments and Methods in Physics Research Section A: Accelerators, Spectrometers, Detectors and Associated Equipment, 2001. **475**(1): p. 498-503.
21. Borland, M., *Coherent synchrotron radiation and microbunching in bunch compressors*. Proc. 2002 Linac Conference, Gyeongju, Korea, 2002: p. 11-15.
22. Mitchell, C., J. Qiang, and P. Emma, *Longitudinal pulse shaping for the suppression of coherent synchrotron radiation-induced emittance growth*. Physical Review Special Topics - Accelerators and Beams, 2013. **16**(6): p. 060703.
23. Piot, P., et al., *Generation and Characterization of Electron Bunches with Ramped Current Profiles in a Dual-Frequency Superconducting Linear Accelerator*. Physical Review Letters, 2012. **108**(3): p. 034801.
24. Penco, G., et al., *Experimental Demonstration of Electron Longitudinal-Phase-Space Linearization by Shaping the Photoinjector Laser Pulse*. Physical Review Letters, 2014. **112**(4): p. 044801.
25. Heifets, S., G. Stupakov, and S. Krinsky, *Coherent synchrotron radiation instability in a bunch compressor*. Physical Review Special Topics - Accelerators and Beams, 2002. **5**(6): p. 064401.
26. Stupakov, G. and S. Heifets, *Beam instability and microbunching due to coherent synchrotron radiation*. Physical Review Special Topics-Accelerators and Beams, 2002. **5**(5): p. 054402.
27. Huang, Z., et al., *Suppression of microbunching instability in the linac coherent light source*. Physical Review Special Topics-Accelerators and Beams, 2004. **7**(7): p. 074401.
28. Di Mitri, S., et al., *Suppression of microbunching instability with magnetic bunch length compression in a linac-based free electron laser*. Physical Review Special Topics-Accelerators and Beams, 2010. **13**(1): p. 010702.

29. Huang, Z., et al., *Measurements of the linac coherent light source laser heater and its impact on the x-ray free-electron laser performance*. Physical Review Special Topics - Accelerators and Beams, 2010. **13**(2): p. 020703.
30. Qiang, J., C.E. Mitchell, and M. Venturini, *Suppression of Microbunching Instability Using Bending Magnets in Free-Electron-Laser Linacs*. Physical Review Letters, 2013. **111**(5): p. 054801.
31. Behrens, C., Z. Huang, and D. Xiang, *Reversible electron beam heating for suppression of microbunching instabilities at free-electron lasers*. Physical Review Special Topics - Accelerators and Beams, 2012. **15**(2): p. 022802.
32. Cornacchia, M. and P. Emma, *Transverse to longitudinal emittance exchange*. Physical Review Special Topics - Accelerators and Beams, 2002. **5**(8): p. 084001.
33. Ruan, J., et al., *First observation of the exchange of transverse and longitudinal emittances*. Physical Review Letters, 2011. **106**(24): p. 244801.
34. Kim, K.J. and A. Sessler, *Transverse - Longitudinal Phase - Space Manipulations and Correlations*. AIP Conference Proceedings, 2006. **821**(1): p. 115-138.
35. Thangaraj, J.C.T., et al., *Experimental studies on coherent synchrotron radiation at an emittance exchange beam line*. Physical Review Special Topics - Accelerators and Beams, 2012. **15**(11): p. 110702.
36. Zholents, A. and M. Zolotarev, *A new type of bunch compressor and seeding of a short wave length coherent radiation*. Advanced Photon Source ANL/APS/LS-327, 2011.
37. Xiang, D., Private communication.
38. Carlsten, B.E., et al., *Using an emittance exchanger as a bunch compressor*. Physical Review Special Topics - Accelerators and Beams, 2011. **14**(8): p. 084403.
39. Xiang, D. and A. Chao, *Emittance and phase space exchange for advanced beam manipulation and diagnostics*. Physical Review Special Topics - Accelerators and Beams, 2011. **14**(11): p. 114001.
40. Thangaraj, J., *Next generation emittance exchangers*. to appear in the Proceedings of the LINAC 2014, 2014.

3.5 Mitigation Plans for the Microbunching-Instability-Related COTR at ASTA/FNAL

A.H. Lumpkin, M. Church, and A.S. Johnson
 Fermi National Accelerator Laboratory, Batavia, IL 60510 USA
 Mail to: lumpkin@fnal.gov

3.5.1 Introduction

At the Advanced Superconducting Test Accelerator (ASTA) now under construction at Fermilab [1], we anticipate the appearance of the microbunching instability related to the longitudinal space charge (LSC) impedances [2,3]. With a photoinjector source and up to two chicane compressors planned, the conditions should result in the shift of some microbunched features into the visible light regime. The presence of longitudinal microstructures (microbunching) in the electron beam or the leading edge spikes can result in strong, spatially localized coherent enhancements of optical transition radiation (COTR) that mask the actual beam profile. Several efforts on mitigation of the effects in the diagnostics task have been identified [4-7]. At ASTA we have designed the beam profiling stations to have mitigation features based on spectral filtering, scintillator choice, and the timing of the trigger to the digital camera's CCD chip. Since the COTR is more intense in the NIR than UV we have selectable bandpass filters centered at 420

nm which also overlap the spectral emissions of the LYSO:Ce scintillators. By delaying the CCD trigger timing of the integration window by 40-50 ns, we can reject the prompt OTR signal and integrate on the delayed scintillator light predominately. This combination of options should allow mitigation of COTR enhancements of order 100-1000 in the distribution.

3.5.2 ASTA Facility and Diagnostics Aspects

3.5.2.1 Facility

The base linac planned includes the L-Band photoinjector gun with a Cs₂Te photocathode, two superconducting (SC) rf booster cavities, a chicane, and up to three L-band cryomodules (CM1-3) that each house 8 SCRF cavities. The first cavity of the cryomodule presently installed has been tested to gradients of 31.5 MV/m so one projects a total acceleration capability of 250 MeV per cryomodule. A schematic of the injector is shown in Fig. 1 with a photograph of the shielded tunnel and installed infrastructure in Fig. 2. The gun is driven by the Yb fiber laser oscillator running at 1300 MHz which has been pulse picked down to a 3 MHz micropulse rate, amplified by several single pass amplifiers, and frequency quadrupled to the UV. The macropulse is specified for up to 1 ms length at 5Hz. Charges per micropulse range from 20-3200 pC which are dictated by the UV energy, the quantum efficiency of the cathode, and the experimental requests. At the time of this writing, we are working towards the first testing of the gun with Cs₂Te cathode and the installation of the beamline to the low energy dump. Depending on the status of the first booster cavity we may run first beam tests through only booster cavity 2 which has already been conditioned at about 20 MV/m.

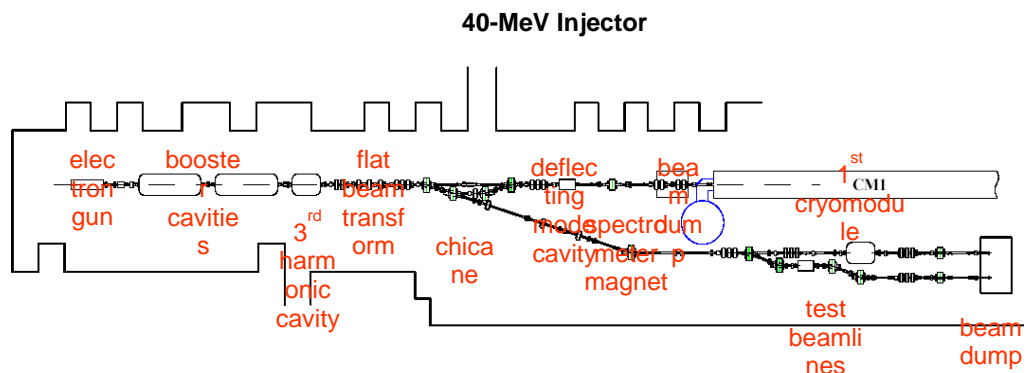


Figure 1: A schematic of the ASTA injector showing gun, booster cavities, and chicane for providing beam into CM1. The straight ahead line to the low energy dump is in assembly stage.



Figure 2: Photographs of an installed cryomodule (left) and the shielded tunnel and installed rf and power supply infrastructure (right).

The proposed buildout path in Stage I indicated in Fig. 3 would add the high energy beamline transport to the high power (30 kW) beam dump, install an experimental and diagnostics area, and install the integrable optics test accelerator (IOTA) storage ring. At present the experimental spur beamline at 50 MeV has been postponed.

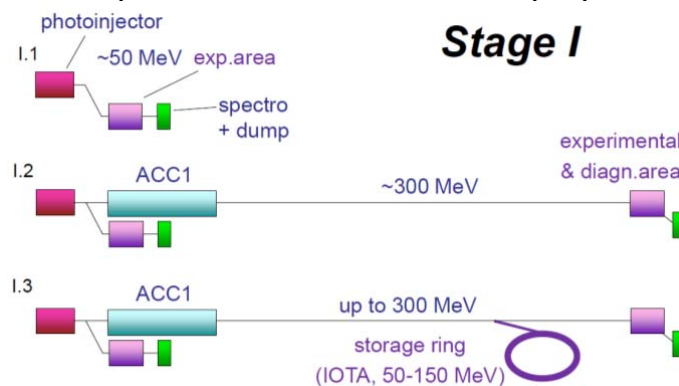


Figure 3: Proposed Stage I buildout of the ASTA facility to include the injector linac, high energy experimental area, and the IOTA ring [1].

3.5.2.2 *Diagnostics Options*

As provided in this workshop's experimental overview talk [8], diagnostics for assessing the μ BI via COTR can be developed with standard beam diagnostics with some adaptations.

- 1) Bunch length monitors for tuning and verifying the compression will be based on coherent radiation aspects of transition radiation (CTR), synchrotron radiation (CSR), edge radiation (CER), diffraction radiation (CDR), etc. in the frequency domain or on incoherent sources in the temporal domain with an ultrafast streak camera or deflecting mode cavity plus an imaging screen. We have planned for a station following the first chicane to provide such capabilities in the injector linac.
- 2) OTR beam profile monitor screens are used for detecting the presence of COTR and its spatial distribution, intensity fluctuations, and intensity enhancements. The latter can be factors of 100 to 10,000 which make the profiles no longer

representative of the true charge distribution and obviate the technique for profiling.

In the event we have COTR, our mitigation techniques include spectral filtering, using the source strength of the scintillator relative to OTR, and temporally sorting the prompt OTR from the delayed scintillator emission with the CCD gate. The spectral aspects are schematically shown in Fig. 4 with the COTR being enhanced in the NIR and the OTR being bluish white to the human eye. A first order mitigation of COTR is provided by a band pass filter centered at 400 nm (violet-rectangle) where the gain is close to one. To improve the signal-to-background ratio, one can employ a scintillator that radiates at

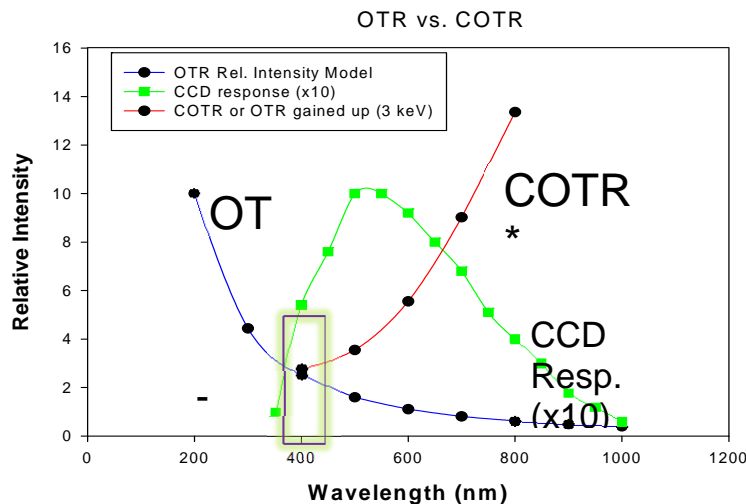


Figure 4: Comparison of the OTR and COTR spectral content and the CCD spectral response. The COTR gain is based on a model using the 3-keV slice energy spread [9].

within the same filter's transmission bandwidth. Some options are shown in Table 1. We have chosen the Yttrium-doped version of the LSO:Ce crystal, or LYSO:Ce, which also radiates in the 420-nm regime and is commercially available. At ASTA the standard stations after BC1 will have these crystals instead of the YAG:Ce crystals that radiate at 530 nm. We have chosen a scintillator thickness of 100 μm as a trade on efficiency (about 100 times that of OTR) and spatial resolution. Empirical evidence suggests we should have 8-10 μm spatial resolution (sigma) from the scintillator term.

The beam profile stations consist of the converter screens on a 4-position pneumatic actuator, the transport optics, and the digital CCD camera as shown in Fig. 5. The positions include an impedance screen, the crystal position, the OTR position, and a calibration target which includes line-pair patterns for checking spatial resolution *in situ*. Our optical imaging resolution term is about 15 μm with an 18-mm FOV. We use the Prosilica 5 Mpix digital cameras with Gig-E format. Image processing is done with a Java-based script online and a Matlab-based script off line. In the production station we use two filter wheels with 5 positions each loaded as listed in Table 2: one to allow the selection of neutral density (ND) filters for signal intensity adjustments and one to select bandpass filters matched to the YAG:Ce or LYSO:Ce scintillator emissions. Additionally, two linear polarizers are available for study of OTR polarization effects and for optimizing the point spread function for the horizontal and vertical planes [10].

Table 1: Summary of the properties of cerium-doped scintillators as compared to an OTR source.

Converter	Spectrum (FWHM)*, Peak	Efficiency	Response Time (FWHM)	Comment
YAG:Ce	487-587, 526 nm	1.0*	89 ns*	460 μ m T
LSO:Ce	380-450, 415 nm	0.46*	40 ns*	530 μ m T
YAP:Ce	350-400, 369 nm	~0.5	28 ns	460 μ m T
OTR	Broadband	0.0013*	~10 fs	Surface

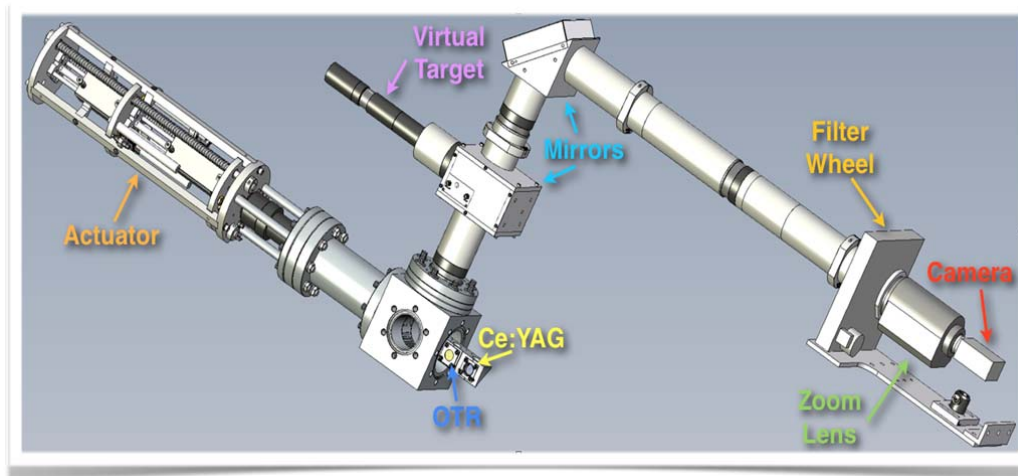


Figure 5: The beam profile station prototype showing the vacuum cube, converter screens, optics transport, filter wheel, final lens, and CCD camera.

Table 2: Summary of the options in the two filter wheels at each standard beam profiling station. The uses of filter wheel 2 options are also indicated.

Position #	Filter Wheel 1	Filter Wheel 2	Use
1	Clear glass	Clear glass	optics
2	ND 0.5	400x50 nm	LYSO:Ce
3	ND 1.0	550x40 nm	YAG:Ce
4	ND 2.0	Horiz. Pol.	OTR
5	ND 3.0	Vert. Pol.	OTR

3.5.3 Temporal Mitigation Option in Diagnostics

It has been established previously that one can sort the source terms for radiation with different response times such as the prompt OTR and the delayed emissions of scintillators. Clean separations have been done using the gating feature of the microchannel plate intensifier (MCP) coupled to the CCD camera and single micropulses [6]. Since the MCP may cost over \$10k, we pursued a less expensive option based on the digital CCD camera's integration gate. In Fig. 6, the upper images are the LYSO:Ce signal with different trigger delays from the reference time of 742.800 μ s. As the trigger moves later in time, the CCD integrated signal level drops as the intensity decays. However for the OTR case, we found a 41 ns delay on the CCD trigger was sufficient to suppress the signal from the prompt OTR as seen in images 6d) and 6e). The rejection ratio is at least 50. For a pulse train in the linac, a fast pulse kicker could be used to direct a single micropulse to the off-axis imaging station.

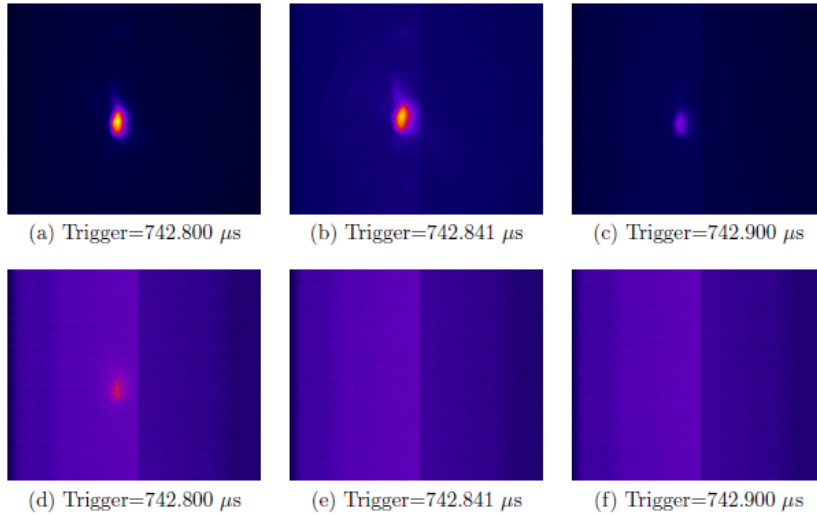


Figure 6: Beam images for different CCD trigger times for the chip integration period for the LYSO:Ce scintillator in (a-c) and the OTR source (d-f).

3.5.4 Summary

In summary, based on the experiences at other laboratories [8], we anticipate the μ BI will be present in our photo-injected beams at ASTA. At a minimum, the appearance of COTR due to the instability is expected after the second compressor. We also have the option to track the visibility of the COTR over a range of charges from 20 to 3200 pC per micropulse. We plan to use the spectral differences between OTR and COTR, the scintillators in combination with bandpass filters to enhance the signal-to-background ratio, and temporal gating techniques to mitigate the diagnostics effects by a total factor of 100-1000. This should address this diagnostics issue sufficiently to provide reliable beam profile measurements under such conditions.

3.5.5 Acknowledgments

The authors acknowledge the support of N. Eddy and R. Dixon of Fermilab and the production of the beam profiling stations by RadiaBeam based on Fermilab specifications.

3.5.6 References

1. Sergei Nagaitsev, “ILC-TA at NML”, ILC-TA Workshop at Fermilab, November 2006; J. Leibfritz, “Status of Plans for a Superconducting RF Test Facility at Fermilab”, Proc. of IPAC12, May 2012
2. E.L. Saldin, E.A. Schneidmiller, and M.V. Yurkov, Nucl. Instr. and Methods, A490, 1 (2002).
3. Z. Huang, M.Borland, P.Emma, J.Wu, C.Limborg, G. Stupakov, and J.Welch, Phys. Rev. ST-AB 7, 077701 (2004).
4. D. Dowell et al., Proc. of FEL07, WEAAU01, JACoW.org.
5. H. Loos et al., Proc. of FEL08, THBAU01, JACoW.org.
6. A.H. Lumpkin et al., Phys. Rev. ST-AB 12, 080702 (2009).
7. C. Behrens et al., Phys. Rev. ST-AB 15, 062801 (2012).
8. Alex H. Lumpkin, “Overview and Issues of Experimental Observations of Microbunching Instabilities”, Proc. of the Fifth Microbunching Instability Workshop, Pohang, Korea, May 8-10, 2013.
9. D. Ratner et al., Proc. of FEL08, Gyeongju Korea, TUPPH041, JACoW.org.
10. A.H. Lumpkin, et al., Phys. Rev. ST-AB 16, 102801 (2013).

3.6 Cancellation of Coherent Synchrotron Radiation Kicks with Optics Balance

S. Di Mitri¹, M. Cornacchia¹, S. Spampinati^{2,3}

¹Elettra Sincrotrone Trieste, S.S. 14 km 163,5 in AREA Science Park, 34149

Basovizza, Trieste, Italy

²University of Liverpool, Department of Physics, Liverpool, UK

³Cockcroft Institute, Sci-Tech Daresbury, Warrington, UK

Mail to: simone.dimitri@elettra.eu

3.6.1 Introduction

The advent of sub-ps electron beams with very high brightness in X-ray free electron lasers (FELs) [1–5] and in linear colliders [6, 7] has raised the awareness of the accelerator community to the effect of the coherent synchrotron radiation (CSR) on beam transverse emittance [8, 9]. The works reported in [10–14] trace the theoretical understanding of the CSR effects for ultra-relativistic beams. Experiments supporting that understanding may be found in [15–17]. In summary, the CSR field affects the electron transverse motion both with radial forces and by changing the particle energy in the dispersive line. In the latter case, the particle starts a betatron oscillation around a new reference trajectory, thus increasing its Courant-Snyder (C-S) invariant [18]. The synchrotron radiation emission is coherent for wavelengths comparable to the electron bunch length and it induces a variation of the particle energy that is correlated with the

longitudinal coordinate along the bunch. The removal of this correlation suppresses the CSR-driven emittance growth [19, 20].

A manner in which to cancel this perturbation by imposing certain symmetric conditions on the electron transport system has been suggested [20]. We first expand on this idea by quantitatively relating the beam C-S parameters to the emittance growth, and by providing a general scheme of CSR suppression with asymmetric optics, provided it is properly balanced along the line. We present the first experimental evidence of this cancellation with the resultant optics balance of multiple CSR kicks: the transverse emittance of a 500pC, sub-ps, high brightness electron beam is being preserved after the passage through the achromatic transfer line of the FERMI free electron laser [21] and emittance growth observed when the optics balance is intentionally broken. We finally show the agreement between the theoretical model and the experimental results. This study holds the promise of compact dispersive lines with relatively large bending angles, thus reducing costs for future electron facilities.

3.6.2 Suppression of CSR-driven Emittance Growth with Optics Symmetry

A way to cancel the CSR perturbations to the transverse emittance by imposing certain symmetric conditions on the electron transport system was suggested by D. Douglas for the special case of identical CSR kicks along the beam line [20]. This is usually the case when a beam is transported from the linac end to the undulator line, where the energy spread is small in order not to reduce the FEL gain, the bunch length is approximately constant and, consequently, CSR emission can be formulated by assuming identical beam parameters at all source points. The transfer line typically includes several identical dipole magnets; quadrupole magnets are also included for beam size control. The idea is that successive CSR kicks separated by π betatron phase advance (in the bending plane) add with opposite sign, and thus cancel the slice transverse mismatch with no or negligible emittance growth. To further explain and clarify, as a beam slice receives its first CSR kick, it starts betatron oscillating around a new dispersive trajectory that is defined by the dispersion function at the kick location times the CSR-induced energy shift. As the same slice is subject to an identical energy shift at the second CSR kick location, it moves to another dispersive trajectory. Owing to the optics symmetry and phase advance, the slice is already on the off-momentum trajectory to which it belongs after the 2nd kick, which thus cancels the action induced by the first one: after a double bend the slice ends on the appropriate off-momentum trajectory and the emittance growth is cancelled.

Several processes can interfere with proper CSR suppression. First, phase advance and optics functions at the homologous points of the lattice will in general depend on particle momentum offset, so that chromatic aberrations could corrupt the cancellation scheme. Second, the CSR single-kick approximation might not be valid for long dipole magnets followed by long drifts, so that CSR suppression may be limited by cross-coupling between energy shifts along the beam line. Third, transport matrix elements R_{51} , R_{52} are in general nonzero and, for a finite emittance beam, an electron path length from the initial excitation point to the compensation point may deviate from its design value, thus leaving the electron at a different longitudinal position along the bunch. This leads to different CSR-driven energy shifts. All these additional effects could partially corrupt the suppression scheme, although not necessarily invalidate the overall optics performance.

Compensating schemes like the one described above are implicitly or explicitly integrated in most high energy transfer lines of existing and up-to-date planned linac-driven FEL facilities [4, 22–24]. Cautious designs usually include short dipole lengths with small bending angles in order to minimize the individual CSR kicks strength, thus to avoid excessive emittance degradation even in case of non-ideal optics. With the only exception discussed in the next Chapter, experimental demonstration of successful CSR suppression in transfer lines is still lacking in the literature.

3.6.3 Cancellation of CSR Kicks Extended to Asymmetric Optics

3.6.3.1 *Theoretical Model*

In [25] we expanded on the idea proposed in [20] by quantitatively relating the beam C-S parameters to emittance growth and by providing a general scheme of CSR suppression with asymmetric optics. Later on, a more rigorous analytical derivation of the particle C-S invariant for arbitrary phase advance along the line was derived in [26] and found to be in good agreement with the experimental results. In the following, we recall the contents previously published in [25] and [26]. The analytical study allows the evaluation of the final emittance growth as a function of the optics *asymmetry*, and thus it applies also to asymmetric designs that may be required by other than optical constraints. The FERMI Spreader incorporates an asymmetric, balanced optics with π betatron phase advance between consecutive dipole magnets. The design has proved successful in preserving the 2 mm mrad normalized emittance of 500 pC, 40 μm and 80 μm long bunches. Emittance growth was observed when the optics balance was intentionally broken, evidence of good agreement between the theoretical model and the experimental results.

Our analysis considers the effect of the CSR on the particle transverse motion through the momentum dispersion only, justified by the fact that the kick provided by the radial forces defined as F_x^{eff} and G_{res} in [27] is small ($\leq 10^{-6}$) compared to $\theta\delta \approx 10^{-5}$, the product of the bending angle and the CSR induced relative energy deviation. The effect of radiation shielding [28–30] is neglected, since the wavelength at which the CSR starts being suppressed by the vacuum chamber [29], $\lambda \geq 2h(h/R)^{1/2} \cong 1\text{mm}$ (h is the vacuum chamber gap and R the bending radius) is much longer than the electron bunch length, $40\mu\text{m} \leq \sigma_z \leq 80\mu\text{m}$. Particle-field interactions on a scale much shorter than the bunch length such as those driving the so-called microbunching instability [31–34] are ignored on the ground that the analysis of the microbunching instability [32, 34] predicts a small gain for the experimental configuration of this study. For the sake of simplicity, the CSR emission and its interaction with the electrons is described below within the bounds of the single-kick approximation. The beam is ultra-relativistic and with a small energy spread relative to the mean energy (σ_δ), so that the small momentum compaction (R_{56}) of the FERMI achromatic system does not significantly change either the bunch length or the longitudinal charge distribution, at any point of the lattice ($|R_{56}\sigma_\delta| \leq 5\mu\text{m} \ll \sigma_z$). This is an important condition since it implies the same CSR energy kick in all the dipoles and it eventually allows the removal of the energy-position correlation established by the radiation emission. The relatively small σ_δ also allows us to neglect chromatic aberrations. The FERMI achromatic system, denoted henceforth as Spreader, is made of two identical double bend achromats (denoted

henceforth as DBA) [21, 35], as sketched in Fig.1. We recall that in a DBA with identical dipoles $|\eta|$ and $\left|\frac{d\eta}{ds}\right|$ (s is the longitudinal coordinate along the beam line) are the same, respectively, in all the dipoles [36]. Each FERMI DBA includes two FODO cells and their nominal setting ensures $\Delta\mu = \pi$ between the dipoles and a symmetric β and α , with values β_1 (α_1) and β_4 (α_4) in the dipoles of the first and the second achromat, respectively. The two DBAs are separated by 7 quadrupoles with a phase advance of π between them. In the following, the C-S formalism is applied to the particle motion in the Spreader with the aforementioned notation. Only the motion in the bending plane is considered.

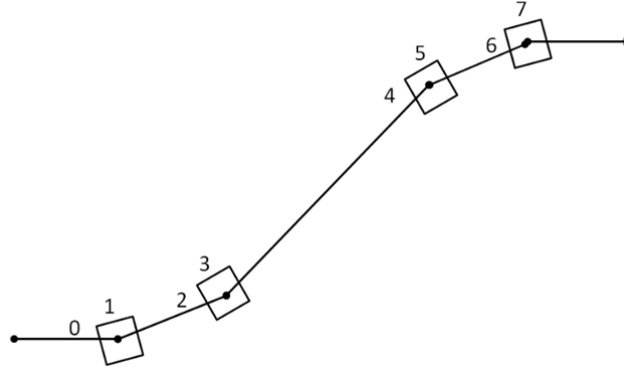


Figure 1. Sketch of the FERMI Spreader (not to scale). The design optics gives a betatron phase advance of π in the bending plane between two consecutive dipoles. There are quadrupoles between the dipoles (not shown here).

To illustrate how the optics balance works in such a rather compact system (approximately 30 m long in total for an operating energy range of 0.9–1.5 GeV), we start by assuming that the initial test particle coordinates relative to the reference trajectory are $x_0 = 0, x'_0 = 0$ and the initial particle invariant is $2J_0 = 0$. The variable subscript refers to the point along the lattice, as indicated in Figure 3.2. After the CSR kick in the first dipole, the particle transverse coordinates become:

$$\begin{cases} x_1 = \eta \delta_{CSR} \equiv \sqrt{2J_1 \beta_1} \cos \Delta\mu|_{\Delta\mu=0} = \sqrt{2J_1 \beta_1} \\ x'_1 = \eta' \delta_{CSR} \equiv -\sqrt{\frac{2J_1}{\beta_1}} (\alpha_1 \cos \Delta\mu + \sin \Delta\mu)|_{\Delta\mu=0} = -\alpha_1 \sqrt{\frac{2J_1}{\beta_1}} \end{cases}, \quad (1)$$

where η and η' are the energy dispersion function and its first longitudinal derivative at the dipole's location. After the CSR kick, the particle C-S invariant has grown to $2J_1 = \gamma_1 x_1^2 + 2\alpha_1 x_1 x'_1 + \beta_1 x_1'^2 = H_1 \delta_{CSR}^2$, where $H_1 = \gamma_1 \eta^2 + 2\alpha_1 \eta \eta' + \beta_1 \eta'^2$ and $\gamma_1 = \left(\frac{1 + \alpha_1^2}{\beta_1}\right)$. The particle coordinates are hereafter transported according to the C-S

formalism, taking into account π phase advance from one dipole magnet to the next. Owing to the symmetry of η and η' along the line and with the additional equality

$J_i = \gamma_i x_i^2 + 2\alpha_i x_i x_i' + \beta_i x_i'^2$ for $i = 3, 5, 7$, each successive CSR kick (particle's invariant) can be expressed in terms of the particle coordinates (particle's invariant) after the first kick. In order to reflect the experiment depicted in [25] and with reference to Fig. 1, we assume a symmetric optics in the first DBA only, arbitrary C-S parameters in the second DBA and arbitrary phase advance between the two achromats (with notation $C_{34} = \cos \Delta\mu_{34}$, $S_{34} = \sin \Delta\mu_{34}$). The particle coordinates at the Spreader's end turn out to be:

$$\begin{aligned} x_7 &= -\sqrt{2J_1\beta_1} \left(1 - \sqrt{\frac{\beta_5}{\beta_7}}\right) - \sqrt{2J_1\beta_7} 2\alpha_1 S_{34} \\ x_7' &= -\sqrt{\frac{2J_1}{\beta_1}} \alpha_1 \left(1 + \sqrt{\frac{\beta_5}{\beta_7}}\right) - \sqrt{\frac{2J_1}{\beta_7}} 2\alpha_1 (C_{34} - \alpha_5 S_{34}) + \sqrt{2J_1} \sqrt{\frac{\beta_1}{\beta_5\beta_7}} (\alpha_5 - \alpha_7) (1 - 2\alpha_1 S_{34}) \end{aligned} \quad (2)$$

For the special case of the nominal FERMI optics ($\beta_5 = \beta_7$, $\Delta\mu_{34} = \pi$), Eq. 2 leads to the C-S invariant:

$$2J_7 = 2J_1 4\alpha_1^2 \left(1 - \sqrt{\frac{\beta_5}{\beta_1}}\right)^2 \equiv 2J_1 X_{17}, \quad (3)$$

CSR-induced rms projected emittance growth can now be estimated by the determinant of the beam matrix, once the single-kick chromatic perturbation of CSR field onto the particles betatron motion is taken into account:

$$\varepsilon \equiv \left[\det \begin{pmatrix} \varepsilon_0 \beta + \eta^2 \sigma_{\delta, CSR}^2 & -\varepsilon_0 \alpha + \eta \eta' \sigma_{\delta, CSR}^2 \\ -\varepsilon_0 \alpha + \eta \eta' \sigma_{\delta, CSR}^2 & \varepsilon_0 \frac{1 + \alpha^2}{\beta} + \eta'^2 \sigma_{\delta, CSR}^2 \end{pmatrix} \right]^{1/2} = \varepsilon_0 \sqrt{1 + \frac{H}{\varepsilon_0} \sigma_{\delta, CSR}^2}, \quad (4)$$

By substituting Eq.3 into Eq.4 with the prescription $2J_1 = H_1 \delta^2$, $\sigma_{\delta, CSR}^2 = \langle \delta_{CSR}^2 \rangle$, we estimate a residual emittance growth at the Spreader's end:

$$\Delta\gamma\varepsilon = \gamma\varepsilon \left[\sqrt{1 + \frac{H_1 \sigma_{\delta, CSR}^2}{\varepsilon} X_{17}} - 1 \right] < 0.1 \mu\text{m}, \quad (5)$$

where ε is the unperturbed geometric emittance and γ is the relativistic Lorentz factor. Repeating the same reasoning for a two source points lattice, it can be shown that the idea reported in [20] (π phase advance between two identical dispersive elements) is a special case of the present treatment and that, in agreement with its finding it requires a fully symmetric optics for a complete CSR suppression.

3.6.3.2 Experimental Results

The experimental demonstration of cancellation of CSR kicks with optics balance is provided in Figures 2 – 4. The emittance growth was measured at the end of the Spreader as the phase advance between the two achromats and the C-S parameters in the second achromat were changed by varying a quadrupole's strength in the intermediate dispersion-free region, thus breaking the optics balance. The perturbed optics was

computed for each quadrupole's strength with the ELEGANT code [37] and used to evaluate Eq. 5. The experimental growth rate was higher for the shorter beam, in agreement with the expected CSR dynamics and well described by the analytical model. Minimum emittance growth was achieved for a π phase advance between the two achromats and design C-S parameters at the second achromat, again in agreement with the theoretical expectation. Since the cancellation of consecutive CSR kicks is independent from the strength of the individual CSR kick, this result suggests that large bending angles, compact dispersive lines can be designed and built in future high brightness electron accelerators-based FELs.

The parameters of the electron beam and of the line that characterize our experiment are listed in Table 1. The bunch length was magnetically compressed at 300 MeV by a factor $CF=8$ in a first experimental session and by $CF=16$ in a second one. The beam optics was matched [38] to the Spreader nominal lattice (see Fig.2) with a mismatch parameter [39] $\xi \cong 1.05$ in both transverse planes. The RMS projected emittance was measured with the quadrupole scan technique [40] at the beginning and at the end of the Spreader, in regions nominally free of momentum dispersion. Details about the emittance measurement can be found in [17]. Standard error propagation led to typical errors of a few percent on the central value of the beam optical parameters. A nonzero spurious dispersion was measured in the proximity of the screen used for the final emittance measurement. The dispersion value was the resultant of a linear, least mean-square fit applied to the beam position measured as the beam mean energy was varied over a normalized range of $\pm 1.0\%$ [41]. The dispersion uncertainty was dominated by the measurement reproducibility.

Table 1. Parameters of the electron beam (measured) and of the Spreader (by design). The beam parameters refer to compression factors of 8 and 16.

<i>Parameter</i>	<i>Value</i>	<i>Units</i>
Charge	500	pC
Mean Energy	1240 / 1155	MeV
Final Bunch Length, RMS	80 / 40	μm
Initial Norm. Emittance, RMS	2.3 ± 0.1 / 1.9 ± 0.1	$\mu\text{m rad}$
Dipole Bending Angle	52	mrad
H_1 -function	15	mm
$ R_{56} $	2.1	mm

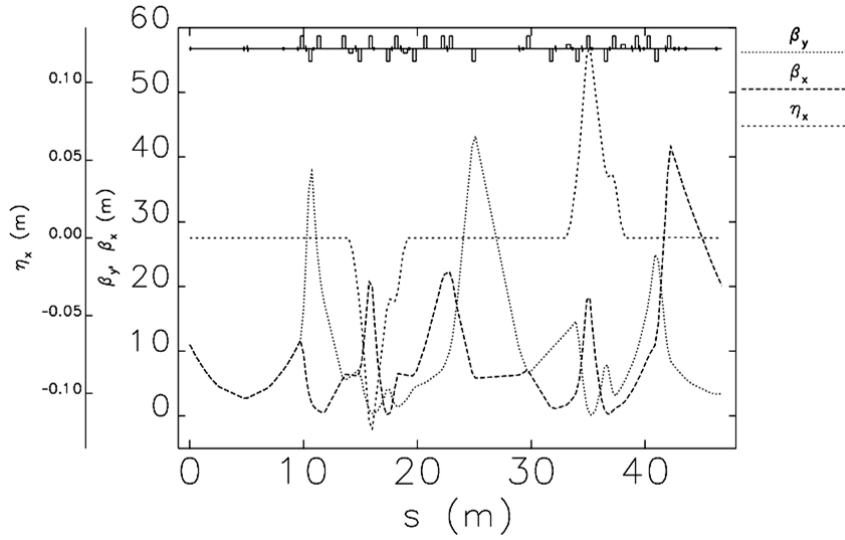


Figure 2. Nominal optics of the Spreader. The two MDBAs are identified by the closed dispersion bumps. The machine layout is sketched at the top.

The emittance and the dispersion was scanned versus the strength of a quadrupole (Q_SFEL01.02) placed between the two DBAs, as shown in Fig.3. While the nominal quadrupole setting is expected to cancel the CSR kicks by implementing asymmetric but properly balanced optics in the two DBAs with $\Delta\mu=\pi$ between the two achromats, any deviation from this setting would affect both the phase advance and the C-S parameters in the second DBA, thus breaking the optics balance. The phase advance was computed with the ELEGANT on the basis of the real machine setting and it is plotted in Fig.4 together with the final emittance increment as the strength of Q_SFEL01.02 was varied. As predicted, almost zero emittance growth was observed when the phase advance between the DBAs was π . As we vary the quadrupole strength away from its optimal setting, the emittance grows with a higher rate for the shorter beam. This can be explained by the fact that the CSR induced energy spread and the associated CSR kicks are inversely proportional to the bunch length [13]. The error bars in Fig.4 are computed as the square-root sum of the errors of the initial and final emittances and the contribution from the spurious dispersion, namely $\Delta\gamma\epsilon_\eta \approx \frac{\gamma(\eta\sigma_\delta)^2}{\beta}$. In this case, the total

relative energy spread is the square-root sum of the initial energy spread ($\sigma_\delta \sim 10^{-3}$, see Table 1) and of that induced by the CSR emission ($\approx 4 \cdot 10^{-4}$ and $\approx 2 \cdot 10^{-4}$ for CF=16 and CF=8, respectively). Given our beam parameters and the dipoles geometry, the latter was computed in the so-called *long bunch, long magnet* regime of CSR emission [13, 17] and used for the evaluation of Eq.6. Although a discrepancy at phase advances far from π is expected, other effects might be contributing to it. For instance, by varying the quadrupole strength in between the two MDBAs we were exciting some spurious dispersion that might have been corrupting the symmetry assumed for η and η' at all the dipoles, thus affecting the efficiency of CSR cancellation.

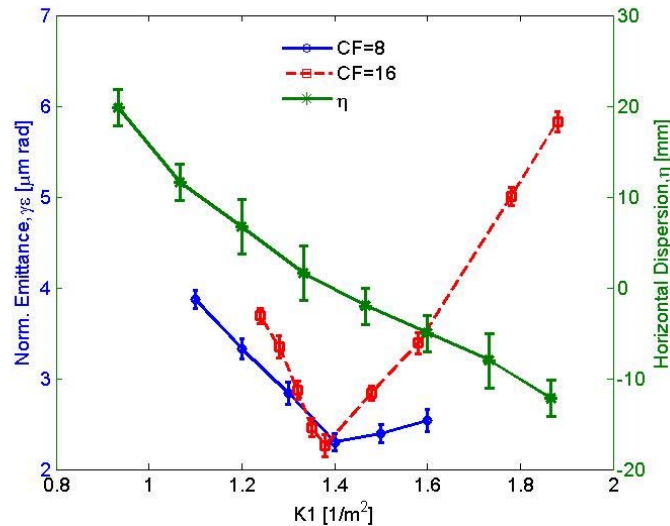


Figure 3. Horizontal emittance (circles for CF=8, squares for CF=16) and spurious horizontal dispersion (stars) measured at the Spreader end versus the strength of the quadrupole $Q_{\text{SFEL01.02}}$ placed between the two DBAs.

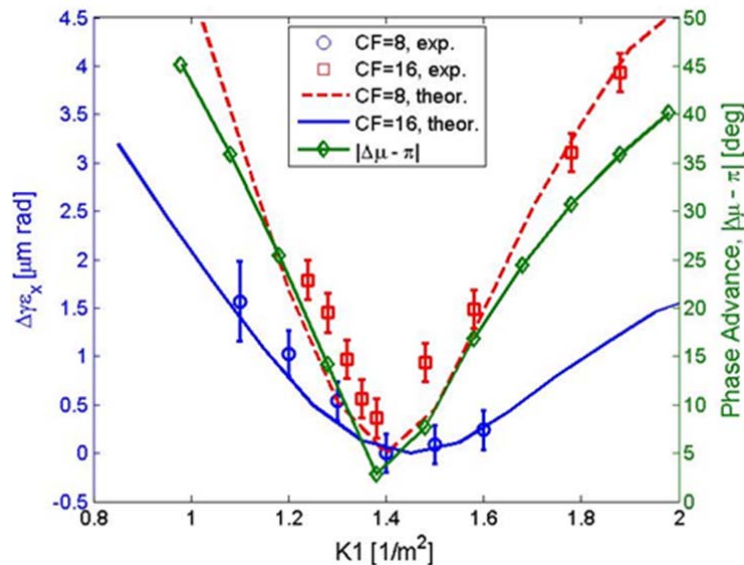


Figure 4. The horizontal normalized emittance growth at the end of the Spreader (markers with error bars) is plotted as a function of the strength of the quadrupole $Q_{\text{SFEL01.02}}$ placed between the two DBAs. The squares (circles) are for a compression factor of 16 (8). The horizontal betatron phase advance between the DBAs (diamonds) was computed with ELEGANT on the basis of the experimental machine settings; the absolute value of its distance from π is also shown. The dashed (solid) line is the evaluation of Eq.6 for CF=16 (8).

3.6.4 Conclusions

The original idea for the suppression of CSR kicks with optics symmetry [25] is explained by applying the C-S formalism to dog-leg-like achromatic lines [26]. Alternative solutions with asymmetric optics are allowed, as shown by Eq.5. More

precisely, this analytical result allows for the evaluation of the final emittance growth as a function of the optics *asymmetry*, and thus it applies also to asymmetric designs that may be required by other than optical constraints. Asymmetric, but properly balanced optics were present in the FERMI Spreader, together with the relative phase advance of π between the achromats, allowing for the preservation of the 2 μm normalized emittance of 500 pC, 40 μm and 80 μm long bunches. The emittance growth was measured as the phase advance was changed and the optics balance was broken. The growth rate was higher for the shorter beam, in agreement with the expected CSR dynamics and the experimental behavior is well described by the analytical model. The results presented in this article suggest that compact dispersive lines can be designed and built in future high brightness electron accelerators, such as linac-based FELs or linear colliders. This study should be continued and extended in order to further explore the development of the CSR instability in the presence of larger bending angles ($\geq 10^\circ$) and very short beams ($\sim 1 \mu\text{m}$). A detailed simulation study that would include the propagation of CSR in the drift sections is pending.

3.6.5 References

1. P. Emma *et al.*, Nature Photon. **4**, 641 (2010).
2. W. Ackermann *et al.*, Nature Photon. **1**, 336 (2007).
3. D. Pile, Nature Photon. **5**, 456 (2011).
4. M. Altarelli, Nucl. Instrum. Methods Phys. Res., Sect. B **269**, 24 (2011).
5. E. Allaria *et al.*, Nat. Photon. **233**, 699 (2012).
6. International Linear Collider, *Reference Design Report* (2007).
<http://www.linearcollider.org/about/Publications/Reference-Design-Report>
7. J. Ellis *et al.*, Nature **409** (2001).
8. R. Talman, Phys. Rev. Lett. **56**, 1429 (1986).
9. T. Nakazato, M. Oyamada, N. Niimura, S. Urasawa, O. Konno, A. Kagaya, R. Kato, T. Kamiyama, Y. Torizuka, T. Nanba, Y. Kondo, Y. Shibata, K. Ishi, T. Ohsaka, and M. Ikezawa, Phys. Rev. Lett. **63**, 2433 (1989).
10. Ya.S. Derbenev, J. Rossbach, E.L. Saldin, and V.D. Shiltsev, TESLA-FEL 95-05 (1995).
11. B. E. Carlsten and T. O. Raubenheimer, Phys. Rev. E **51**, 1453 (1995).
12. Ya.S. Derbenev and V.D. Shiltsev, SLAC-PUB-7181 (1996).
13. E.L. Saldin, E.A. Schneidmiller, and M.V. Yurkov, Nucl. Instrum. Methods Phys. Res., Sect. A **398**, 373 (1997).
14. R. Li and Ya.S. Derbenev, JLAB-TN-02-054 (2002).
15. M. Dohlus and T. Limberg, Nucl. Instrum. Methods Phys. Res., Sect. A **393** 494 (1997).
16. H. Braun, F. Chautard, R. Corsini, T.O. Raubenheimer, and P. Tenenbaum, Phys. Rev. Lett. **84**, 658 (2000).
17. S. Di Mitri, E.M. Allaria, P. Craievich, W. Fawley, L. Giannessi, A. Lutman, G. Penco, S. Spampinati, and M. Trovo', Phys. Rev. ST Accel. Beams **15**, 020701 (2012).
18. E.D. Courant and H.S. Snyder, Annals of Phys. **3** 1 (1958). See also: S.Y. Lee, *Accelerator Physics*, published by World Scientific Publishing Co. Pte. Ltd., reprinted 2007, ISBN-13 978-981-256-182-4 (2007).
19. P. Emma and R. Brinkmann, SLAC-PUB-7554 (1997).
20. D. Douglas, JLAB-TN-98-012 (1998).
21. C. J. Bocchetta *et al.*, "FERMI@Elettra FEL Conceptual Design Report", ST/F-TN-07/12(2007). <https://www.elettra.trieste.it/FERMI/index.php?n=Main.CDRdocument>
22. "LCLS Conceptual Design Report", SLAC Report No. SLAC-R-593 (2002).
<http://www-ssrl.slac.stanford.edu/lcls/cdr/>
23. "SwissFEL Conceptual Design Report", edited by R. Ganter, PSI Bericht 10-04 (2012).

- <http://www.psi.ch/swissfel/internal-reports>
24. H.S. Kang and S.H. Nam, in Proceedings of the 32th Intern. Free Electron Laser Conf., MOPC19, Malmö, Sweden (2010).
 25. S. Di Mitri, M. Cornacchia, S. Spampinati, Phys. Rev. Letters **110**, 014801 (2013).
 26. S. Di Mitri and M. Cornacchia, “Electron beam brightness in linac-drivers for free electron lasers”, Physics Reports (2014), in press.
 27. R. Li and Ya.S. Derbenev, JLAB-TN-02-054 (2002).
 28. J.S. Nodvick and D. Saxon, Phys. Rev. **96**, 1 (1954).
 29. R.L. Warnock, SLAC-PUB-5375 (1990).
 30. G.V. Stupakov and I.A. Kotelnikov, Phys. Rev. ST Accel. Beams **6**, 034401 (2003).
 31. E.L. Saldin, E.A. Schneidmiller, and M.V. Yurkov, Nucl. Instrum. Methods Phys. Res., Sect. A **490** 1 (2002).
 32. S. Heifets, S. Krinsky, and G. Stupakov, Phys. Rev. ST Accel. Beams **5**, 064401 (2002).
 33. Z. Huang and K.-J. Kim, Phys. Rev. ST Accel. Beams **5**, 074401 (2002).
 34. Z. Huang, M. Borland, P. Emma, J. Wu, C. Limborg, G. Stupakov, and J. Welch, Phys. Rev. ST Accel. Beams **7**, 074401 (2004).
 35. A. Zholents, K. Chow, R. Wells, D. Bacescu, B. Diviacco, M. Ferianis, and S. Di Mitri, ST/F-TN-07/01 (2007) and LBNL-62345 (2007). The design lattice was later modified by one of the authors (S. Di Mitri).
 36. A. Jackson, Part. Accel. **22** (1987).
 37. M. Borland, Advanced Photon Source LS-287 (2000).
 38. S. Di Mitri, M. Cornacchia, C. Scafuri, and M. Sjoström, Phys. Rev. ST Accel. Beams **15**, 012802 (2012).
 39. M. Sands, Report No. SLAC-AP-85 (1991).
 40. M. G. Minty and F. Zimmermann, Report No. SLAC-R-621 (2003).
 41. S. Di Mitri, L. Froehlich, and E. Karantzoulis, Phys. Rev. ST Accel. Beams **15**, 061001 (2012).

4 Workshop and Conference Reports

4.1 ICFA Mini Workshop on SuperKEKB beam commissioning

U. Wienands, SLAC
Mail to: uli@slac.stanford.edu

About 70 registered attendees from half-a dozen labs around the world met for 2 1/2 days in November 2013 at KEK to review the state-of the art in beam-commissioning tools and their application to SuperKEKB. The workshop was held under ICFA and EuCARD2 auspices. Agenda and slides can be found at

<http://kds.kek.jp/conferenceDisplay.py?ovw=True&confId=12760>.

SuperKEKB will be using beams of extremely small emittance (5 by 0.05 nm-r) and high intensity (up to 3.6 A) to achieve close to 10^{36} cm⁻²s⁻¹ luminosity in asymmetric e^+e^- collisions, exceeding that of KEKB and PEP-II by close to two orders of magnitude. Needless to say the challenges in commissioning this facility will be formidable.

Besides giving an overview of SuperKEKB design features the sessions were loosely grouped by topic: Emittance tuning and optics, electron-cloud effects, Intensity and HOM effects, and IR and background issues.

- Emittance tuning and getting the beam optics under control may present one of the foremost challenges for SuperKEKB, however, progress in this field has been very impressive. At the LHC, betas within 5% of the design values are achieved by lattice tuning using the ac dipole to excite the beam. This technique can be (and has been) used at lepton colliders even easier as radiation damping prevents permanent emittance growth. Expanding on the technique, SVD can be used to clean up the tune spectrum, thus improving data quality (which often limits the effectiveness). At LNF, a new low-emittance tuning algorithm has been developed and tested at Diamond and the SLS that achieves low emittance possibly in a more efficient and faster way than other techniques. Cornell uses a system based on turn-by-turn oscillations and BMAD to reach new lows in beam emittance, although interestingly enough the results are not always reproducible. All-in-all a vast body of experience is now at hand.
- Electron-cloud effects came to the fore in PEP-II and KEKB, and in the wake of these machines a vast body of information and experimental data has been amassed through experiments at ANL, PEP-II, CERN and CEsrTA. In fact, the CEsrTA program is ongoing and providing detailed, quantitative understanding of the effect and the efficiency of its mitigation. It is through all of this work that one may argue that everything reasonable was done at SuperKEKB (chamber-wall coating, antechambers, grooves, and cleaning electrodes) and there is reason for optimism that e-cloud will not limit the machine performance.
- HOM heating and discharges are an ever-present threat for high-current machines especially with short bunches. The HOM-absorbing techniques developed at PEP-II will go a long way to mitigate such events, although if they happen they can be somewhat tricky to diagnose given their transient nature. Various instabilities with rather unusual signature were seen at PEP-II that were eventually traced to vacuum events caused by voltage break-down.
- IR and background tuning were a major challenge at the first *B*-Factories and are expected to be just that at SuperKEKB also. A temporary background detection system (“BEAST”) will be installed before the Belle II detector rolls in. Especially with continuing injection being an integral part of the design due to the short beam lifetime, background may be an operational limit until mitigated enough by vacuum scrubbing and beam-collimation. Background estimation and beam collimation being notoriously difficult to do there is an area ripe for increased collaborative effort; this workshop may have provided the initial spark for a collaborative effort between KEK and LNF in this field; LNF having done a significant amount of work in this topic for the Super*B* project and also being involved in TLEP background estimation. In this context it is to be remarked that a body of data exists from both KEKB and PEP-II that allows to anticipate the vacuum processing (scrubbing) rate *vs* the accumulated Ah of beam current with a high degree of confidence.
- Last-not-least the demands on the SuperKEKB injector chain are considerably higher than at KEKB, with relatively high charges and the demands of continuing injection for low emittance and good matching. We were shown the impressive new rf gun and linac on our tour. As it is, wakefields will limit the

performance and the experience at the SLAC linac should provide important guidance.

4.1.1 **Review of Extant Facilities and Lessons Learned (Convenor: J.T. Seeman, SLAC)**

Work and lessons-learned from several facilities around the world were presented: LHC (R. Tomas, F. Zimmermann, CERN), CESR-TA (D. Rubin, Cornell), BEPC-II (J. Zhou, IHEP), PEP-II (M. Sullivan, SLAC) and the τ -Charm plans at LNF (M. Biagini, LNF). Optics and emittance tuning have reached a high state of maturity, and the agreement between expectation and measured emittance esp. at CESR-TA is impressive. Electron-cloud effects have been parametrized to a significant extent, giving some confidence in the degree of effectiveness of mitigation methods. IBS and other emittance-diluting effects are to a certain degree understood although some differences to simulation results remain to be understood.

4.1.2 **More Lessons-learned for SuperKEKB (Convenor: Y. Funakoshi, KEK)**

This session heard reports on beam dynamics work and tuning from CESR-TA (J. Shanks, K. Sonnad, M. Ehrlichman, Cornell) and ATF-II and FACET (G. White, SLAC).

At SuperKEKB, emittance tuning is one of the most critical issues. The target vertical emittance at zero current is 5...7 pm. The vertical emittance routinely obtained at CEsrTA is less than 10.5 pm for the positron beam. Simulation shows that 5 pm emittance should be possible, and the residual vertical emittance and x-y coupling in the ring after tuning are as small as the expectation. This means that low emittance tuning in the sense of the optics corrections is successful. This is encouraging for SuperKEKB. However, the achieved value of the vertical emittance at CEsrTA is twice as high as that in tracking studies. The reason for this discrepancy seems interesting for SuperKEKB. It should be also noted that there is no low-beta insertion at CEsrTA unlike SuperKEKB. Emittance preservation in the injector linac is another critical issue, since the required linac beam emittance for SuperKEKB is much smaller than that for KEKB. The following table summarizes linac emittance related parameters.

The parameters at the SuperKEKB linac and FACET are not very different. Beam commissioning of the SuperKEKB linac has started. The experience of emittance preservation at FACET such as tuning with BBA and wake-field bumps should be fully utilized at SuperKEKB.

Table: Comparison of linac emittance related parameters.

	SuperKEKB	KEKB	FACET
initial energy (e^+)	20 MeV		1.2 GeV
initial emittance (e^+) ($\gamma\epsilon_x$)	6 μm		30 μm
initial emittance (e^+) ($\gamma\epsilon_y$)	6 μm		3 μm
bunch charge (e^+)	5 nC		1.6 / 3.2 nC
emittance at exit (e^+) ($\gamma\epsilon_x$)	50 μm (target)	300 μm (achieved)	60 μm (achieved)
emittance at exit (e^+) ($\gamma\epsilon_y$)	20 μm (target)	300 μm (achieved)	6 μm (achieved)
energy at exit (e^+)	4 GeV	3.5 GeV	20.35 GeV
Initial energy (e^-)	1.1 GeV		
Initial emittance (e^-) ($\gamma\epsilon_x$)	92 μm		
Initial emittance (e^-) ($\gamma\epsilon_y$)	7 μm		
bunch charge (e^-)	4 nC		
emittance at exit (e^-) ($\gamma\epsilon_x$)	100 μm (target)	2100 μm (achieved)	
emittance at exit (e^-) ($\gamma\epsilon_y$)	20 μm (target)	2100 μm (achieved)	
energy at exit (e^-)	7 GeV	8 GeV	

4.1.3 Linac and DR Commissioning (Convenor: K. Oide, KEK)

A series of talks by T. Mura, T. Mori, M. Kikuchi, H. Ikeda (all KEK) presented the upgraded injector chain for SuperKEKB. Electron and positron source will be new as will be a new positron damping ring. The new electron source is undergoing first beam-commissioning. With significantly higher performance requirement than for KEKB, the beam commissioning team will be challenged to achieve the required beam emittance at intensity up to 5 nC. Y. Renier (CERN) presented emittance tuning results for the ATF ring pushing the emittance down to 6.5 pmr in only two iterations.

Each subsystem of the injector chain appears well designed and manufactured taking a number of new effects and ideas into account. Technically, no fatal issues have been found so far although there are issues with limited human resources to finish construction & commissioning within the given schedule. As there is no “damping ring group”, coordination will be extremely important.

4.1.4 Ring Optics and Intensity Effects (Convenor: F. Zimmermann, CERN)

The Session on Ring Optics and Intensity Effects featured presentations by Hiroshi Sugimoto (KEK), Akio Morita (KEK), Demin Zhou (KEK), Kazuhito Ohmi (KEK),

John Flanagan(KEK), Alexander Novokhatski (SLAC), and Uli Wienands (SLAC). The topics covered are illustrated in the following diagram.

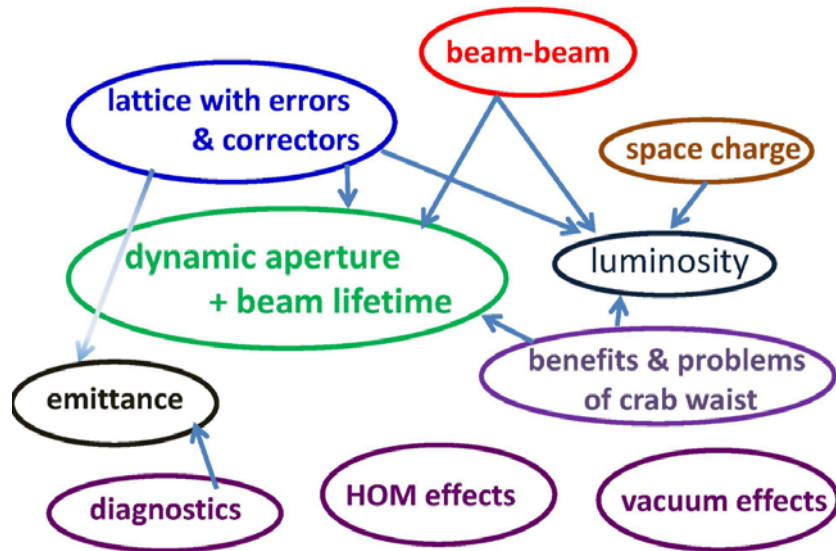


Figure: Themes discussed at the SuperKEKB Commissioning Workshop in the Session on Ring Optics and Intensity Effects.

This workshop session concluded that several important issues have been settled, such as low emittance tuning, electron cloud, vacuum design, and beam-size diagnostics. However, a number of issues are still outstanding, including the off-momentum optics, and the effects of nonlinear fields, beam-beam interaction, and space charge. To address the latter, the session established a “to do” list, which features off-momentum optics correction, identification of dominant lattice nonlinearities affecting the luminosity in both rings, development of nonlinear optics measurement & correction schemes, optimization of the nonlinear optics and dynamic aperture including space-charge and beam-beam effects, compensation scheme for space charge, and correction scheme with/for crab waist.

4.1.5 IP Commissioning/Background and Lifetime (Convenor: M. E. Biagini, INFN-LNF)

We heard presentations regarding the PEP-II IR (W. Kozanecki, Saclay), Background and lifetime studies (M. Boscolo, LNF) and SuperKEKB background and IR work (T. Oki, Y. Arimoto, T. Ishibashi, H. Nakayama, all KEK).

Among all the subsystems of the SuperKEKB accelerator, the Interaction Region is probably the most crucial and difficult to handle with. Many SC magnets are packed in a relatively small space, including those for the correction of the detector field, nonlinearities, orbit and magnets leakage. The magnets will need to be accurately measured and positioned, since any error will reflect on the machine performances. Very tiny beams must be put in collision and kept stable, in spite of disturbances such as vibrations, orbit deviations, injection jitter, errors, etc. For this reason fast IP feedbacks are needed to keep the beams in collision and assure a constant peak luminosity.

The detector has to be protected from the high background that is a consequence of the beam parameters (like Touschek and beam-gas processes) and of the high luminosity (such as Radiative Bhabha, Gammas). Accurate simulations of all possible sources, with tracking of lost particles and estimate of beam loss rates are crucial to take adequate countermeasures (mask, collimators, shielding). The collimators will help in reducing background, however they introduce additional complications: their influence on the ring impedance has to be minimized, a clever geometry studied and materials able to cope with HOM heating and wake fields need to be tested. A proper choice of the collimator locations is also very important, to maximize their effect and at the same time reduce the impact on the core beam. In SuperKEKB the same collimators used in KEKB are kept for HER ring, while newly designed ones will be mounted on the LER.

A huge effort is being put on the optimization of the IR design and construction. The experience of the previous B-Factories, with similar problems and different solutions, is extremely useful for comprehension of the possible issues and remediation techniques. Possible perturbations are being taken into account, and solutions for most of the issues have been found. IP feedbacks are being studied. Different design and materials for collimators have been tested, keeping in mind the high beam current. Simulations of beam background and design of mitigation are in progress. It is very important that there is an active collaboration between the people who simulate them for checking the results and take proper countermeasures, and it is essential that the Detector and Machine groups strictly collaborate in understanding and mitigating the backgrounds sources.

4.1.6 Feedback, Injection and Commissioning Strategies, (Convenor: J. Flanagan, KEK)

Wednesday morning's session focused on RF and bunch-by-bunch feedback systems, with a Dafne status report and discussion of general commissioning issues. We heard presentations by C. Rivetta and U. Wienands (SLAC), M. Tobiya (KEK) and A. Drago (LNF). The common theme in these talks revolved about high-beam-current issues and how to prevent instability due to beam-loading and impedance-related effects. Notably, feedback systems e.g. at DAFNE adopt lower-noise and higher-resolution (going from 8 to 12 bits) electronics to prevent luminosity reduction at higher gain. Model-assisted tuning for the rf systems was used at PEP-II and has been brought to bear on the LHC as well. The session ended with a well-received presentation by J. Seeman (SLAC) on general commissioning strategies at colliders, outlining the various trade-offs and balancing acts that need to be mastered for beam commissioning to be rapid and successful.

In summary, the workshop provided for an overview of state-of-the-art accelerator tuning techniques and their applicability to SuperKEKB. While challenging, the body of data in existence is now so large that commissioning progress can be anticipated with at least some degree of confidence.

An expanded version of this summary can be found at the workshop website.

5 Recent Doctorial Theses

5.1 Study on Electron Beam Optimization at PAL-XFEL Injector Test Facility

Moonsik Chae

Mail to: cmswill@postech.ac.kr

Graduation date: 14 February 2014

Institution: Pohang Accelerator Laboratory, Korea

Supervisor: Prof. In Soo Ko

Abstract:

Pohang Accelerator Laboratory started the construction of the fourth-generation synchrotron radiation facility, PAL-XFEL, in April 2011. This project aims to generate a 0.1 nm hard X-ray radiation using an electron beam of 0.2 nC charge and 10 GeV energy. To get operation experiences and to demonstrate the performances of sub-systems for the PAL-XFEL, Injector Test Facility (ITF) has been constructed. This facility includes an RF gun, two accelerating structures, two modulator and klystron systems, a laser system, a laser heater and several diagnostics. The current RF gun installed at ITF has four holes at the second cell so as to suppress undesirable multipole modes. PARMELA simulation has been carried out to analyse the effect of each multipole mode in the gun cavity to the emittance growth. Experimental calibration was carried out for screens, spectrometers and a transverse RF deflector. The projected emittance were measured at the end of the beamline with various conditions, i.e. various RF phases, transverse laser sizes, laser pulse lengths in order to find an optimized operating condition of an electron beam. The emittance was measured by the single quadrupole scan. The emittance of a low charge electron beam was also measured with various laser beam sizes. Requirements to measure an smaller optimized emittance value are also discussed.

6 Forthcoming Beam Dynamics Events

6.1 55th ICFA Advanced Beam Dynamics Workshop on High Luminosity Circular e^+e^- Colliders for Higgs Factory (HF2014)

The 55th ICFA Advanced Beam Dynamics Workshop on High Luminosity Circular e^+e^- Colliders – Higgs Factory (HF2014) will take place October 9-12, 2014 in Hotel Wanda Realm, Beijing, China. It will be hosted by the Institute of High Energy Physics (IHEP), Chinese Academy of Sciences (CAS).

Since the discovery of the Higgs particle in 2012 at CERN, there have been two new initiatives for a very large future circular collider, namely, the FCC in Europe and the CEPC-SppC in China. Both would serve as a Higgs factory in the first stage. ICFA encouraged these initiatives and issued a statement that “*ICFA supports studies of*

energy frontier circular colliders and encouraged global coordination.” The HF2014 workshop will focus on a circular e⁺e⁻ collider for a Higgs factory. The topics include:

- Parameters
- Optics
- Interaction region and machine-detector interface
- Synchrotron radiation and shielding
- Superconducting RF
- Injectors and injection
- Orbit stability and beam instability
- Polarization
- Instrumentation and control
- “Green” Higgs factory

The workshop website is:

<http://hf2014.ihep.ac.cn>

Deadline for abstract submission: July 15, 2014

Deadline for registration: August 31, 2014

International Organizing Committee (IOC):

Michael Benedikt (CERN)
 Marica Biagini (INFN-LNF)
 Alain Blodel (U. of Geneva)
 Alex Chao (SLAC)
 Swapan Chattopadhyay (Cockcroft Inst.)
 Weiren Chou (Fermilab, Co-Chair)
 Jie Gao (IHEP)
 Stuart Henderson (Fermilab)
 Andrew Hutton (JLab)
 Eugene Levichev (BINP)
 Xinchou Lou (IHEP)
 Katsunobu Oide (KEK)
 Qing Qin (IHEP, Co-Chair)
 Dave Rice (Cornell U.)
 John Seeman (SLAC)
 Chuanxiang Tang (Tsinghua U.)
 Jorg Wenninger (CERN)
 Frank Zimmermann (CERN)

Local Organizing Committee (LOC):

Huiping Geng (IHEP)
 Yinghua Jia (IHEP)
 Shuzhen Liu (IHEP)
 Qian Pan (IHEP)
 Tongzhou Xu (IHEP, Chair)
 Shan Zeng (IHEP)
 Ning Zhao (IHEP)

Contact:

For administrative support:

Ms. Qian Pan, hf2014@ihep.ac.cn, tel: +86-10-88235014, fax: +86-10-88233374

For scientific program support:

Dr. Huiping Geng, hf2014@ihep.ac.cn, tel: +86-10-88236505

6.2 International Beam Instrumentation Conference (IBIC 2014)

The Third International Beam Instrumentation Conference, IBIC 2014 will be held in Monterey, California, USA on September 14 through 18, 2014. Like its predecessors, the Beam Instrumentation Workshop (BIW) and the Diagnostics and Instrumentation for Particle Accelerators Conference (DIPAC), this conference is dedicated to exploring the physics and engineering challenges of beam diagnostics and measurement techniques for charged particle beams. IBIC 2014 will be hosted by the SLAC National Accelerator Lab. The 3.5 day scientific program will include tutorials, invited, and contributed talks as well as poster sessions. Following the conference there will be the opportunity for tours of the SLAC National Accelerator Lab.

Registration will open in April 2014. An exhibition for vendors of beam instrumentation and diagnostics related products is an integral part of the conference. Further information about this exhibition will be available on the conference website. We look forward to seeing you in Monterey.

Conference website:

<http://conf-slac.stanford.edu/ibic-2014/>

6.3 XXIV Russian Particle Accelerators Conference

The Program and Organizing Committees of the Conference invite you to participate in the serial XXIV Russian Particle Accelerators Conference, RuPAC 2014

Scope

Information exchange and discussion of various aspects of the accelerator science and technology, physics of charged particle beams, development of new accelerators, upgrade of the existing facilities, application of accelerators for basic and applied R&D

Conference Topics

- 1 Modern trends in accelerators
- 2 Particle dynamics in accelerators, optimization of their operation modes, cooling methods, new methods of acceleration
- 3 Colliders
- 4 Cyclic and linear accelerators of high intensity
- 5 Synchrotron radiation sources and free-electron lasers
- 6 Magnetic and vacuum systems, power supplies
- 7 Superconducting technologies in accelerators
- 8 Accelerating structures and high power RF systems
- 9 Control and diagnostic systems
- 10 Ion sources and electron guns
- 11 Accelerators for medical and industrial applications
- 12 Radiation problems in accelerators

Venue

The Conference will be held in the First Science City of Russia, Obninsk, from October 6 to 10, 2014, and will be hosted by the Institute for Physics and Power Engineering named after A.I. Leypunsky.

Procedure

The working languages of the Conference are Russian and English. The Conference program includes invited and oral talks as well as poster presentations. The information on the time given for each presentation, on the office equipment installed in the lecture hall, and on the size of the poster session posterboards will be available on the Conference website.

Dates and Deadlines

Second Announcement	May 30, 2014
Registration and abstract submission deadline	July 30, 2014
Program Committee's notification of acceptance and form of paper submission	August 15, 2014

Registration

All participants and accompanying persons should pass the preliminary registration procedure on the Conference website <http://www.ippe.ru/ninf/rupac.php> by filling the relevant Registration form.

Speaking authors of the Conference contributions have to pass registration at web-page <http://oraweb.cern.ch/pls/rupac2014/profile.html> as well (that is indispensable condition for the contribution to be accepted for presentation at the Conference)

Publication of the Conference Proceedings

All papers accepted by the Program Committee and presented at the Conference will be published in electronic format at website www.jacow.org.

For the papers to be included in the Conference program their abstracts in English have to be submitted before July 30, 2014 via web-page <http://oraweb.cern.ch/pls/rupac2014/profile.html>.

The procedure of submitting the abstracts mentioned above is required for all contributions (invited, oral and poster). The abstracts' size should not exceed 1200 symbols.

The authors will be informed on the Program Committee's decision concerning the acceptance of their papers before August 15, 2014. The list of authors and paper titles will be available on the Conference website.

7 Announcements of the Beam Dynamics Panel

7.1 ICFA Beam Dynamics Newsletter

7.1.1 Aim of the Newsletter

The ICFA Beam Dynamics Newsletter is intended as a channel for describing unsolved problems and highlighting important ongoing works, and not as a substitute for journal articles and conference proceedings that usually describe completed work. It is published by the ICFA Beam Dynamics Panel, one of whose missions is to encourage international collaboration in beam dynamics.

Normally it is published every April, August and December. The deadlines are 15 March, 15 July and 15 November, respectively.

7.1.2 Categories of Articles

The categories of articles in the newsletter are the following:

1. Announcements from the panel.
2. Reports of beam dynamics activity of a group.
3. Reports on workshops, meetings and other events related to beam dynamics.
4. Announcements of future beam dynamics-related international workshops and meetings.
5. Those who want to use newsletter to announce their workshops are welcome to do so. Articles should typically fit within half a page and include descriptions of the subject, date, place, Web site and other contact information.
6. Review of beam dynamics problems: This is a place to bring attention to unsolved problems and should not be used to report completed work. Clear and short highlights on the problem are encouraged.
7. Letters to the editor: a forum open to everyone. Anybody can express his/her opinion on the beam dynamics and related activities, by sending it to one of the editors. The editors reserve the right to reject contributions they judge to be inappropriate, although they have rarely had cause to do so.

The editors may request an article following a recommendation by panel members. However anyone who wishes to submit an article is strongly encouraged to contact any Beam Dynamics Panel member before starting to write.

7.1.3 How to Prepare a Manuscript

Before starting to write, authors should download the template in Microsoft Word format from the Beam Dynamics Panel web site:

<http://www-bd.fnal.gov/icfabd/news.html>

It will be much easier to guarantee acceptance of the article if the template is used and the instructions included in it are respected. The template and instructions are expected to evolve with time so please make sure always to use the latest versions.

The final Microsoft Word file should be sent to one of the editors, preferably the issue editor, by email.

The editors regret that LaTeX files can no longer be accepted: a majority of contributors now prefer Word and we simply do not have the resources to make the conversions that would be needed. Contributions received in LaTeX will now be returned to the authors for re-formatting.

In cases where an article is composed entirely of straightforward prose (no equations, figures, tables, special symbols, etc.) contributions received in the form of plain text files may be accepted at the discretion of the issue editor.

Each article should include the title, authors' names, affiliations and e-mail addresses.

7.1.4 Distribution

A complete archive of issues of this newsletter from 1995 to the latest issue is available at

<http://icfa-usa.jlab.org/archive/newsletter.shtml>.

This is now intended as the primary method of distribution of the newsletter.

Readers are encouraged to sign-up for electronic mailing list to ensure that they will hear immediately when a new issue is published.

The Panel's Web site provides access to the Newsletters, information about future and past workshops, and other information useful to accelerator physicists. There are links to pages of information of local interest for each of the three ICFA areas.

Printed copies of the ICFA Beam Dynamics Newsletters are also distributed (generally some time after the Web edition appears) through the following distributors:

Weiren Chou	chou@fnal.gov	North and South Americas
Rainer Wanzenberg	rainer.wanzenberg@desy.de	Europe ⁺⁺ and Africa
Toshiyuki Okugi	toshiyuki.okugi@kek.jp	Asia ^{**} and Pacific

⁺⁺ Including former Soviet Union.

^{**} For Mainland China, Jiu-Qing Wang (wangjq@mail.ihep.ac.cn) takes care of the distribution with Ms. Su Ping, Secretariat of PASC, P.O. Box 918, Beijing 100039, China.

To keep costs down (remember that the Panel has no budget of its own) readers are encouraged to use the Web as much as possible. In particular, if you receive a paper copy that you no longer require, please inform the appropriate distributor.

7.1.5 Regular Correspondents

The Beam Dynamics Newsletter particularly encourages contributions from smaller institutions and countries where the accelerator physics community is small. Since it is impossible for the editors and panel members to survey all beam dynamics activity worldwide, we have some Regular Correspondents. They are expected to find interesting activities and appropriate persons to report them and/or report them by themselves. We hope that we will have a "compact and complete" list covering all over the world eventually. The present Regular Correspondents are as follows:

Liu Lin	Liu@ns.lnls.br	LNLS Brazil
Sameen Ahmed Khan	Rohelakan@yahoo.com	SCOT, Oman
Jacob Rodnizki	Jacob.Rodnizki@gmail.com	Soreq NRC, Israel
Rohan Dowd	Rohan.Dowd@synchrotron.org.au	Australian Synchrotron

We are calling for more volunteers as Regular Correspondents.

7.2 ICFA Beam Dynamics Panel Members

Name	eMail	Institution
Rick Baartman	baartman@lin12.triumf.ca	TRIUMF, 4004 Wesbrook Mall, Vancouver, BC, V6T 2A3, Canada
Marica Biagini	marica.biagini@lnf.infn.it	INFN-LNF, Via E. Fermi 40, C.P. 13, Frascati, Italy
John Byrd	jmbyrd@lbl.gov	Center for Beam Physics, LBL, 1 Cyclotron Road, Berkeley, CA 94720-8211, U.S.A.
Yunhai Cai	yunhai@slac.stanford.edu	SLAC, 2575 Sand Hill Road, MS 26 Menlo Park, CA 94025, U.S.A.
Swapan Chattopadhyay	swapan@cockcroft.ac.uk	The Cockcroft Institute, Daresbury, Warrington WA4 4AD, U.K.
Weiren Chou (Chair)	chou@fnal.gov	Fermilab, MS 220, P.O. Box 500, Batavia, IL 60510, U.S.A.
Wolfram Fischer	wfisher@bnl.gov	Brookhaven National Laboratory, Bldg. 911B, Upton, NY 11973, U.S.A.
Yoshihiro Funakoshi	yoshihiro.funakoshi@kek.jp	KEK, 1-1 Oho, Tsukuba-shi, Ibaraki-ken, 305-0801, Japan
Jie Gao	gaoj@ihep.ac.cn	Institute for High Energy Physics, P.O. Box 918, Beijing 100039, China
Ajay Ghodke	ghodke@cat.ernet.in	RRCAT, ADL Bldg. Indore, Madhya Pradesh, 452 013, India
Ingo Hofmann	i.hofmann@gsi.de	High Current Beam Physics, GSI Darmstadt, Planckstr. 1, 64291 Darmstadt, Germany
Sergei Ivanov	sergey.ivanov@ihep.ru	Institute for High Energy Physics, Protvino, Moscow Region, 142281 Russia
In Soo Ko	isko@postech.ac.kr	Pohang Accelerator Lab, San 31, Hyoja-Dong, Pohang 790-784, South Korea
Elias Metral	elias.metral@cern.ch	CERN, CH-1211, Geneva 23, Switzerland
Yoshiharu Mori	mori@rri.kyoto-u.ac.jp	Research Reactor Inst., Kyoto Univ. Kumatori, Osaka, 590-0494, Japan
George Neil	neil@jlab.org	TJNAF, 12000 Jefferson Ave., Suite 21, Newport News, VA 23606, U.S.A.
Toshiyuki Okugi	toshiyuki.okugi@kek.jp	KEK, 1-1 Oho, Tsukuba-shi, Ibaraki-ken, 305-0801, Japan
Mark Palmer	mapalmer@fnal.gov	Fermilab, MS 221, P.O. Box 500, Batavia, IL 60510, U.S.A.
Chris Prior	chris.prior@stfc.ac.uk	ASTeC Intense Beams Group, STFC RAL, Chilton, Didcot, Oxon OX11 0QX, U.K.
Yuri Shatunov	Yu.M.Shatunov@inp.nsk.su	Acad. Lavrentiev, Prospect 11, 630090 Novosibirsk, Russia
Jiu-Qing Wang	wangjq@ihep.ac.cn	Institute for High Energy Physics, P.O. Box 918, 9-1, Beijing 100039, China
Rainer Wanzenberg	rainer.wanzenberg@desy.de	DESY, Notkestrasse 85, 22603 Hamburg, Germany

*The views expressed in this newsletter do not necessarily coincide with those of the editors.
The individual authors are responsible for their text.*